Advanced Transceiver Algorithm Design for Cognitive Radio Physical Layer

by

Anjana Gardiye Punchihewage

B.Sc.Eng., The University of Peradeniya, 2004
M.Eng., Memorial University of Newfoundland, 2008

A THESIS SUBMITTED IN PARTIAL FULFILLMENT OF
THE REQUIREMENTS FOR THE DEGREE OF

DOCTOR OF PHILOSOPHY

in

The Faculty of Graduate Studies

(Electrical and Computer Engineering)

THE UNIVERSITY OF BRITISH COLUMBIA

(Vancouver)

January 2011

Abstract

With the ever increasing demand for wireless applications, current wireless systems are challenged to meet the higher data rate and higher reliability requirements. Although the current and future technological developments allow making these requirements reachable, some other resources remain limited. The radio spectrum is one such natural resource. Previous studies have shown that the radio spectrum is not efficiently utilized. Therefore, recent studies are focused on fully utilizing this unexpandable radio spectrum. Cognitive radio (CR) has emerged as a possible solution to improve the spectrum utilization by opportunistically exploiting the licenced users transmit spectrum in dynamically changing environments. On the other hand, the development of CR technology raises new challenges of proper design of transmission and receive schemes for CR to facilitate high data rate access and better performance along with high spectral efficiency. To achieve these objectives, in this thesis, advanced transceiver algorithms for CR physical layer are designed to improve the throughput and the error rate performance in hostile wireless channels.

We first designed a linear precoder for orthogonal space-time block coded, orthogonal frequency division multiplexing (OFDM)-based multiple-input multiple-output antenna CR when operating in correlated Rayleigh fading channels. The linear precoder is designed by minimizing an upper bound on the average pairwise error probability, constrained to a set of per subcarrier power constraints at CR transmitter and a set of primary users interference power thresholds. An efficient algorithm is proposed to obtain the optimal precoder

matrices. We then proposed a power allocation policy to achieve a lower-bound on the ergodic sum capacity of single-input single-output opportunistic spectrum sharing multiple access channel with imperfect channel estimates. An efficient algorithm is proposed to obtain the optimal power allocation for each CR transmitter. Finally, we proposed a blind parameter estimation algorithm for OFDM signal affected by a time-dispersive channel, carrier phase, timing offset, carrier frequency offset and additive Gaussian noise. The cyclostationarity properties of received OFDM signal in time-dispersive channel is exploited to estimate the OFDM parameters. These parameters includes OFDM symbol period, useful symbol period, cyclic prefix factor, number of subcarriers and carrier frequency offset.

Table of Contents

Appendices

List of Tables

List of Figures

Abbreviations

ADC	:	Analog to digital converter
ADSL	:	Asymmetric digital subscriber line
BS	:	Base station
BER	:	Bit error rate
CSI	:	Channel state information
CSCG	:	Circular symmetric complex Gaussian
CR	:	Cognitive radio
CF	:	Cycle frequency
CAF	:	Cyclic autocorrelation function
DAB	:	Digital audio broadcasting
DAC	:	Digital to analog converter
DVB-T	:	Digital video broadcasting-Terrestrial
FCC	:	Federal Communications Commission
4G	:	Fourth generation
IST	:	Information society technologies
IEEE	:	Institute of Electrical and Electronics Engineers
ISI	:	Inter-symbol interference
IFFT	:	Inverse fast Fourier transform

KKT	:	Karush-Kuhn-Tucker
LTE	:	Long term evolution
M-PSK	:	M-ary phase shift keying
M-PAM	:	M-ary pulse amplitude modulation
M-QAM	:	M-ary quadrature amplitude modulation
ML	:	Maximum likelihood
MMSE	:	Minimum mean square error
MAC	:	Multiple access channels
MIMO	:	Multiple-input multiple-output
NBI	:	Narrow band interference
NMSE	:	Normalized mean square error
OFDM	:	Orthogonal frequency division multiplexing
OSTBC	:	Orthogonal space-time block coding
PEP	:	Pairwise error probability
PU	:	Primary user
QoS	:	Quality of services
RF	:	Radio frequency
SU	:	Secondary user
SP	:	Serial-to-parallel
SNR	:	Signal to noise ratio
SISO	:	Single-input single-output
STBC	:	Space-time block coding
STTC	:	Space-time trellis coding
3GPP	:	Third generation partnership project

3G+	:	Third generation plus
WiFi	:	Wireless fidelity
WLAN	:	Wireless local area network
WMAN	:	Wireless metropolitan area network
WPAN	:	Wireless personal area network
WRAN	:	Wireless regional area network
WINNER	:	Wireless world initiative new radio
WiMAX	:	Worldwide interoperability for microwave access

Acknowledgements

I have received numerous support from a number of different people during the course of this thesis work. I honestly believe this thesis work would not have been possible without their encouragement, guidance and great support.

First and foremost, I am deeply indebted to my supervisor, Prof. Vijay K. Bhargava, whose suggestions, guidance and encouragement helped me throughout my thesis work. In addition, I extend my sincere thanks to Prof. Vijay K. Bhargava for giving me the opportunity to be a part of the Information Theory and Systems (ITS) group.

I take this opportunity to thank Prof. Charles Despins from the INRS-ÉMT, Montréal, Québec, Canada, for his support and encouragement during my thesis work.

I would like to thank Prof. Robert Schober, Prof. Lutz Lampe, Prof. Vikram Krishnamurthy, and Prof. David L. Pulfrey, for their valuable time serving on my qualifying examination. Their important comments and suggestions have considerably improved the quality of my thesis work.

The work of this thesis is supported by the Natural Sciences and Engineering Research Council (NSERC) of Canada under the strategic project grant support. I am grateful to NSERC for their support.

I would like to thank my former and current ITS group mates for their help, cheerfulness, friendship and continuous encouragement during this thesis work. I am thankful to my Sri Lankan friends, Mr. Lalinda Weerasekara, Mr. Gamini Siriwardana, Dr. Chandika

Wavegedara, Mr. Thissa Bandara and Mr. Eranda Harinath for their continuous encouragement and numerous support in different ways.

I would like to acknowledge the sacrifice, support and affection extended by my family during this period, with special thanks extending to my elder brother and sister-in-law. I would like to thank my loving wife, to her unwavering support, love, dedication, continuous encouragement, patient and many sacrifices she has made during my thesis work.

Lastly, and most importantly, I wish to thank my parents. They gave birth to me, raised me, supported me and loved me.

To My Parents . . .

Statement of Co-Authorship

I identified and formulated the research problems presented in this thesis work in consultation with my graduate supervisor Prof. Vijay K. Bhargava. Prof. Charls Despins provided some important feedbacks during formulation of the research problems in this thesis work. He also provided editorial feedbacks during my preparation of the manuscripts for publications. I, myself, performed all mathematical derivations. Computer simulations and analyzes of the results were totally carried out by myself.

Chapter 1

Introduction

1.1 Overview

With the increasing advancements in the digital technology, current and future wireless communications systems are promising to support higher throughput, higher reliability, wider coverage area and higher mobile speeds. Initial wireless systems were mainly designed and developed to support only the voice. However, the role of current wireless communications has changed considerably due to extensive deployment of multimedia applications and vast growth of internet. Therefore, current and future wireless networks need to be designed to carry voice, data and multimedia applications.

There are several current broadband wireless standards such as wireless fidelity (WiFi), worldwide interoperability for microwave access (WiMAX) and third generation plus (3G+) systems, which support high throughput with the help of large bandwidth. In addition, the Institute of Electrical and Electronics Engineers (IEEE) and the Information Society Technologies (IST) have been proposed future fourth generation (4G) technologies such as the long term evolution (LTE), LTE-advanced standards by the 3G partnership project (3GPP) and the wireless world initiative new radio (WINNER) to support future wireless communications services and networks.

In spite of all these technological advancement, the scarcity and the static allocation of

the radio spectrum become crucial concern for increasing the throughput in current wireless services. The electromagnetic radio spectrum is a precious resource available for wireless communications, which demands efficient usage. According to the current measurements by the Federal Communications Commission's (FCC's) spectrum policy task report [1], the usage of allocated spectrum varies from fifteen to eighty-five percent at specific time and geographical location. Wide span of licensed spectrum is rarely used most of the time, while other spectrum segments are heavily occupied. This low spectrum utilization coupled with spectrum scarcity motivates the development of novel spectrum sharing technologies with the aim of improving the spectrum utilization.

Recently, a new development for improving the spectrum under utilization, while accommodating the growing amount of services and applications in wireless communications has been suggested by proposing the use of cognitive radio (CR) [2–6]. CR is capable of dynamically sensing and identifying the unoccupied spectrum bands which are initially allocated to licensed users, also called primary users (PUs) and allowing an unlicensed users, also called secondary users (SUs) to communicate through these available spectrum segments. SUs, however, can only operate in licensed bands without causing harmful interference to PUs or they do not block the active PUs in the network. CR can significantly improve the spectral utilization by implementing this approach. CR is an intelligent wireless system which is aware of its surrounding propagation environment through sensing, measurements and adapts to it by making real time changes in certain operating parameters, such as output power, operating frequency, modulation and demodulation strategy [3]. Making this real time processing is possible since it is a particular extension of software defined radio [7], as such allowing CR transceiver to perform baseband processing functionalities using software and digital logic. Thus, in addition to the efficient usage of

spectrum, CR provides reconcilability and highly reliable communication.

1.2 Motivation and Objective of the Thesis

CR has been proposed as a novel technique to improve the spectrum utilization while supporting the increasing amount of services and applications in wireless communications. In CR network, CR users may coexist or opportunistically share the spectrum with PUs either on a non-interfering basis or interference tolerance basis [8, 9]. Examples of several opportunistic spectrum access methods for CR are proposed in [9]. One of the major challenging problems in CR networks is to ensure the successful coexistence of PUs and CR users in the same frequency band while maximizing the CR users performance and avoid or minimize the interference introduced to the PUs. Due to the presence of PUs in the CR networks, strategies proposed in conventional radios to improve the throughput and the system error performance may not be optimal and not directly applicable for CRs. Thus, managing the quality of services (QoS) offered by a CR system while maintaining the QoS of the PUs, in opportunistic spectrum sharing and dynamically changing environments is challenging. Hence, proper design of a transmitter and receiver schemes for CRs to facilitate high data rate access and better performance along with high spectral efficiency is very important. Therefore, there is a need to optimize the transceiver design to achieve a higher throughput and a better error rate performance over the utilized spectrum. To achieve these objectives, it is crucial to integrate recent physical layer technical advances into the CR systems. Therefore, the overall goal of this thesis is to study and design of advanced transceiver algorithms for CR physical layer with the aim of improving the throughput and the system error performance.

Multiple-input multiple-output (MIMO) antenna systems and space-time block coding (STBC) in wireless communications have attached considerable attention in conventional radio systems due to their ability to increase throughput and improve error rate performance. Orthogonal frequency division multiplexing (OFDM) is also gained vast attention due to its several advantages such as scalability, robustness against multipath fading etc. In conventional radio systems, efficient precoding techniques in combination with STBC have been exploited to improve the system error performance and to minimize the induced interference to the other active users. Therefore, these vital techniques motivate us to employ them in the CRs for improving the error rate performance while minimizing the interference introduced to other active PUs in the network. In a heterogeneous CR environment several SUs and PUs coexist, and moreover, the CR users are mobile and sporadic (e.g. mobile military mission). In such coexisting CR network, the QoS of PUs is maintained by introducing a interference power constraint to the SU's resource allocation problem. The interference power is measured at the PU receiver and should be below a threshold specified by the regulatory bodies. Unlike the linear precoder design problems for conventional radio systems, additional interference power constraints are added to the liner precoder design problem for CRs. Thus, linear precoders proposed for conventional radio systems cannot be directly applied to CR systems. In this thesis, we propose a solution to this problem by designing a linear precoder for orthogonal space-time block coded (OSTBC) MIMO-OFDM based CR. Theoretical analysis and the linear precoder design proposed in this work are based on a comprehensive signal model that takes into account of multiple antennas at both SUs and PUs, multi-carrier transmission scheme and the correlation effect at SU's both transmit and receive antennas.

Many power allocation algorithms developed for CRs in previous studies have assumed

either point-to-point communication or perfect channel state information (CSI) is available at the CR transmitter. However, CR network is naturally a multiuser communication environment and therefore, it is necessary to consider power allocation schemes between multiple SUs in a CR network. Furthermore, the assumption of perfect CSI for the channels between SU transmitters and SU receivers and the channels between SU transmitters and PU receivers is not practical. In practice, these CSI is often imperfect and SU performance can be highly depended on the accuracy of these CSI. In particular, the induced interference on the PUs by the SUs can depend on the accuracy of the available CSI. This motivates us to design a power allocation scheme for CR multiple access channels (MAC) by considering the channel estimation errors for both the aforementioned set of channels.

Since the CR is an intelligent device, it has the capability of adjusting to the propagating environment by making real time changes to its operating parameters such as modulation strategy, demodulation strategy, operating frequency etc. Due to this dynamic change of operating parameters, CR transmitter has to frequently send information necessary to demodulate the signal to the receiver side with the cost of additional bandwidth. This will reduce the spectrum utilization, which is the primary objective of the CR. This motivates us to design a blind parameter estimation algorithms for CRs with the intention of improving the system throughput. This will reduce the impact of various practical impairments to wireless signals. The received signal signal-to-noise ratio can be considerably improved by minimizing the impact of these impairments. Thus, this will allow CR systems to support higher order modulation formats and consequently higher data rates. In addition, since we employ a blind method, the spectrum utilization is also improved.

In the sequel, we present briefly the specific objectives of this thesis:

1. To design a linear precoder for OSTBC MIMO-OFDM based CR when operating

in correlated Rayleigh fading channels. In designing the linear precoder, we intend to improve the error rate performance of the CR while minimizing the interference introduced to the active PUs.

2. To design a robust power allocation algorithm for opportunistic spectrum sharing single-input single-output (SISO) MAC in Rayleigh fading channels with imperfect channel estimations.

3. To design a blind parameter estimation algorithm for OFDM based CR when operating in time-dispersive channel.

1.3 Background

In this section, the background pertinent to the research areas of this thesis work is reviewed. First, we present the operation of a CR followed by some physical layer advances which can be exploited for CRs.

1.3.1 Operation of a Cognitive Radio

The CR operation was first modeled through a cognitive cycle, with states named as *observe*, *orient*, *learn*, *plan*, *decide* and *act* [2]. The cognitive cycle starts with sensing the radio spectrum, and finishes with an action taken based on the sensed spectrum [2]. A modified representation of the cognitive cycle was introduced in [3] and depicted in Fig. 1.1. The cognitive cycle consists of three cognitive tasks; radio-scene analysis, channel identification, and transmit power control and dynamic spectrum management [3]. The first task in the cognitive cycle, comprises two sub tasks; estimation of interference tem-

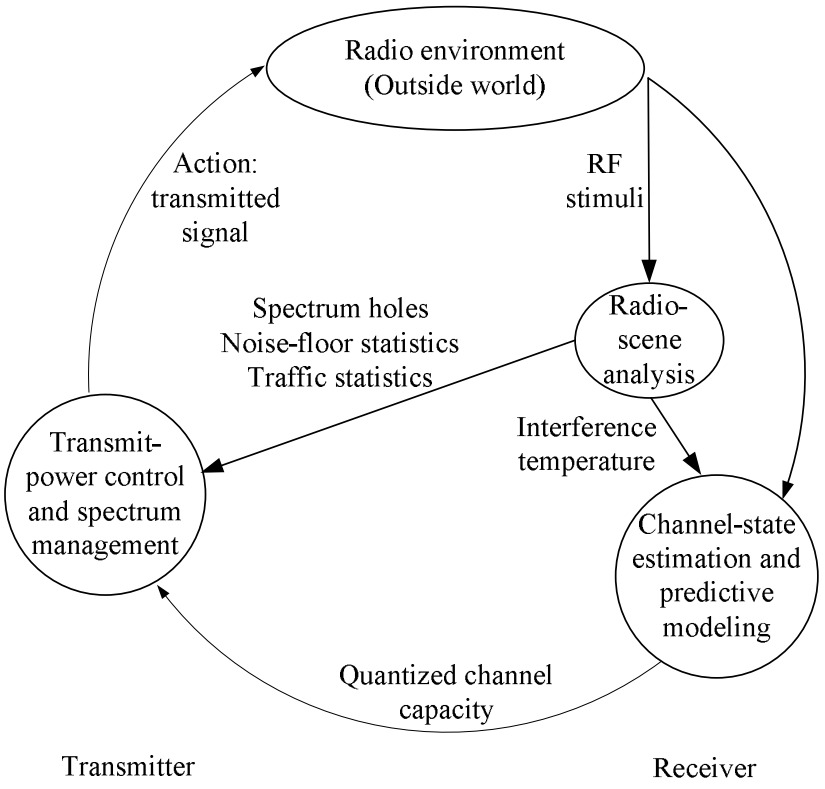

Figure 1.1: Basic cognitive cycle.

perature and detection of spectrum holes [3]. A spectrum hole is a frequency segment assigned to a PU, that can be available for a SU at a particular time and a geographical location [3]. The interference temperature is a metric introduced by FCC and represents the temperature equivalent of the radio frequency (RF) power available at a receive antenna, per unit bandwidth. The interference temperature is intended to quantify and manage interference among different services in a radio environment. The maximum acceptable level of interference temperature provides a *worst case* characterization of the radio frequency environment in a particular frequency band, time and geographical location, where the receiver could be expected to operate satisfactory. Three types of spectrum holes, *black*, *gray*

and *white* spaces, can be identified by exploring the power spectrum of an incoming RF signal [3]. The frequency bands currently occupied by PUs are *black* spaces, and thus, they are characterized by high RF power. These *black* spaces must be avoided in the CR environment. However, these *black* spaces become spectrum holes when the PUs are switched off. Then, these can be shared with CR users. The *gray* and *white* spaces are defined as low and free of RF interferences, respectively. It appears that *gray* and *white* spaces are candidates to be employed by CR users.

The second task in the cognitive cycle consist of two sub tasks; estimation of CSI and prediction of channel capacity [3]. In the CR environment, computation of channel capacity requires the knowledge of CSI. In previous studies, two approaches are used to CSI estimation; differential detection and pilot transmission [10]. The differential detection has the advantage of implementation simplicity, at the expense of frame error rate degradation at the receive-side. On the other hand, the pilot transmission offers an improved performance, at the expense of transmit power and bandwidth. It should be noted that the differential detection is a blind method whereas the pilot transmission is data aided. Due to the drawbacks of the two aforementioned methods, CR is intended to employ a semi-blind approach to estimate CSI [11]. After carrying out the first two tasks in the cognitive cycle, the transmit power control of the CR is performed at the transmit-side [3].

1.3.2 OFDM Technology

OFDM is one of the widely exploited efficient transmission techniques in current wireless communications systems. This multi-carrier transmission scheme has been exploited in current physical layer standards such as wireless local area networks standards (WLAN) [12], wireless metropolitan area networks standards (WMAN) [13], digital audio broadcast-

ing (DAB) [14], digital video broadcasting-terrestrial (DVB-T) standards [15] and asymmetric digital subscriber line (ADSL) [16]. In addition, it has been proposed as a strong candidate for future wireless technologies such as LTE, LTE-advanced [17] standard proposed by 3GPP, and the wireless personal area network standard (WPAN) [18]. Further, OFDM has been proposed as the transmission technique in the wireless regional area networks (WRAN), which is the first CR standard [19].

There are several benefits of OFDM over single carrier transmission schemes such as robustness against multipath fading, simplicity in channel equalization and coding, multiple access mechanism, ease of implementation. In the OFDM transmission scheme, a broadband frequency channel is divided into narrow-band sub-channels which are modulated using orthogonal subcarriers. Therefore, each sub-channel becomes flat fading in the frequency-selective channel, since the sub-channel bandwidth becomes smaller than the coherence bandwidth of the channel. In addition, the introduction of cyclic prefix (CP) reduces the inter-symbol interference (ISI) caused by multipath propagation [20]. In general, the length of the cyclic prefix should be greater than the length of the channel [20].

A simplified block diagram of a basic wireless communications system using OFDM over a SISO channel is presented in Fig. 1.2. First, the channel encoded and interleaved data are fed into the modulator to generate the data symbols. In OFDM transmission, interleaving is applied to increase immunity to burst errors and randomize the occurrence of bit errors. Coding is exploited to improve the system performance over the channel. Second, modulated data symbols are passed through serial-to-parallel (S/P) converter to form a parallel data stream. Third, the parallel data symbols are fed into the inverse fast Fourier transform (IFFT) block to obtain the time domain samples of the OFDM symbols. Fourth, parallel-to-serial (P/S) converter forms a serial data stream. Fifth, at the cyclic

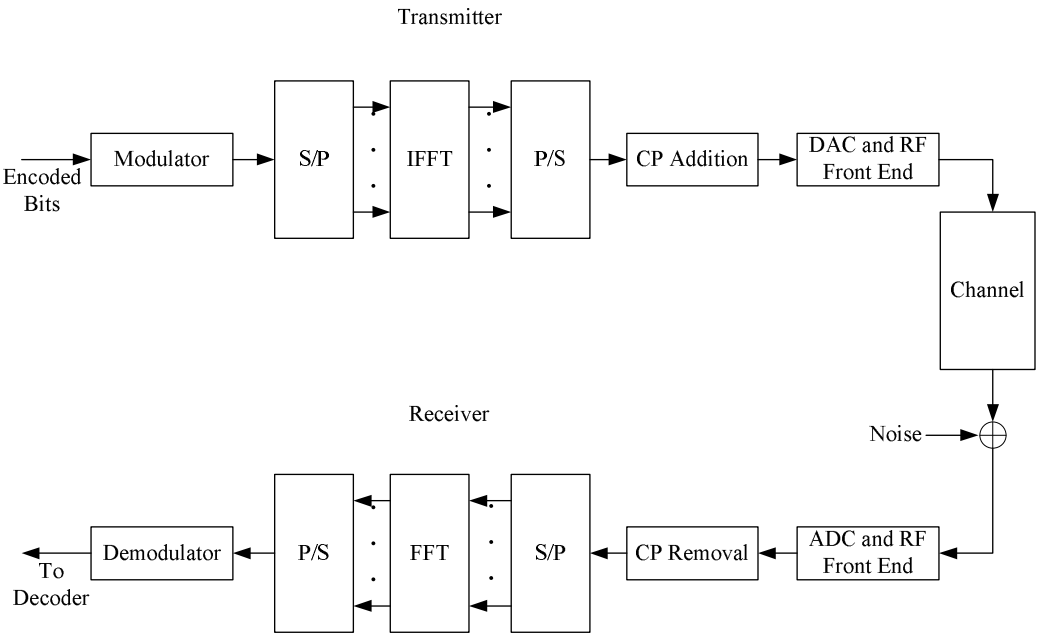

Figure 1.2: A simplified block diagram of a SISO OFDM system.

prefix (CP) addition block, a CP, which is the portion of the last part of the symbols is added to each symbol to avoid residual ISI from the previous OFDM symbols. Finally, the digital to analog converter (DAC) and the RF front end process the serial data stream to transmit by the transmit antennas through the channel. At the receive side, the received signal is first passed through a band pass noise rejection filter, RF front end circuits and analog to digital converter (ADC) to process the data and then send to the CP removal block. Then, the CP removal block removes the CP and the S/P converter passes the parallel time domain samples to the FFT block to generate the frequency domain samples of the received signal. These samples are then demodulated, deinterleaved, and decoded to obtain the transmitted data bits. In Table 1.1, we present some key parameters of current OFDM-based standards.

OFDM has been exploited as transmission technique in CRs due to its several attractive

Table 1.1: Key OFDM parameters exploited in current wireless standards.

Standard	IEEE 802.11a	IEEE 802.16d	IEEE 802.22	DVB-T2
Channel spacing (MHz)	20	1.25, 5, 10, 20	6, 7, 8	1.7, 5, 6, 7, 8, 10
FFT size (k=1024)	64	128, 256, 512, 1k, 2k	1k, 2k, 4k	2k, 8k
CP size/FFT size	1/4	1/4, 1/8, 1/16, 1/32	variable	1/4, 1/8, 1/16, 1/32
Subcarrier modulation format	BPSK, QPSK, 16-QAM, 64-QAM	BPSK, QPSK, 16-QAM, 64-QAM	QPSK, 16-QAM, 64-QAM	QPSK, 16-QAM, 64-QAM, 256-QAM
Maximum achievable net bit rate (Mbps)	54	63	19	48

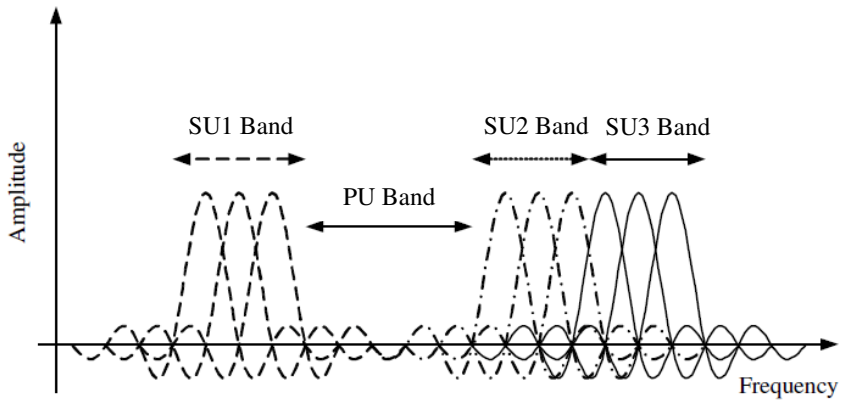

Figure 1.3: Allocation of the available spectrum among SUs using OFDM.

features in addition to the aforementioned advantages such as, flexibility in dynamically allocating unused spectrum among CR users, ease of analysis of PUs spectral activity, ability of adaptively change operating parameters for individual subcarriers based on the

channel conditions and the user needs [21–24]. Fig. 1.3 presents the dynamic allocation of the available spectrum among CR users using the OFDM. It can be seen from Fig. 1.3 that the PU transmission is protected by simply turning off the subcarriers which are occupied by the PU in that frequency segment.

1.3.3 MIMO Antenna Systems

A wireless communications system which employs multiple antennas at both the transmitter and receiver is referred to as a MIMO antenna system [25]. MIMO technique is basically initiated by the theoretical work developed in [25] and [26]. The use of MIMO technique proffers numerous advantages such as spatial degree of freedom, increased spectral efficiency and diversity gain [27]. A simplified block diagram of a single user MIMO system is presented in Fig. 1.4. The transmission technologies developed for MIMO systems can be broadly classified in to two: Maximize the throughput over MIMO channels; maximize the diversity gain to improve the system performance.

The first category is generally referred to as the spatial multiplexing. In spatial multiplexing, independent data streams are transmitted simultaneously from each transmit antenna in parallel and separated at the receiver. This provides a liner increase in the throughput for a given bandwidth without additional transmit power. It is shown in the previous studies that the capacity of a MIMO system increases linearly with the minimum of the number of transmit and receive antennas. With these vital features, MIMO systems will play an important role in CR systems. Recently, MIMO antenna systems have been exploited for CRs in previous studies to improve the throughput and minimize the error rate performance [28–33].

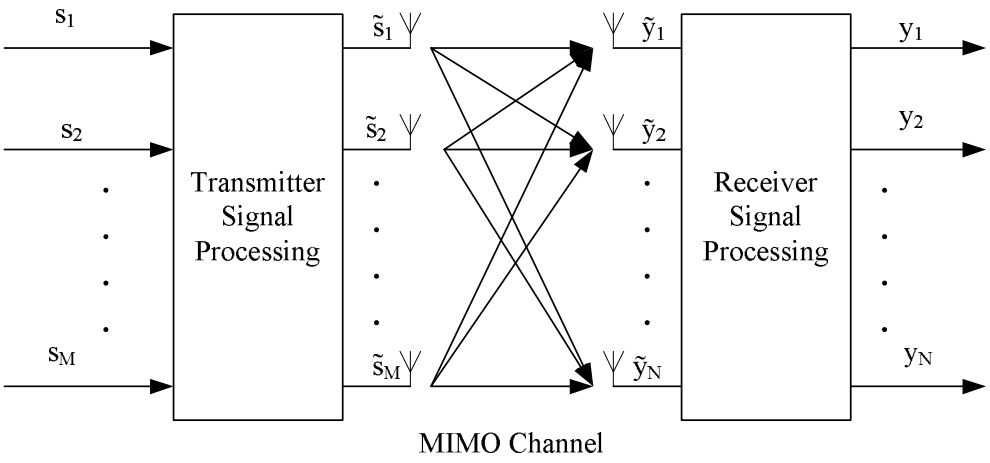

Figure 1.4: A simplified block diagram of a MIMO system.

1.3.4 Space-Time Coding

The second category of the MIMO systems is the transmit diversity techniques, which exploits the diversity advantages offered by the multiple transmit antennas. In wireless communications, diversity techniques such as time (temporal), antenna (space), and frequency can be effectively exploited to suppress the determinantal effect of channel fading [34, 35]. However, in practice it might not be able to employ all the above diversity techniques in most of the wireless communications applications. In spectral diversity, the diversity advantage can be achieved by increasing the number of transmit and/or receive antennas for a given frequency band. On the other hand, in frequency diversity, the diversity advantage is achieved with fixed number of transmit and receive antennas and by increasing the frequency band. In practice, spatial diversity is preferred among the aforementioned diversity techniques, since it can be exploited without the loss of spectral efficiency by increasing the number of transmit and receive antennas [36].

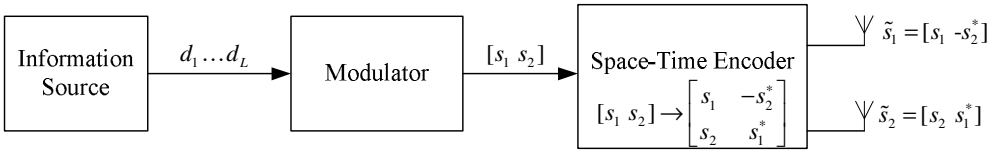

Figure 1.5: A simplified block diagram of the Alamouti space-time block encoder.

Space-time codes were originally investigated and developed for frequency flat fading channels. Two basic space-time coding techniques, space-time trellis coding (STTC) and STBC were introduced in [35] and [37], respectively to improve the link level performance based on the diversity. The STTC decoding requires the multidimensional Viterby algorithm at the receiver. On the other hand, the maximum likelihood (ML) decoding of STBC is possible only using linear processing at the receiver [38]. Therefore, this lower decoding complexity of STBC makes it more attractive when compared with the STTC.

In Fig. 1.5, we present a simplified block diagram of the Alamouti space-time block encoder. During the first symbol period, the transmit antennas one and two transmit symbols s_1 and s_2, respectively. During the second symbol period, the transmit antennas one and two transmit symbols $-s_2^*$ and s_1^*, respectively with $(\cdot)^*$ as the conjugate operation. Therefore, Alamouti scheme provides the full diversity with full transmission rate [37]. Furthermore, Alamouti scheme is capable of achieving the overall diversity gain of $2N$ with N as the number of receive antennas [39]. The Alamouti scheme was then generalized to arbitrary number of transmit antennas using the theory of orthogonal design in [38]. These codes are referred to as OSTBC and can achieve the full transmit diversity of MN with M as the number of transmit antennas, and yet allow receiver with simple ML decoding algorithm [38].

The performance of STBC was investigated in [34]. Furthermore, in [38] it was shown that, complex orthogonal design for STBC, which provides full diversity and full rate, does not exist for more than two transmit antennas. The design of quasi-orthogonal STBC was proposed in [40] to achieve the full rate but only with the partial diversity.

1.3.5 Signal Cyclostationarity

In general, signal cyclostationarity is present in communications, signal processing, telemetry, radar and control systems. The cyclostationarity properties of signals have been extensively studied for communications, radar, sonar applications and biomedical. Most of the signal encountered in wireless communications exhibits cyclostationary associated with the carrier frequency, symbol period, chip rate, pilot position, and combination of these [41–53]. In previous studies, the signal cyclostationarity have been exploited for different purposes including signal identification, blind equalization, parameter estimation and synchronization [41–53]. In conventional radios, first-, second-, and higher-order cyclostationarity of signals is employed for aforementioned applications [54–58].

In CR networks, the signal cyclostationarity have been exploited for parameter estimation, modulation classification and signal detection [59–61]. For the spectrum sensing, the cyclostationarity feature detector employs cycle spectral correlation to detect the presence of a signal. The correlation at certain spectral and cycle frequencies is used to detect the signal presence [62]. The cyclostationarity feature detector has the ability to discriminate noise from a modulated signal, as noise is a wide-sense stationary signal with zero cyclic spectral correlation [62]. Therefore, the noise influence in the detection process is less for cyclostationarity feature detector [63].

1.4 Outline of the Thesis

The remainder of the thesis is organized as follows:

- In Chapter 2, we present a linear precoder design for OSTBC MIMO-OFDM based CR when operating in correlated Rayleigh fading channels. Unlike the previous studies on precoder design for CR, our proposed linear precoder is capable of handling both transmit and receive correlation in a multi-carrier based CR system. The proposed linear precoder is designed to minimize an upper bound on the average pairwise error probability, constrained to a set of per subcarrier transmit power constraints at the CR transmitter and a set of interference power thresholds at PU receivers. The CR transmitter exploits the knowledge of transmit and receive correlation matrices while designing the precoder. We have shown that the linear precoder design problem is convex with these constraints, and convex optimization techniques are exploited to derive an efficient algorithm to obtain the optimal precoder matrices. We have also presented simulation results to show performance benefits of the proposed linear precoder in a CR system.

- In Chapter 3, we study a ergodic sum capacity of SISO opportunistic spectrum sharing MAC in Rayleigh fading channels with imperfect channel estimates. Unlike the previous studies, we consider the channel estimation errors for both set of channels, between the SU transmitters and the SU receiver and the channels between the SU transmitters and the PU receivers. By considering these channel estimation errors, an optimal power allocation policy for each SU transmitter is derived to achieve a lower bound of the ergodic sum capacity of opportunistic spectrum sharing MAC, subject to set of SU transmitters power constraints and a set of interference power

constraints at each PU receiver. Furthermore, convex optimization techniques are exploited to derive an efficient algorithm to obtain the optimal power allocation for each SU transmitter.

- In Chapter 4, we develop a blind parameter estimation algorithm for OFDM signal affected by a time-dispersive channel, carrier phase, timing offset, carrier frequency offset and additive Gaussian noise. Unlike the previous studies, we present the second-order cyclostationarity of OFDM signal considering the effect of time-dispersive channel. The cyclostationarity properties of received OFDM signal in time-dispersive channel is exploited to estimate the OFDM parameters. These parameters includes OFDM symbol period, useful symbol period, cyclic prefix factor, number of subcarriers and carrier frequency offset. Simulations are performed to investigate the performance of OFDM parameter estimation algorithm in diverse channel conditions.

- In Chapter 5, we conclude the thesis by summarizing our contributions. Furthermore, suggestions for future research directions are also presented.

Bibliography

[1] Federal Communication Commission, *Spectrum Policy Task Force*, ET Docket No. 02-155, Nov. 2002.

[2] J. Mitola III, "Cognitive radio for flexible mobile multimedia communications," *Proc. IEEE Int. Work. MoMuC*, pp. 3-10, Nov. 1999.

[3] S. Haykin, "Cognitive radio: Brain-empowered wireless communications," *IEEE J. Sel. Areas Commun.*, vol. 23, no. 2, pp. 201-220, Feb. 2005.

[4] B. A. Fette, *Cognitive Radio Technology*, Elsevier, 2009.

[5] A. M. Wyglinski, M. Nekovee, and Y. T. Hou, *Cognitive Radio Communications and Networks: Principles and Practice*, Elsevier, 2010.

[6] L. Berlemann and S. Mangold, *Cognitive Radio and Dynamic Spectrum Access*, Wiley, 2009.

[7] J. Mitola, "The software radio architecture," *IEEE Commun. Mag.*, vol. 33, no. 5, pp. 26-38, May 1995.

[8] W. Wei, P. Tao, and W. Wenbo, "Optimal power control under interference temperature constraint in cognitive radio network," *Proc. IEEE WCNC*, pp. 116-120, Mar. 2007.

[9] I. F. Akyildiz, W. Y. Lee, M. C. Vuran, and S. Mohanty, "NeXt generation/dynamic spectrum access/cognitive radio wireless networks: A survey," *Comput. Netw.*, vol. 50, no. 13, pp. 2127-2159, Sep. 2006.

[10] S. Haykin and M. Moher, *Modern Wireless Communications*, Prantice Hall, 2004.

[11] C. J. Foschini, "Bayesian sequential state estimation for MIMO wireless communications," *Proceedings of the IEEE*, vol. 92, no. 3, pp. 439-454, Mar. 2004.

[12] Supplement to IEEE Standard for Information Technology - Telecommunications and Information Exchange Between Systems - Local and Metropolitan Area Networks - Specific Requirements. Part 11: Wireless LAN Medium Access Control (MAC) and Physical Layer (PHY) Specifications: High-Speed Physical Layer in the 5 GHz Band, IEEE Std 802.11a-1999, Aug. 1999.

[13] IEEE standard for local and metropolitan area networks part 16: Air interface for fixed broadband wireless access systems, IEEE Std. 802.16-2004, 2004.

[14] Radio broadcasting systems; digital audio broadcasting (DAB) to mobile, portable and fixed receivers, ETSI Std. EN 300 401, 2001.

[15] Digital video broadcasting (DVB); framing structure, channel coding and modulation for digital terrestrial television, ETSI Std. EN 300 744, 2001.

[16] Asymmetric digital subscriber line (ADSL), ANSI Std. T1.413, 1995.

[17] E. Seidel, "Progress on LTE Advanced-the new 4G standard,", *White Paper, Nomor Research*, Jul. 2008.

[18] IEEE 802.15 WPAN high rate alternative PHY task group 3a (TG3a), [Online]. Available: http://www.ieee802.org/15/pub/TG3a.html.

[19] "IEEE 802.22 working group on wireless regional area networks." [Online]. Available: http://www.ieee802.org/22/

[20] L. L. Hanzo, M. Munster, B. J. Choi, and T. Keller, *OFDM and MC-CDMA for Broadband Multi-User Communications, WLANs and Broadcasting*, Wiley, 2003.

[21] T. Weiss and F. K. Jondral, "Spectrum pooling: An innovative strategy for the enhancement of spectrum efficiency," *IEEE Commun. Mag.*, vol. 43, no. 3, pp. S8-S14, Mar. 2004.

[22] G. Bansal, M. J. Hossain, and V. K. Bhargava, "Optimal and suboptimal power allocation schemes for OFDM-based cognitive radio systems," *IEEE Trans. Wireless Commun.*, vol. 7, no. 11, pp. 4710-4718, Nov. 2008.

[23] E. Hossain and V. K. Bhargava, *Cognitive Wireless Communication Networks*, Springer, 2007.

[24] T. Keller and L. Hanzo, "Adaptive modulation techniques for duplex OFDM transmission," *IEEE Trans. Veh. Techn.*, vol. 49, no. 5, pp. 1893-1906, Sep. 2004.

[25] E. Telatar, "Capacity of multiantenna Gaussian channels," *European Trans. Telecommun.*, vol. 10, no. 6, pp. 585-595, Nov. 1999.

[26] G. J. Foschini and M. J. Gans, "On limits of wireless communications in a fading environment when using multiple antennas," *Wirel. Pers. Commun.*, vol. 6, no. 3, pp. 311-335, Mar. 1998.

[27] S. Haykin and M. Moher, *Modern Wireless Communications*, Prentice-Hall, 2004.

[28] X. Kang, A. Nallanathan, Y. C. Liang, H. K. Garg, and R. Zhang, "Optimal power allocation for fading channels in cognitive radio networks: Ergodic capacity and outage capacity," *IEEE Trans. Wireless Commun.*, vol. 8, no. 2, pp. 940-950, Feb. 2009.

[29] R. Zhang and Y. C. Liang, "Exploiting multi-antennas for opportunistic spectrum sharing in cognitive radio networks," *IEEE J. Sel. Topics Signal Proc.*, vol. 2, no. 1, pp. 88-102, Feb. 2008.

[30] N. Devroye, P. Mitran, and V. Tarokh, "Achievable rates in cognitive radio channels," *IEEE Trans. Info. Theory*, vol. 52, no. 5, pp. 1813-1827, May 2006.

[31] S. Sridharan and S. Vishwanath, "On the capacity of a class of MIMO cognitive radios," *IEEE J. Sel. Topics Signal Proc.*, vol. 2, no. 1, pp. 103-117, Feb. 2008.

[32] C. X. Wang, X. Hong, H. H. Chen, and J. Thompson, "On capacity of cognitive radio networks with average interference power constraints," *IEEE Trans. Wireless Commun.*, vol. 8, no. 4, pp. 1620-1625, Apr. 2009.

[33] U. Phuyal, A. Punchihewa, V. K. Bhargava, and C. Despins, "Power loading for multicarrier cognitive radio with MIMO antennas," *Proc. IEEE WCNC*, pp. 1-5, Apr. 2009.

[34] V. Tarokh, H. Jafarkhani, and A. R. Calderbank,"Space-time block coding for wireless communications: performance results," *IEEE J. Sel. Areas Commun.*, vol. 17, no. 3, pp. 451-460, Mar. 1999.

[35] V. Tarokh, N. Seshadri, and A. R. Calderbank, "Space-time codes for high data rate wireless communication: performance criterion and code construction," *IEEE Trans. Inf. Theory*, vol. 44, no. 2, pp. 744-765, Mar. 1998.

[36] H. Bolcskei and A. J. Paulraj, "Space-frequency coded broadband OFDM systems," *Proc. IEEE WCNC*, pp. 1-6, Sep. 2000.

[37] S. M. Alamouti, "A simple transmit diversity technique for wireless communications," *IEEE J. Sel. Areas Commun.*, vol. 16, no. 8, pp. 1451-1458, Oct. 1998.

[38] V. Tarokh, H. Jafarkhani, and A. R. Calderbank, "Space-time block codes from orthogonal designs," *IEEE Trans. Inf. Theory*, vol. 45, no. 5, pp. 1456-1467, Jul. 1998.

[39] H. Jafarkhani, *Space-time coding: Theory and practice*, 1st. ed. Cambridge University Press, 2005.

[40] H. Jafarkhani, "A quasi-orthogonal space-time block code," *IEEE Trans. Commun.*, vol. 49, no. 1, pp. 1-4, Jan. 1998.

[41] H. Bolcskei, "Blind estimation of symbol timing and carrier frequency offset in wireless OFDM systems," *IEEE Trans. Commun.*, vol. 49, no. 6 , pp. 988-999, Jun. 2001.

[42] M. Shi, Y. Bar-Ness, and W. Su, "Blind OFDM systems parameters estimation for software defined radio," *Proc. IEEE DySPAN*, pp. 119-122, Apr. 2007.

[43] H. Li, Y. Bar-Ness, A. Abdi, O. S. Somekh, and W. Su, "OFDM modulation classification and parameter extraction," *Proc. IEEE CROWCOM*, pp. 1-6, Jun. 2006.

[44] A. Bouzegzi, P. Jallon, and P. Ciblat, "A second order statistics based algorithm for blind recognition of OFDM based systems," *Proc. IEEE GLOBECOM*, pp. 1-5, Nov. 2008.

[45] R. W. Heath Jr. and G. B. Giannakis, "Exploiting input cyclostationarity for blind channel identification in OFDM systems," *IEEE Trans. Sig. Proc.*, vol. 47, no. 3, pp. 848-856, Mar. 1999.

[46] C. M. Spooner and W. A. Gardner, "Robust feature detection for signal interception," *IEEE Trans. Commun.*, vol. 42, no. 5, pp. 2165-2173, May 1994.

[47] D. Cabric, "Cognitive radios: System design perspective," University of California at Berkley, 2007.

[48] Q. Zhang, O. A. Dobre, S. Rajan, and R. Inkol, "On the second-order cyclostationarity for joint signal detection and classification in cognitive radio systems," *Proc. IEEE CCECE*, pp. 204-208, May 2009.

[49] M. Oner and F. Jondral, "On the extraction of the channel allocation information in spectrum pooling system," *IEEE J. Sel. Areas Commun.*, vol. 25, no. 3, pp. 558-565, Apr. 2007.

[50] K. Kim, C. M. Spooner, I. Akbar, and J. H. Reed, "Specific emitter identification for cognitive radio with application to IEEE 802.11," *Proc. IEEE GLOBECOM*, pp. 1-5, Nov. 2008.

[51] O. A. Dobre, Y. Bar-Ness, and W. Su, "Cyclostationarity-based modulation classification of linear digital modulations in flat fading channels," *Springer Wireless Personal Communications*, DOI: 10.1007/s11277-009-9776-2, 2009.

[52] W. A. Gardner and C. M. Spooner, "The cumulant theory of cyclostationary time-series. I. Foundation," *IEEE Trans. Sig. Proc.*, vol. 42, no. 12, pp. 3387-3408, Dec. 1994.

[53] C. M. Spooner and W. A. Gardner, "The cumulant theory of cyclostationarity time-series. II. Development and applications," *IEEE Trans. Sig. Proc.*, vol. 42, no. 12, pp. 3409-3429, Dec. 1994.

[54] P. Marchand, J. L. Lacouume, and C. Martret, "Classification of linear modulations by a combination of different orders cyclic cumulants," *Proc. Workshop on HOS*, pp. 47-51, Jul. 1997.

[55] C. M. Spooner, "Classification of co-channel communication signal using cyclic cumulants," *Proc. IEEE ASILOMAR*, pp. 531-536, Nov. 1995.

[56] C. M. Spooner, W. A. Brown, and G. K. Yeung, "Automatic radio frequency environment analysis," *Proc. IEEE ASILOMAR*, pp. 1181-1186, Oct. 2000.

[57] F. Gini and G. B. Giannakis, "Frequency offset and symbol timing recovery in flat-fading channels: A cyclostationary approach," *IEEE Trans. Commun.*, vol. 46, no. 3, pp. 400-411, Mar. 1998.

[58] W. A. Gardner, *Cyclostationarity in Communication and Signal Processing*, IEEE Press, 1994.

[59] K. L. Du and W. H. Mow, "Affordable cyclostationarity-based spectrum sensing for cognitive radio with smart antennas," *IEEE Trans. Veh. Technol.*, vol. 59, no. 4, pp. 1877-1886, May 2010.

[60] K. W. Choi, W. S. Jeon, and D. G. Jeong, "Sequential detection of cyclostationary signal for cognitive radio systems," *IEEE Trans. Wireless Commun.*, vol. 8, no. 9, pp. 4480-4485, Sep. 2009.

[61] H. Ishii and G. W. Wornell, "OFDM blind parameter identification in cognitive radio," *Proc. IEEE PIMRC*, pp. 700-705, Sep. 2005.

[62] W. A. Gardner and C. M. Spooner, "Signal interception: Performance advantages of cyclic-feature detectors," *IEEE Trans. Commun.*, vol. 40, no. 1, pp. 149-159, Jan. 1992.

[63] D. Cabric and R. W. Brodersen, "Physical layer design issues unique to cognitive radio systems," *Proc. PIMRC*, pp. 759-763, Sep. 2005.

Chapter 2

Linear Precoding for Orthogonal Space-Time Block Coded MIMO-OFDM Cognitive Radio[1]

2.1 Introduction

The electromagnetic radio spectrum is a precious resource available for wireless communications, which demands efficient usage. However, it has become increasingly scarce due to a wide deployment of wireless services. According to the Federal Communications Commission's spectrum policy task report [1], the usage of allocated spectrum varies from fifteen to eighty-five percent at specific time and geographical location. This low spectrum utilization coupled with spectrum scarcity motivates the development of novel spectrum-sharing technologies with the aim of improving spectrum utilization. Cognitive radio (CR) has emerged as a promising technology to improve spectrum utilization, while accommodating the growing amount of services and applications in wireless communications [2, 3]. CR is capable of dynamically sensing and identifying unoccupied spectrum bands that are

[1] A version of this chapter has been accepted for publication. Punchihewa, A. Bhargava V. K. and Despins, C. "Linear Precoding for Orthogonal Space-Time Block Coded MIMO-OFDM Cognitive Radio," IEEE Transaction on Communications.

initially allocated to licensed (primary) users (PUs), and allowing unlicensed (secondary) users (SUs) to communicate through these available spectrum segments without causing harmful interference to PUs, thus having the potential to efficiently improve spectrum utilization. Since CR operates with opportunistic spectrum sharing in dynamically changing environments, managing the quality of services (QoS) offered by a CR system while maintaining the QoS of the PUs, is challenging. Hence, proper design of a transmission scheme for CR to facilitate high data rate access and better performance along with high spectral efficiency is very important. To achieve this objective, it is crucial to integrate recent physical layer technical advances into the CR systems.

Multiple-input multiple-output (MIMO) antenna systems and space-time block coding (STBC) in wireless communications have attached considerable attention due to their ability to increase capacity and improve system performance over hostile wireless channels [4–7]. Orthogonal frequency division multiplexing (OFDM) is a promising transmission technique in CR systems due to its several advantages such as scalability, robustness against multipath fading, multiple access mechanisms, simplicity in channel equalization and coding [8–10]. Therefore, with these valuable features, incorporating MIMO, STBC and OFDM into CR would promise enhanced performance in terms of spectral efficiency, capacity and bit error rate over hostile wireless channels.

It is shown in previous studies that the performance of conventional MIMO systems is degraded in spatially correlated channels based on the available channel state information (CSI) at the transmitter [11–13]. However, efficient precoding techniques in combination with STBC can be used to further improve the system performance in such channel conditions, when the knowledge of CSI is available at the transmitter [14–19]. Therefore, linear precoding is a vital technique to combat the correlation effect of MIMO channels. In prac-

tice a perfect CSI is seldom available and is difficult to obtain at the transmitter. Thus, a common practice is to assume partial channel knowledge at the transmitter, for example, in terms of transmit or both transmit and receive correlation matrices [14–19]. In conventional MIMO systems [14–19], the linear precoder is designed with the knowledge of transmit or both transmit and receive correlation matrices at the transmitter by minimizing a metric related to average error probability and constrained only to total transmit power.

Although this topic has been extensively studied for conventional MIMO systems, less attention is given in previous studies for design of a linear precoder for MIMO-based CR, where additional constraints need to be incorporated in precoder design. The linear precoder designed in [20] for CR with the intention of improving the error rate performance assumes only the SU transmit antenna correlation, single antenna at the PU receiver and considers the single carrier transmission scheme. However, this work extends the linear precoder design for CR in several ways. The theoretical analysis of the linear precoder design is based on a comprehensive signal model that takes into account of multiple antennas at both SU and PUs, multi-carrier transmission scheme and the correlation effects of SU's both transmit and receive antennas. A linear precoder is designed for orthogonal space-time block coded (OSTBC) MIMO-OFDM based CR, when operating in frequency-flat correlated Rayleigh fading channels. The linear precoder is designed to minimize an upper bound on the average pairwise error probability (PEP) when the SU transmitter has the knowledge of transmit and receive correlation matrices, while imposing a set of interference power constraints at the PUs and a set of per subcarrier transmit power constraints at the SU transmitter. It is shown that the precoder design problem for CR is convex with these constraints. Furthermore, an efficient algorithm based on the Lagrange dual-decomposition is proposed to obtain the linear precoder. The individual effects of the SU transmit and re-

ceive antenna correlation on the linear precoder design for CR is also addressed in this work. A closed-form solutions for power loading in each OFDM subcarrier for simplified correlation scenarios are also presented.

The rest of the Chapter is organized as follows. The system model and OSTBC MIMO-OFDM transmission scheme are introduced in Section 2.2. The optimal linear precoder design problem is formulated in Section 2.3. The linear precoder design with SU's different correlation scenarios are investigated in Section 2.4, and the Lagrangian dual-decomposition-based efficient algorithm is proposed to obtain the linear precoder. Simulation results are provided in Section 2.5. Finally, conclusions are drawn in Section 2.6. Proofs of the theorems are given in the Appendix A.

The following notations are used throughout this Chapter. Vectors are denoted by boldfaced lowercase letters, e.g., **a**, **b**, and matrices are denoted by boldface uppercase letters, e.g., **A**, **B**. The superscripts $(\cdot)^{-1}$, $(\cdot)^T$, $(\cdot)^\dagger$, and $(\cdot)^{1/2}$ stand for inverse, transpose, conjugate transpose, and square root, respectively. $Tr\{\cdot\}$ is the trace of a square matrix, $\det[\cdot]$ is the determinant of a matrix, $E\{\cdot\}$ is the expectation operation, $\text{vec}(\cdot)$ is the vectorization operation, $\|\cdot\|_F$ is the Frobenius norm of a matrix and $\otimes$ is the Kronecker product. $\mathbf{I}_n$ is the $n \times n$ identity matrix and $\mathbf{A} \succeq 0$ indicates that the square matrix **A** is positive semi-definite.

2.2 System Model

2.2.1 System Description

A CR network as illustrated in Fig. 2.1 is considered, where a single pair of SU transmitter and receiver coexist with the L PUs' receivers. We assume that PUs and SU share the same bandwidth. The SU pair are equipped with M_{st} and M_{sr} transmit and receive antennas,

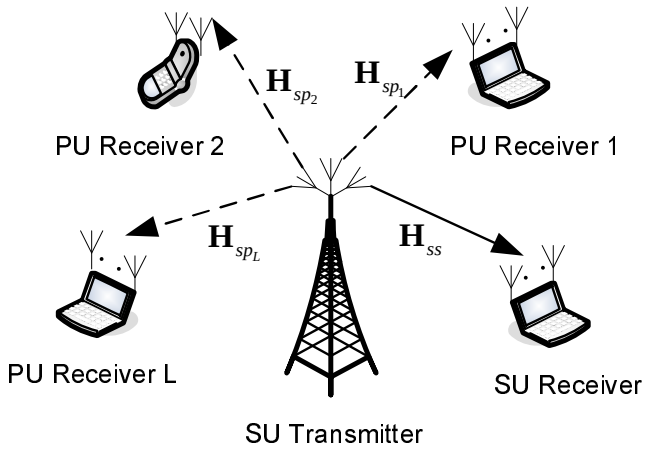

Figure 2.1: A cognitive radio network.

respectively, while the PUs have M_{pr} receive antennas each. The SU transmitter employs K subcarriers to modulate the signal using OFDM. Furthermore, we assume that only the transmit and receive correlation matrices for the MIMO channels, between the SU transmitter and PU receivers, and between the SU transmitter and SU receiver, are available at the SU transmitter. These matrices are obtained at the SU transmitter by periodically sensing the transmitted signals from the PU and SU receivers. In addition, perfect CSI is assumed at the SU receiver.

2.2.2 Correlated Channel Model

Quasi-static frequency-flat correlated Rayleigh MIMO channels between the SU transmitter and PU receivers, and between the SU transmitter and SU receiver are considered. Under the assumption of SU transmit and SU, PUs' receive scattering radii are large compared to the distance between the SU transmitter and SU, PUs receivers, the MIMO channels between the SU transmitter and SU receiver and between the SU transmitter and PU receivers

for the kth subcarrier can be respectively written as [21]

$$\mathbf{H}_{ss}(k) = \mathbf{R}_{rx,ss}^{1/2}(k)\mathbf{H}_{w,ss}(k)\mathbf{R}_{tx,ss}^{1/2}(k),\ k = 1, \ldots, K, \tag{2.1}$$

and

$$\mathbf{H}_{sp_l}(k) = \mathbf{R}_{rx,sp_l}^{1/2}(k)\mathbf{H}_{w,sp_l}(k)\mathbf{R}_{tx,sp_l}^{1/2}(k),\ k = 1, \ldots, K,\ l = 1, \ldots, L, \tag{2.2}$$

where $\mathbf{R}_{tx,ss}(k)$, $\mathbf{R}_{rx,ss}(k)$ are the transmit and receive correlation matrices of sizes $M_{st} \times M_{st}$ and $M_{sr} \times M_{sr}$, respectively, for the MIMO channels between SU transmitter and SU receiver; and $\mathbf{R}_{tx,sp_l}(k)$, $\mathbf{R}_{rx,sp_l}(k)$, are the transmit and receive correlation matrices of sizes $M_{st} \times M_{st}$ and $M_{pr} \times M_{pr}$, respectively, for the MIMO channels between SU transmitter and PU receivers. $\mathbf{H}_{w,ss}(k)$ and $\mathbf{H}_{w,sp_l}(k)$ are matrices of sizes $M_{sr} \times M_{st}$ and $M_{pr} \times M_{st}$, respectively, with independent and identically distributed (i.i.d.) zero-mean circular symmetric complex Gaussian (CSCG) entries with unit variance. The transmit and receive correlation matrices for the MIMO channels between the SU transmitter and SU receiver, and between the SU transmitter and PU receivers can be respectively written as [21]

$$\begin{aligned} \mathbf{R}_{tx,i}(k) &= \mathbf{R}_{tx,i}^{1/2}(k)^{\dagger}\mathbf{R}_{tx,i}^{1/2}(k), \\ &= E\left\{\mathbf{H}_i(k)^{\dagger}\mathbf{H}_i(k)\right\},\ i = \{ss, sp_l\},\ k = 1, \ldots, K,\ l = 1, \ldots, L, \end{aligned} \tag{2.3}$$

and

$$\begin{aligned} \mathbf{R}_{rx,i}(k) &= \mathbf{R}_{rx,i}^{1/2}(k)\mathbf{R}_{rx,i}^{1/2}(k)^{\dagger}, \\ &= E\left\{\mathbf{H}_i(k)\mathbf{H}_i(k)^{\dagger}\right\},\ i = \{ss, sp_l\},\ k = 1, \ldots, K,\ l = 1, \ldots, L. \end{aligned} \tag{2.4}$$

The full autocorrelation matrices, $\mathbf{R}_{ss}(k)$ and $\mathbf{R}_{sp_l}(k)$, can be obtained in terms of the Kronecker product of the transmit and receive correlation matrices:

$$\mathbf{R}_{ss}(k) = \mathbf{R}_{tx,ss}(k)^T \otimes \mathbf{R}_{rx,ss}(k),\ k = 1, \ldots, K, \tag{2.5}$$

$$\mathbf{R}_{sp_l}(k) = \mathbf{R}_{tx,sp_l}(k)^T \otimes \mathbf{R}_{rx,sp_l}(k),\ k = 1, \ldots, K,\ l = 1, \ldots, L. \tag{2.6}$$

By applying the vectorization operation to the equations (2.1) and (2.2), we have $\text{vec}\left(\mathbf{H}_{ss}(k)\right) = \mathbf{R}_{ss}^{1/2}(k)\text{vec}\left(\mathbf{H}_{w,ss}(k)\right)$, and $\text{vec}(\mathbf{H}_{sp_l}(k)) = \mathbf{R}_{sp_l}^{1/2}(k)\text{vec}(\mathbf{H}_{w,sp_l}(k))$, respectively. This Kronecker model has been widely exploited in the previous studies for correlated MIMO systems [17–19, 22, 23].

2.2.3 Transmission Scheme

A block diagram of the proposed OSTBC MIMO-OFDM based CR transmission scheme with linear precoding is shown in Fig. 2.2. The SU transmitter includes an OSTBC encoder and a linear precoder followed by an OFDM modulator. At the SU transmitter, the input symbols are first serial to parallel (S/P) converted and fed into the OSTBC encoder. Secondly, the output symbols of the OSTBC encoder are multiplied by $M_{st} \times M_{st}$ precoder matrices $\mathbf{F}(k),\ k = 1, \ldots, K$. Third, the precoded data to be transmitted by each transmitting antenna are subjected to typical OFDM transmit processing, such as S/P conversion, inverse fast Fourier transform operation, parallel to serial (P/S) conversion and the addition of a cyclic prefix (CP). Fourth, the precoded data are transmitted over the wireless MIMO channel. Then at the SU receiver, the received signal in each antenna is subjected to typical OFDM processing such as removal of CP, S/P conversion, fast Fourier transform operation and P/S conversion. Finally, the maximum likelihood (ML) detector recovers the received

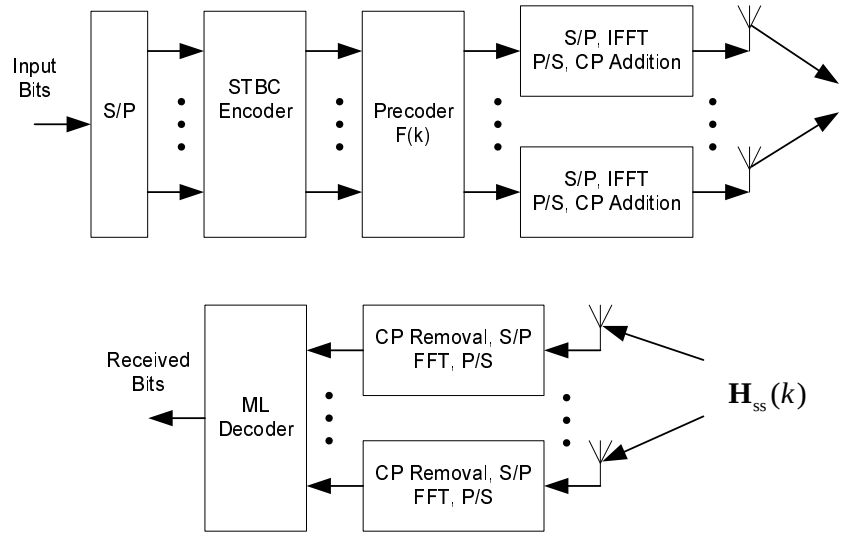

Figure 2.2: System block diagram of the precoded OSTBC MIMO-OFDM based CR transmission scheme.

data symbols.

For this system, the received signal at the SU receiver for the kth subcarrier can be written as

$$\mathbf{Y}_{ss}(k) = \mathbf{H}_{ss}(k)\mathbf{F}(k)\tilde{\mathbf{C}}(k) + \mathbf{N}(k),\ k = 1, \ldots, K, \tag{2.7}$$

where $\tilde{\mathbf{C}}(k)$ is the transmitted OSTBC matrix of size $M_{st} \times T_{\text{ofdm}}$, with T_{ofdm} as the total OFDM symbols transmitted in a block of data. Individual data symbols of $\tilde{\mathbf{C}}(k)$ are drawn from a finite complex signal constellation with unit energy. $\mathbf{N}(k)$[2] is the complex additive white Gaussian noise matrix of size $M_{rt} \times T_{\text{ofdm}}$ with zero-mean and variance $\sigma_n^2\mathbf{I}_{M_{sr}}$. In addition, the same noise statistics are assumed for all subcarriers.

Under the assumption of perfect CSI at the SU receiver, the ML decoding of codeword

[2]Note that the noise at the SU receiver also contains the interference from the PU transmitters in the network and therefore non-white in general. By applying the noise-whitening filter at the SU receiver and incorporating the filter effects into MIMO channel matrix between the SU transmitter and SU receiver, the effective noise is assumed to be approximately white Gaussian.

C from the received signal matrices $\mathbf{Y}_{ss}(k),\ k = 1, \ldots, K$, yields

$$\mathbf{C} = \arg\min_{\mathbf{C}\in\mathcal{C}} \sum_{k=1}^{K} \left\| \mathbf{Y}_{ss}(k) - \mathbf{H}_{ss}(k)\mathbf{F}(k)\tilde{\mathbf{C}}(k) \right\|_F^2 . \tag{2.8}$$

2.3 Optimal Linear Precoder Design Problem Formulation

The main objective is to find a set of linear precoder matrices $\mathbf{F}(k),\ k = 1, \ldots, K$, at the SU transmitter, so as to minimize an upper bound on the average PEP under a set of per subcarrier power constraints at the SU transmitter and a set of PUs' interference power thresholds. Upper bounds on the average PEP have been extensively exploited as design criterions of the linear precoder in conventional MIMO systems [14–19]. In our framework, an upper bound on the average PEP is also adopted as a design criteria, but for OSTBC MIMO-OFDM based CR transmission scheme. The PEP, $P(\mathbf{C}_i \rightarrow \mathbf{C}_j)$ is the probability that ML decoding decides in favour of the codeword $\mathbf{C}_j$ instead of the actually transmitted codeword $\mathbf{C}_i$.

Theorem 2.1: An upper bound of the average PEP of the OSTBC MIMO-OFDM, when SU's transmit and receive antennas are correlated, can be written as:

$$P(\mathbf{C}_i \rightarrow \mathbf{C}_j) \leq \prod_{k=1}^{K} \prod_{j=1}^{M_{sr}} \left\{ \det \left[\mathbf{I}_{M_{st}} + \eta \lambda_{rx,ss}(k)_j \tilde{\mathbf{F}}(k) \mathbf{\Lambda}_{tx,ss}(k) \right] \right\}^{-1}, \tag{2.9}$$

where η is a factor that depends on the codeword pair $\mathbf{C}_i$ and $\mathbf{C}_j$, $\lambda_{rx,ss}(k)_j$ is the jth eigenvalue of the receive eigenvalue matrix $\mathbf{\Lambda}_{rx,ss}(k)$, $\tilde{\mathbf{F}}(k) = \mathbf{F}(k)\mathbf{F}(k)^{\dagger}$, and $\mathbf{\Lambda}_{tx,ss}(k)$ is the transmit eigenvalue matrix of the transmit correlation matrix $\mathbf{R}_{tx,ss}(k)$.

Proof. See the Appendix A. □

In CR networks, CR users may coexist with PUs either on a non-interfering basis or on an interference tolerance basis [24]. Therefore, one fundamental challenge of the CR is to maintain the QoS of the PUs while maximizing the SU's performance. Since PUs have a higher priority than the SUs while opportunistically sharing the spectrum in an interference tolerance basis, SUs have to maintain interference introduced to the PUs by SUs below a certain threshold, known as the interference temperature constraint and defined by regulatory bodies. Therefore, the QoS of the PUs in the CR network is maintained by introducing the additional interference power constraints, measured at the PUs' receivers [25, 26] into the precoder design problem for CR. In previous studies, two basic interference power constraints have been exploited to protect PUs transmission, i.e., peak interference power constraint and the average interference power constraints [24–27]. The peak interference power constrains are exploited when the channel is constant over a fixed-time slot or a fixed-frequency bin. On the other hand, in the average interference power constraints, the channel is assumed to be constant over a block of data transmission or a block of frequency band. A main drawback of peak interference power constraint is that the SU has to measure the instantaneous channels between the SUs and PUs perfectly each channel instant to predict the induced interference at PUs. This is difficult in practice since channels usually subject to space, time, and frequency variation due to multi-path propagation, shadowing and mobility. Therefore, in this thesis, we exploit the average interference power constraint to protect PUs transmission [24–27]. The average interference power measure is appropriate for delay-insensitive communications and has been extensively exploited in the previous studies to limit the interference from SU transmission to the PUs [24–27]. Following considers the average interference power introduced to the PU receivers by SU transmission.

The interference power introduced by SU transmission at the lth PU receiver, conditioned on the input signal constellation and the channel realization, can be written as

$$\mathcal{Q}_l\left(k|\tilde{\mathbf{C}}(k),\mathbf{H}(k)\right) = Tr\left\{\mathbf{H}_{sp_l}(k)\mathbf{F}(k)\tilde{\mathbf{C}}(k)\tilde{\mathbf{C}}(k)^{\dagger}\mathbf{F}(k)^{\dagger}\mathbf{H}_{sp_l}(k)^{\dagger}\right\}, \quad k=1,\ldots,K,\ l=1,\ldots,L. \tag{2.10}$$

Therefore, the total average interference power introduced by the SU transmission to each PU can be obtained under the assumption of independent channel realization for each subcarrier and by taking the expectation of (2.10) with respect to input signal and the channel realization as

$$\begin{aligned}\bar{\mathcal{Q}}_{tot,l} &= \sum_{k=1}^{K} Tr\left\{\mathbf{F}(k)E_{\mathbb{C}}\left\{\tilde{\mathbf{C}}(k)\tilde{\mathbf{C}}(k)^{\dagger}\right\}\mathbf{F}(k)^{\dagger}E_{\mathbb{H}}\left\{\mathbf{H}_{sp_l}(k)^{\dagger}\mathbf{H}_{sp_l}(k)\right\}\right\}, \\ &= \sum_{k=1}^{K} Tr\left\{\tilde{\mathbf{F}}(k)\mathbf{R}_{tx,sp_l}(k)\right\},\ l=1,\ldots,L,\end{aligned} \tag{2.11}$$

where the unit variant input signal constellation is assumed (i.e., $E_{\mathbb{C}}\{\tilde{\mathbf{C}}(k)\tilde{\mathbf{C}}(k)^{\dagger}\} = \mathbf{I}_{M_{st}}$).

In OFDM transmission schemes, the transmitted signal power should be limited to avoid generating strong interference to other active users and the systems, and to avoid requirement of linear amplifiers with large dynamic range. Furthermore, decreasing the transmit power will prolong the battery lifespan. Therefore, in this CR network per subcarrier power constraint is imposed at the SU transmitter. Under the assumption of unit variant constellation, the transmit power from the kth subcarrier can be written as

$$\mathrm{P}(k) = Tr\{\tilde{\mathbf{F}}(k)\},\ k=1,\ldots,K. \tag{2.12}$$

An upper bound on the average PEP of OSTBC is exploited to obtain a set of linear

precoder matrices $\mathbf{F}(k),\ k = 1, \ldots, K$ at the SU transmitter. By exploiting the property that the logarithmic function is monotonic increasing for nonnegative values, we can obtain the optimum linear precoder matrices $\mathbf{F}(k),\ k = 1, \ldots, K$, that minimize an upper bound on the average PEP by solving the following optimization problem (**P1**):

$$\underset{\tilde{\mathbf{F}}(k),\ k=1,\ldots,K}{\text{minimize}} \quad \sum_{k=1}^{K}\sum_{j=1}^{M_{sr}} -\log\det\left[\mathbf{I}_{M_{st}} + \eta\lambda_{rx,ss}(k)_j\tilde{\mathbf{F}}(k)\mathbf{\Lambda}_{tx,ss}(k)\right], \tag{2.13}$$

$$\text{subject to} \quad \sum_{k=1}^{K} Tr\left\{\tilde{\mathbf{F}}(k)\mathbf{R}_{tx,sp_l}(k)\right\} \leq \mathrm{I}_{int,l},\ l = 1, \ldots, L, \tag{2.14}$$

$$Tr\left\{\tilde{\mathbf{F}}(k)\right\} \leq \mathrm{P}_{tot}(k),\ k = 1, \ldots, K, \tag{2.15}$$

$$\tilde{\mathbf{F}}(k) \succeq 0,\ k = 1, \ldots, K, \tag{2.16}$$

where $\mathrm{I}_{int,l}$ is the interference power threshold specified by the lth PU and $\mathrm{P}_{tot}(k)$ is the transmit power available for the kth subcarrier at the SU transmitter. Equations (2.14) and (2.15) represent the average interference power constraint over all receive antennas for lth PU receiver and the per subcarrier transmit power constraint at the SU transmitter, respectively. The third constraint implies that the matrices $\tilde{\mathbf{F}}(k),\ k = 1, \ldots, K$, should be positive semi-definite. Note that this linear precoder design problem is different from the precoder design for conventional systems due to the additional interference power constraints in (2.14). Therefore, the precoder obtained by standard multi-level water-filling is not optimal for this problem. Based on the convexity of the optimization problem **P1** and the structure of the optimal precoder, the following theorem and the lemma can be stated.

Theorem 2.2: The linear precoder design problem **P1** is convex with constraints (2.14)-(2.16).

Proof. See the Appendix A. □

Lemma 2.1: If $\mathbf{F}(k), k = 1, \ldots, K$ is an optimal solution to the problem **P1**, then the linear precoder $\mathbf{F}(k)\mathbf{U}(k), k = 1, \ldots, K$, where $\mathbf{U}(k), k = 1, \ldots, K$ is a $M_{st} \times M_{st}$ unitary matrix is also optimal.

Proof. Since $\mathbf{U}(k), k = 1, \ldots, K$ is a unitary matrix and by insertion of $\mathbf{F}(k)\mathbf{U}(k)$, $k = 1, \ldots, K$, into the objective function (2.13) and the constraints (2.14)-(2.16) remain unchanged. Therefore, $\mathbf{F}(k)\mathbf{U}(k), k = 1, \ldots, K$, is also an optimal solution to the problem **P1**. □

Since the optimization problem **P1** is convex, standard numerical optimization techniques, e.g., the interior-point method [28] can be employed to obtain the optimal linear precoder. The details of this method are omitted for brevity. However, to get more insight into the system performance, Lagrange dual-decomposition-based algorithm is proposed in the next section to obtain the set of linear precoder matrices.

2.4 Precoder Designs for CR in Correlated MIMO Channel

Standard convex optimization techniques are exploited to derive efficient algorithms to obtain the optimal precoder matrices for SU's different transmit and receive correlation scenarios. This section will present the solution to the precoder design problem **P1** using eigen-beamforming. It is shown in the previous studies that eigen-beamforming is optimal for error rate minimization [29]. In eigen-beamforming, the linear precoder $\mathbf{F}(k)$ functions as a multi-mode beamformer based on the knowledge of the transmit and receive correlation matrices of the MIMO channels between the SU transmitter and SU receiver

and between the SU transmitter and PU receivers. The optimal precoder $\mathbf{F}(k)$ has its orthogonal beams directions with the left eigenvectors of the SU's transmit correlation matrix $\mathbf{R}_{tx,ss}(k)$, and the power loading across the beams as the square values of the eigenvalues of the matrix $\tilde{\mathbf{F}}(k)$. Thus, by taking eigenvalue decomposition of $\tilde{\mathbf{F}}(k) = \mathbf{U}_{\tilde{\mathbf{F}}}(k)\Lambda_{\tilde{\mathbf{F}}}(k)\mathbf{U}_{\tilde{\mathbf{F}}}(k)^{\dagger}$, choosing optimal eigen beam directions to be $\mathbf{U}_{\tilde{\mathbf{F}}}(k) = \mathbf{U}_{tx,ss}(k)$, and using the properties of eigenvalue, the optimization problem (**P2**) in eigen-beamforming can be rewritten as

$$\underset{\{\boldsymbol{\lambda}_{\tilde{\mathbf{F}}}(k)\}}{\text{minimize}} \quad \sum_{k=1}^{K}\sum_{i=1}^{M_{st}}\sum_{j=1}^{M_{sr}} -\log\left(1+\eta\lambda_{rx,ss}(k)_j\lambda_{tx,ss}(k)_i\boldsymbol{\lambda}_{\tilde{\mathbf{F}}}(k)_i\right), \tag{2.17}$$

$$\text{subject to} \quad \sum_{k=1}^{K}\sum_{i=1}^{M_{st}}\left(\boldsymbol{\lambda}_{\tilde{\mathbf{F}}}(k)_i\mathbf{u}_{tx,ss}(k)_i^{\dagger}\mathbf{R}_{tx,sp_l}(k)\mathbf{u}_{tx,ss}(k)_i\right) \leq \mathrm{I}_{int,l}, \quad l=1,\ldots,L, \tag{2.18}$$

$$\sum_{i=1}^{M_{st}}\boldsymbol{\lambda}_{\tilde{\mathbf{F}}}(k)_i \leq \mathrm{P}_{tot}(k),\ k=1,\ldots,K, \tag{2.19}$$

$$\boldsymbol{\lambda}_{\tilde{\mathbf{F}}}(k)_i \geqslant 0,\ i=1,\ldots,M_{st},\ k=1,\ldots,K, \tag{2.20}$$

where $\lambda_{tx,ss}(k)_i$, $\boldsymbol{\lambda}_{\tilde{\mathbf{F}}}(k)_i$ are the ith eigenvalues of $\boldsymbol{\Lambda}_{tx,ss}(k)$ and $\boldsymbol{\Lambda}_{\tilde{\mathbf{F}}}(k)$, respectively; and $\mathbf{u}_{tx,ss}(k)_i$ is the ith eigenvector of the $\mathbf{U}_{tx,ss}(k)$. Next, the Lagrange dual-decomposition method is applied to obtain the optimal power allocation across each antenna and for each subcarrier in different SU's transmit and receive antenna correlation scenarios. In previous studies, the Lagrangian dual-decomposition method has been extensively exploited for resource allocation in communication systems [30–32].

2.4.1 Precoder Design With the SU's Both Transmit and Receive Correlation

The general scenario, considering both SU transmit and receive antenna correlation is presented. This is the common situation encountered in the uplink of a communication link, where a multi-antenna access point is located high above the multi-antenna subscriber transmit units. Since the access point is installed at a high location, the receive antennas are having a small spread of angle of arrival due to the less scatters around it. Therefore, causing a high receive antenna correlation at the receive side. In the case of multi-antenna subscriber transmit unit, the possible causes of transmit correlation are lack of spacing between antennas, antenna arrangement and the antenna configurations. It can be noticed from the optimization problem **P2** that the SU's transmit and receive antenna correlations have different effects on the linear precoder design for CR. Particularly, the objective function in (2.17) depends on the SU's both transmit and receive correlation matrices $\mathbf{R}_{tx,ss}(k)$ and $\mathbf{R}_{rx,ss}(k)$ through the eigenvalues $\lambda_{tx,ss}(k)_i$, and $\lambda_{rx,ss}(k)_j$, respectively. Furthermore, the interference power constraint depends on the transmit correlation matrices $\mathbf{R}_{tx,sp_l}(k)$.

The Lagrange dual-decomposition method is applied here to obtain the optimal values of the $\boldsymbol{\lambda}_{\tilde{\mathbf{F}}}(k)_i$. The optimal power allocation policy for the kth subcarrier and the optimal precoder matrix, $\mathbf{F}_{opt}(k)$, can be obtained according to the following theorem.

Theorem 2.4: The optimal power allocation for the ith transmit antenna and for the kth subcarrier, $\boldsymbol{\lambda}^*_{\tilde{\mathbf{F}}}(k)^+_i$, $i = 1, \ldots, M_{st}$, with $x^+ = \max\{0, x\}$ can be obtained by solving the following set of equations:

$$\sum_{j=1}^{M_{sr}} \frac{\eta\lambda_{rx,ss}(k)_j}{\left(\lambda_{tx,ss}(k)_i^{-1} + \eta\lambda_{rx,ss}(k)_j \boldsymbol{\lambda}^*_{\tilde{\mathbf{F}}}(k)_i\right)} = \mu_k + \sum_{l=1}^{L} \nu_l \left(\mathbf{u}_{tx,ss}(k)_i^{\dagger} \mathbf{R}_{tx,sp_l}(k) \mathbf{u}_{tx,ss}(k)_i\right), \quad i = 1, \ldots, M_{st}, \qquad (2.21)$$

where μ_k and ν_l are the non-negative Lagrange multipliers associated with per subcarrier power constraint and the interference power constraint, respectively. Therefore, the optimum linear precoder matrix $\mathbf{F}_{opt}(k)$ for the kth subcarrier can be obtained as $\mathbf{F}_{opt}(k) = \mathbf{U}_{tx,ss}(k)\Lambda^*_{\tilde{\mathbf{F}}}(k)$.

Proof. See the Appendix A. □

It can be noticed from equation (2.21) that for this scenario, the optimal power loading across the ith transmit antenna and for kth subcarrier depends on the eigenvalues of the SU's transmit and receive correlation matrices, eigenvectors of the SU's transmit correlation matrix and the transmit correlation matrices of the MIMO channels between the SU transmitter and the PU receivers. Furthermore, the interference power introduced at the PU receivers are controlled by ν_l and μ_k, which are calculated based on the constraints (2.18) and (2.19).

Normally, the cross-correlation between pairs of antennas is much smaller than one and, as a result for a well behaved receive correlation matrix, the values of $\lambda_{rx,ss}(k)_j$ are close to each other and can be approximated as $\bar{\lambda}_{rx,ss}(k)_j = M_{sr}^{-1} Tr\{\mathbf{\Lambda}_{rx,ss}(k)\}$. In this scenario, the optimal solution $\bar{\boldsymbol{\lambda}}^*_{\tilde{\mathbf{F}}}(k)_i^+$, $i = 1, \ldots, M_{st}$, for the kth subcarrier can be obtained from the following closed-form solution

$$\bar{\boldsymbol{\lambda}}^{*}_{\tilde{\mathbf{F}}}(k)_i = \left(M_{sr} \left(\mu_k + \sum_{l=1}^{L} \nu_l \left(\mathbf{u}_{tx,ss}(k)_i^{\dagger} \mathbf{R}_{tx,sp_l}(k) \mathbf{u}_{tx,ss}(k)_i \right) \right)^{-1} - M_{sr} \left(\eta Tr\{\boldsymbol{\Lambda}_{rx,ss}(k)\} \right)^{-1} \right)^{+}, \; i = 1, \ldots, M_{st}. \tag{2.22}$$

To summarize, the complete algorithm for precoder design with both transmit and receive correlation is given below.

Algorithm 1 Computation of optimal precoder matrix

1: Given $\mathcal{E}_{\boldsymbol{\nu}}^{(0)}$, $\mathcal{E}_{\boldsymbol{\mu}}^{(0)}$, initial ellipsoids centered at $\boldsymbol{\nu}^{(0)}$, $\boldsymbol{\mu}^{(0)}$, which contain the optimal dual solutions $\boldsymbol{\nu}^{*}$ and $\boldsymbol{\mu}^{*}$, respectively.
2: Set $t = 0$.
3: **repeat**
4: For each subcarrier $k = 1, \ldots, K$ obtain the optimal power allocation $\boldsymbol{\lambda}^{*}_{\tilde{\mathbf{F}}}(k)_i$, $i = 1, \ldots, M_{st}$ by solving (2.21).
5: Update $\mathcal{E}_{\boldsymbol{\nu}}^{(t+1)}$, $\mathcal{E}_{\boldsymbol{\mu}}^{(t+1)}$ using $\mathcal{E}_{\boldsymbol{\nu}}^{(t)}$, $\mathcal{E}_{\boldsymbol{\mu}}^{(t)}$ and the sub-gradients of $\nu_l^{(t)}$, $l = 1, \ldots, L$, and $\mu_k^{(t)}$, $k = 1, \ldots, K$, respectively [33].
6: Set $\boldsymbol{\nu}^{(t+1)}$ and $\boldsymbol{\mu}^{(t+1)}$ as the centers of new ellipsoids $\mathcal{E}_{\boldsymbol{\nu}}^{(t+1)}$ and $\mathcal{E}_{\boldsymbol{\mu}}^{(t+1)}$, respectively.
7: Set $t \leftarrow t + 1$.
8: **until** the stopping criteria of the ellipsoid method is satisfied [33].

Note that the solution derived for the linear precoder problem in this paper is for a general scenario. The solution for conventional MIMO systems can be straightforwardly obtained by simply setting the Lagrange multipliers corresponding to average interference power constraints to zero (i.e., $\boldsymbol{\nu} = \mathbf{0}$). Furthermore, the linear precoder design for the single carrier systems in a CR system can be obtained with $K = 1$. In addition, in the case of a single PU, there is only one Lagrange multiplier ν for the interference power constraint. In such a scenario, this *Algorithm 1* can be further simplified and the ν can be updated by the bisection method [28].

2.4.2 Precoder Design with Only the SU Transmit Correlation

The linear precoder design considering only the SU transmit antenna correlation is presented in this Subsection. In practice, this situation is encountered in a downlink of a communication system when the multi-antenna subscriber units have sufficient antenna spacing between them. In this scenario, the multi-antenna base station is situated high above the ground in a low scattering environment and thus, results a high transmit antenna correlation. The multi-antenna subscriber unit is situated in rich scattering environment and with sufficient spacing between antennas, thus no receive antenna correlation. For this scenario, the SU receive correlation matrix is equivalent to the identity matrix, i.e., $\mathbf{R}_{rx,ss}(k) = \mathbf{I}_{M_{sr}}$, or equivalently $\mathbf{\Lambda}_{rx,ss}(k) = \mathbf{I}_{M_{sr}}$. Therefore, using the properties of the determinant, the Kronecker product, and applying some mathematical manipulations to **P1**, the optimization problem (**P4**) in eigen-beamforming for this scenario can be written as

$$\begin{aligned} &\underset{\{\boldsymbol{\lambda}_{\tilde{\mathbf{F}}}(k)\}}{\text{minimize}} && \sum_{k=1}^{K}\sum_{i=1}^{M_{st}} -\log\left(1+\eta\lambda_{tx,ss}(k)_i\boldsymbol{\lambda}_{\tilde{\mathbf{F}}}(k)_i\right), \\ &\text{subject to} && (2.18),\ (2.19),\ \text{and}\ (2.20). \end{aligned} \tag{2.23}$$

It can be seen that the problem **P4** has a similar structure as problem **P2**. Therefore, the Lagrange dual-decomposition method can be exploited to solve problem **P4** and derive an efficient algorithm to obtain the optimal precoder matrices $\mathbf{F}(k)$ for $k = 1, \ldots, K$. A similar analysis can be performed as described in Section 2.4.1. However, the analysis is presented to obtain the optimal precoder matrix for a OFDM subcarrier as described in sub problem **P3**, in order to obtain the dual function $\mathcal{G}(\boldsymbol{\nu}, \boldsymbol{\mu})$, for given $\boldsymbol{\nu}$ and $\boldsymbol{\mu}$. Therefore, sub problem **P5** for the kth OFDM subcarrier can be written as

$$\begin{aligned} \underset{\boldsymbol{\lambda}_{\tilde{\mathbf{F}}}(k)_i,\ i=1,\ldots,M_{st}}{\text{minimize}} \quad & \sum_{i=1}^{M_{st}} -\log\left(1+\eta\lambda_{tx,ss}(k)_i\boldsymbol{\lambda}_{\tilde{\mathbf{F}}}(k)_i\right)+\mu_k\sum_{i=1}^{M_{st}}\boldsymbol{\lambda}_{\tilde{\mathbf{F}}}(k)_i \\ & +\sum_{l=1}^{L}\nu_l\left(\sum_{i=1}^{M_{st}}\left(\boldsymbol{\lambda}_{\tilde{\mathbf{F}}}(k)_i\mathbf{u}_{tx,ss}(k)_i^{\dagger}\mathbf{R}_{tx,sp_l}(k)\mathbf{u}_{tx,ss}(k)_i\right)\right), \\ \text{subject to} \quad & \boldsymbol{\lambda}_{\tilde{\mathbf{F}}}(k)_i\geq 0,\ i=1,\ldots,M_{st}. \end{aligned} \tag{2.24}$$

The optimal power allocation, $\boldsymbol{\lambda}^*_{\tilde{\mathbf{F}}}(k)_i,\ i=1,\ldots,M_{st}$, for this scenario can be obtained as in the sub problem **P3**, by applying the KKT condition for the convex sub problem **P5**. Therefore, the optimal power allocation, $\boldsymbol{\lambda}^*_{\tilde{\mathbf{F}}}(k)_i$, $i=1,\ldots,M_{st}$, for the kth subcarrier with no receive correlation is given by the following closed-form water-filling like solution for given $\boldsymbol{\nu}$ and $\boldsymbol{\mu}$:

$$\boldsymbol{\lambda}^*_{\tilde{\mathbf{F}}}(k)_i=\left(\left(\mu_k+\sum_{l=1}^{L}\nu_l\left(\mathbf{u}_{tx,ss}(k)_i^{\dagger}\mathbf{R}_{tx,sp_l}(k)\mathbf{u}_{tx,ss}(k)_i\right)\right)^{-1}-\left(\eta\lambda_{tx,ss}(k)_i\right)^{-1}\right)^{+}, \quad i=1,\ldots,M_{st}. \tag{2.25}$$

Algorithm 1 proposed in Section 2.4.1 to obtain the precoder matrices $\mathbf{F}(k)$ for $k=1,\ldots,K$ now needs to be slightly modified for this scenario. In Step 4, the optimal solution $\boldsymbol{\lambda}^*_{\tilde{\mathbf{F}}}(k)_i$, $i=1,\ldots,M_{st}$, for each OFDM subcarrier $k=1,\ldots,K$, can now be obtained by (2.25). Therefore, the main advantage of this method in multicarrier transmission scheme is that the same computational routine can be simultaneously applied to all K subcarriers in order to obtain the optimal $\mathbf{F}(k)$'s. Thus, the overall computational time will be maintained regardless of the number of subcarriers K. This is a significant advantage in CR networks since the number of subcarriers is dynamically assigned and the overall computational time

of the linear precoder design algorithm will remain approximately the same as the single carrier systems. Furthermore, for this scenario the convergence time of the overall algorithm is further improved due to the closed-form solution on $\boldsymbol{\lambda}^{*}_{\tilde{\mathbf{F}}}(k)_i$, $i = 1, \ldots, M_{st}$ in (2.25).

2.4.3 Precoder Design with Only the SU Receive Correlation

In this Subsection, the linear precoder design considering the SU receive correlation and no SU transmit correlation is explored. This situation is encountered in an uplink of a communication system when the multi-antenna subscriber units are located in a rich scattering environment with sufficient antenna spacing. There are two possible cases involving the receive-side correlation, i.e., either $\mathbf{R}_{tx,ss}(k) = \mathbf{I}_{M_{st}}$ or $\mathbf{R}_{tx,ss}(k) = \mathbf{R}_{tx,sp_l}(k) = \mathbf{I}_{M_{st}}$, $l = 1, \ldots, L$. The latter is considered to be the case when only the SU's receive-side correlation is considered, with no transmit side correlation. The former case is considered first. For this scenario, $\mathbf{R}_{tx,ss}(k) = \mathbf{I}_{M_{st}}$, or equivalently $\boldsymbol{\Lambda}_{tx,ss}(k) = \mathbf{I}_{M_{st}}$. Therefore, using the properties of the determinant, the Kronecker product, and some trivial calculations to problem **P1**, the optimization problem (**P6**) in eigen-beamforming for this scenario can be written as

$$\begin{aligned} \underset{\{\boldsymbol{\lambda}_{\tilde{\mathbf{F}}}(k)\}}{\text{minimize}} \quad & \sum_{k=1}^{K} \sum_{i=1}^{M_{st}} \sum_{j=1}^{M_{sr}} -\log\left(1 + \eta \lambda_{rx,ss}(k)_j \boldsymbol{\lambda}_{\tilde{\mathbf{F}}}(k)_i\right), \\ \text{subject to} \quad & (2.18),\ (2.19),\ \text{and}\ (2.20). \end{aligned} \tag{2.26}$$

It is apparent from problem **P6** that it has a similar structure to problems **P2** and **P4**. Therefore, as previously discussed, the Lagrange dual-decomposition method can also be exploited for this scenario, to solve and derive an efficient algorithm to obtain the precoder

matrices $\mathbf{F}(k)$, $k = 1, \ldots, K$. However, only the procedure to obtain the precoder matrix $\mathbf{F}(k)$ for a OFDM subcarrier, similar to the sub problem **P3**, is explored here in order to obtain the dual function $\mathcal{G}(\boldsymbol{\nu}, \boldsymbol{\mu})$, for given $\boldsymbol{\nu}$ and $\boldsymbol{\mu}$. Therefore, the sub problem (**P7**) for the kth subcarrier in this scenario can be written as

$$\begin{aligned} \underset{\boldsymbol{\lambda}_{\tilde{\mathbf{F}}}(k)_i,\ i=1,\ldots,M_{st}}{\text{minimize}} \quad & \sum_{i=1}^{M_{st}} \sum_{j=1}^{M_{sr}} -\log\left(1+\eta\lambda_{rx,ss}(k)_j \boldsymbol{\lambda}_{\tilde{\mathbf{F}}}(k)_i\right) + \mu_k \sum_{i=1}^{M_{st}} \boldsymbol{\lambda}_{\tilde{\mathbf{F}}}(k)_i \\ & + \sum_{l=1}^{L} \nu_l \left(\sum_{i=1}^{M_{st}} \left(\boldsymbol{\lambda}_{\tilde{\mathbf{F}}}(k)_i \mathbf{u}_{tx,ss}(k)_i^{\dagger} \mathbf{R}_{tx,sp_l}(k) \mathbf{u}_{tx,ss}(k)_i \right) \right), \\ \text{subject to} \quad & \boldsymbol{\lambda}_{\tilde{\mathbf{F}}}(k)_i \geq 0,\ i = 1, \ldots, M_{st}. \end{aligned} \tag{2.27}$$

Applying the Lagrangian multiplier method to sub problem **P7**, one can find the optimal $\boldsymbol{\lambda}^*_{\tilde{\mathbf{F}}}(k)_i,\ i = 1, \ldots, M_{st}$ for the kth subcarrier by solving the following system of equations:

$$\sum_{j=1}^{M_{sr}} \eta\lambda_{rx,ss}(k)_j \left(1+\eta\lambda_{rx,ss}(k)_j \boldsymbol{\lambda}^*_{\tilde{\mathbf{F}}}(k)_i\right)^{-1} = \mu_k + \sum_{l=1}^{L} \nu_l \left(\mathbf{u}_{tx,ss}(k)_i^{\dagger} \mathbf{R}_{tx,sp_l}(k) \mathbf{u}_{tx,ss}(k)_i \right), \quad i = 1, \ldots, M_{st}. \tag{2.28}$$

Similarly, the optimal $\boldsymbol{\lambda}^*_{\tilde{\mathbf{F}}}(k)_i,\ i = 1, \ldots, M_{st}$ for the kth subcarrier for the latter case where, $\mathbf{R}_{tx,ss}(k) = \mathbf{R}_{tx,sp_l}(k) = \mathbf{I}_{M_{st}}$, $l = 1, \ldots, L$, can be obtained by solving the following system of equations:

$$\sum_{j=1}^{M_{sr}} \eta\lambda_{rx,ss}(k)_j \left(1+\eta\lambda_{rx,ss}(k)_j \boldsymbol{\lambda}^*_{\tilde{\mathbf{F}}}(k)_i\right)^{-1} = \mu_k + \sum_{l=1}^{L} \nu_l,\ i = 1, \ldots, M_{st}. \tag{2.29}$$

It can be noticed from the Equations (2.28) and (2.29) that the optimal matrix $\Lambda_{\tilde{\mathbf{F}}}(k)$ for the kth subcarrier has equal diagonal elements $\boldsymbol{\lambda}^*_{\tilde{\mathbf{F}}}(k)_i$, $i = 1, \ldots, M_{st}$ for given $\boldsymbol{\nu}$ and $\boldsymbol{\mu}$. Since this is the uncorrelated scenario and as CSI is not available at the SU transmitter, an equal diagonal precoder is expected. The algorithm proposed in Section 2.4.1, to obtain the precoder matrices $\mathbf{F}(k)$, $k = 1, \ldots, K$ now needs to be modified for these scenarios. Step 4 of *Algorithm 1* can now be obtained by (2.28) and (2.29), for the cases $\mathbf{R}_{tx,ss}(k) = \mathbf{I}_{M_{st}}$ and $\mathbf{R}_{tx,ss}(k) = \mathbf{R}_{tx,sp_l}(k) = \mathbf{I}_{M_{st}}$, $l = 1, \ldots, L$, respectively.

2.5 Numerical Results

In this section, numerical results are presented to illustrate the performance of the proposed linear precoder in an OSTBC MIMO-OFDM based CR system. Throughout the simulations, the bit error rate (BER) is used as the performance measure.

In all the simulations, quasi-static frequency-flat correlated Rayleigh fading MIMO channels and zero-mean uncorrelated CSCG noise with unit variance are assumed. The elements of the MIMO channel matrices $\mathbf{H}_{w,ss}(k)$ and $\mathbf{H}_{w,sp_1}(k)$, for $k = 1, \ldots, K$, are generated as i.i.d. samples of CSCG distribution with zero-mean and unit variance. Furthermore, it is assumed that the transmit and receive antennas form linear arrays for both SUs and PUs. The correlation coefficient between the mth and the nth transmit antennas for the kth subcarrier with a small angle spread can be approximately obtained as [11]:

$$
\begin{aligned}
[\mathbf{R}_{tx,i}(k)]_{m,n} &\approx \sigma^2_{tx,i} \int_0^{2\pi} \exp^{-j2\pi|m-n| \sin \Delta_{tx,i}(k) d_{tx,i} \lambda_s^{-1} \sin\phi} \, d\phi, \\
&= \sigma^2_{tx,i} J_0(2\pi|m-n| \sin \Delta_{tx,i}(k) d_{tx,i} \lambda_s^{-1}), \\
&\qquad\qquad i = \{ss, sp_l\},\ k = 1, \ldots, K,\ l = 1, \ldots, L.
\end{aligned}
$$

Here, $J_0(\cdot)$ is the zeroth-order Bessel function of the first kind, $\Delta_{tx,i}(k)$ is the transmit angle spread for the kth subcarrier, $d_{tx,i}$ is the spacing between the transmit antennas, λ_s is the wavelength of the carrier and $\sigma^2_{tx,i}$ is the transmit antenna array power gain. The $\Delta_{tx,i}(k), i = \{ss, sp_l\}$, for each subcarrier is generated from a uniform distribution in the range $[\bar{\Delta}_{tx,i} - \Delta/2, \bar{\Delta}_{tx,i} + \Delta/2]$ with $\bar{\Delta}_{tx,i}, i = \{ss, sp_l\}$ as the mean transmit angle spread and $\Delta = 6^0$. The receive correlation matrices $\mathbf{R}_{rx,ss}(k)$ and $\mathbf{R}_{rx,sp_l}(k)$, $k = 1, \ldots, K,\ l = 1, \ldots, L$ are also obtained similarly as the transmit correlation matrices. Furthermore, antennas at transmitter and receiver are assumed to be uniformly spaced with half wavelength distance between them for both SUs and PUs. Two PUs are assumed to be present in the system. The number of subcarriers is set to 16. The number of receive antennas for both PUs and SU are either set to 1 and 2. The transmit power varies to obtain the average signal to noise ratio (SNR) presented. The PU receiver interference temperature power threshold is set to 0.1 [20]. A similar or larger interference threshold values have been exploited in previous studies to protect PUs in CR networks [20, 34–37]. With this setup, the distances between the CR transmitter and the nearest PU receiver are two and ten meters for indoor and outdoor environment, respectively [37]. Therefore, the PUs which are beyond these ranges are protected by this interference threshold value [37]. Binary phase shift keying symbols are generated with unit variant signal constellation for signal transmission. The Alamouti code was exploited as the OSTBC for the SU transmission [7]. Simulation results are obtained by averaging 1000 trials, with each block consisting of 10000 OSTBC OFDM symbols. Finally, the SNR is defined as the signal power to noise power at the SU receiver.

The average BER of the CR system is plotted versus SNR in Fig. 2.3 for proposed precoded system and with non-precoded system. In order to have a fair compression, the trans-

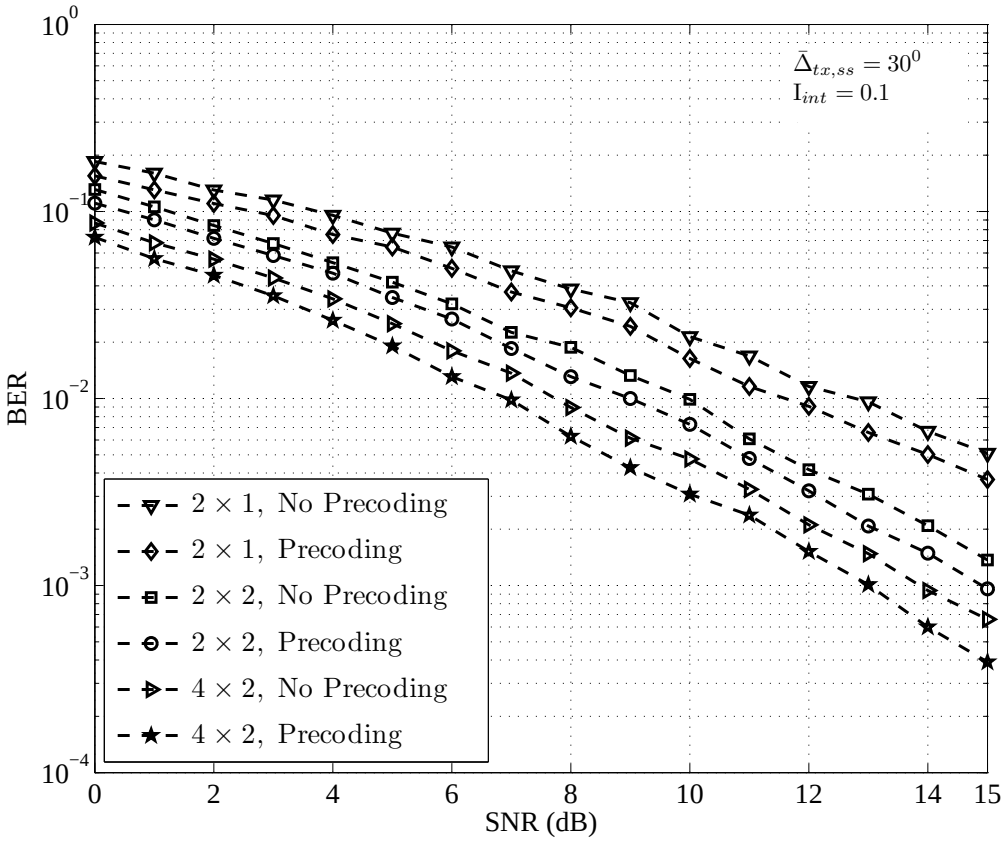

Figure 2.3: The average BER versus SNR for the CR transmission scheme with and without precoding.

mit power is uniformly loaded in non-precoding such that the interference power constraint satisfied. In this scenario, the transmit power from the ith transmit antenna is obtained by $\boldsymbol{\lambda}_{\tilde{\mathbf{F}},\mathrm{u}}(k)_i = \mathrm{I}_{int,l} M_{st}^{-1} \left(\mathbf{u}_{tx,ss}(k)_i^{\dagger} \mathbf{R}_{tx,spl}(k) \mathbf{u}_{tx,ss}(k)_i \right)$, $i = 1, \ldots, M_{st}$, $k = 1, \ldots, K$. This will ensure in uniform power loading that the total interference introduced is below the prescribed threshold value. The BER results are presented for 2×1, 2×2 and 4×2 SU antenna configurations with a 0.1 interference power threshold. From the plots, it can be seen that the proposed precoder in CR outperforms the non-precoding scheme. The precoding gain

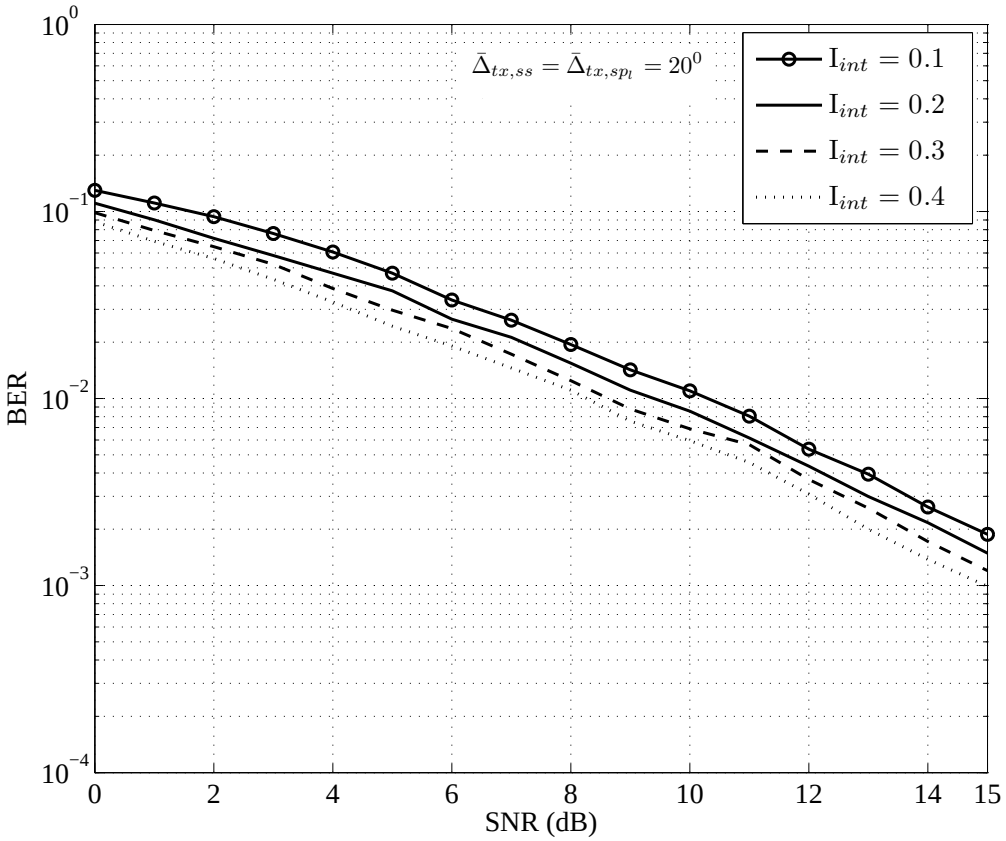

Figure 2.4: The BER performance of the precoded OSTBC MIMO-OFDM based CR transmission scheme with different interference power thresholds.

is around 1.2 dB for the presented SNR range. Similar performance results are achieved for all three antenna configurations. Furthermore, it is noticed that significant improvement in performance by adding more antennas to the SU receiver with the same interference power constraint. Thus, employing multiple antennas at the CR transmitter and receiver, system error performance can be improved significantly for a fixed interference power threshold.

In Fig. 2.4, the average BER is plotted against SNR for the 2×2 CR system with different interference power thresholds. As expected, BER performance improvement can be

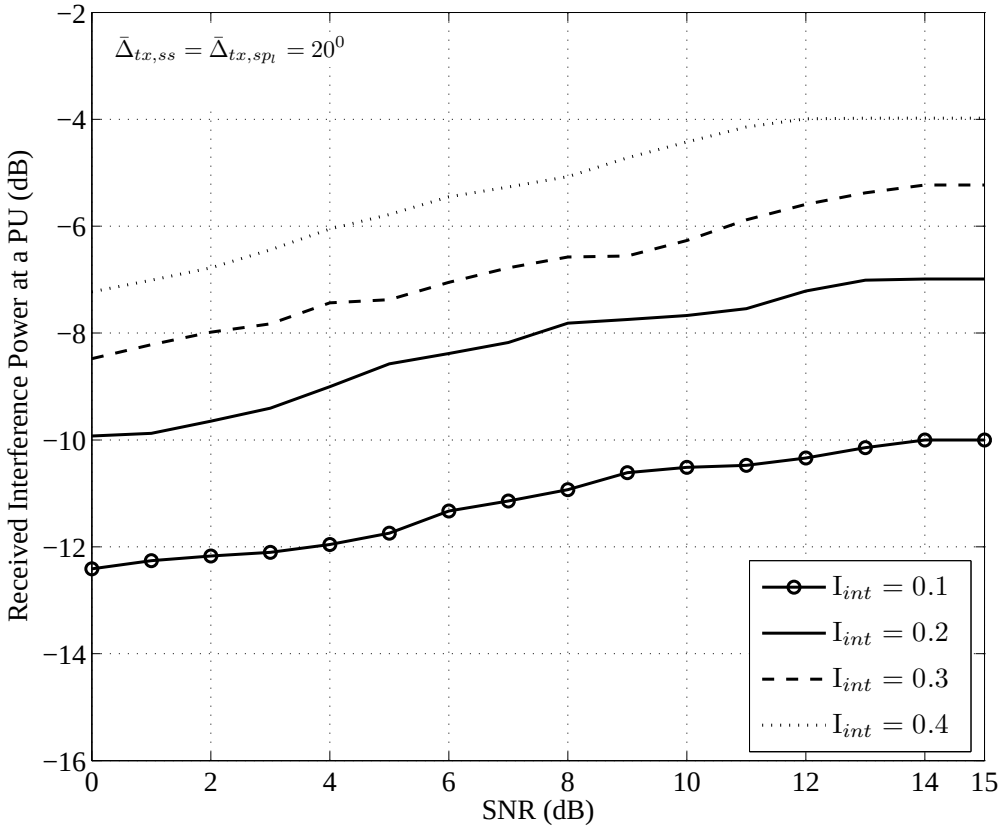

Figure 2.5: The average received interference power versus SNR for different interference power thresholds.

seen with increased interference power thresholds. The increase of the interference power limit allows the CR transmitter to allocate higher power to the precoder matrices. However, interference power cannot be increased significantly, since it could increase an unacceptable interference receive at the PU receivers. In Fig. 2.5, the average received interference power at a PU receiver is plotted against the SNR for different interference power thresholds. It is apparent from Fig. 2.5 that as the interference power threshold increases the amount of received interference also increases. In addition, it can be seen from Fig. 2.5

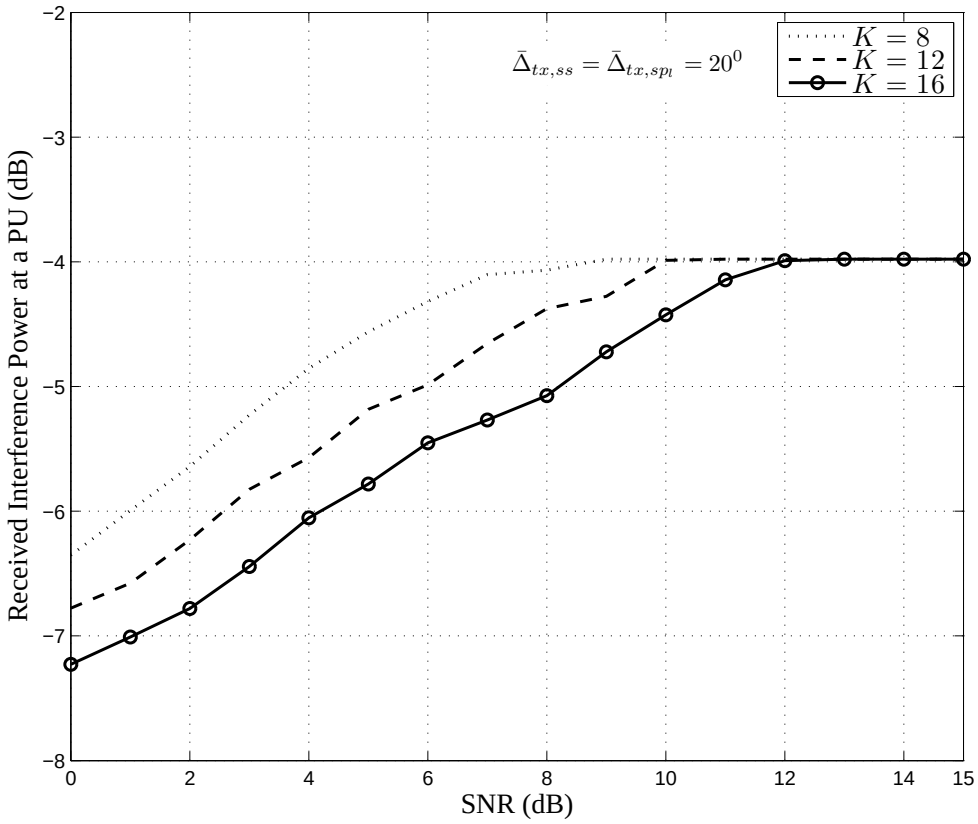

Figure 2.6: The average received interference power versus SNR for different number of subcarriers.

that for all the cases, the received interference power at the PU is below or equal to the respective interference power thresholds, thus allowing CR and PU to coexist in the same frequency band.

The average received interference power at a PU receiver is plotted against SNR for different number of subcarriers. From Fig. 2.6 it is apparent that for all the subcarriers the received interference power at the PU remain below or equal to the interference power threshold. Furthermore, as the number of subcarriers increases, the received interference

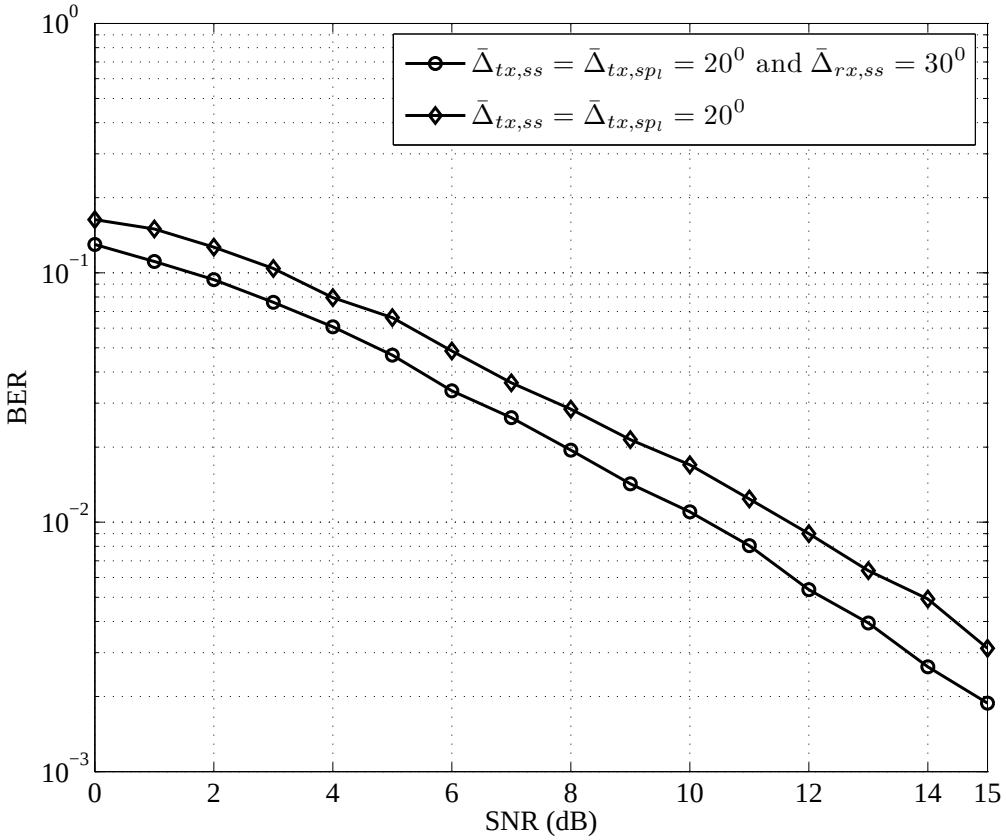

Figure 2.7: The average BER performance of a CR system for SU's transmit correlation and both transmit and receive correlation scenarios.

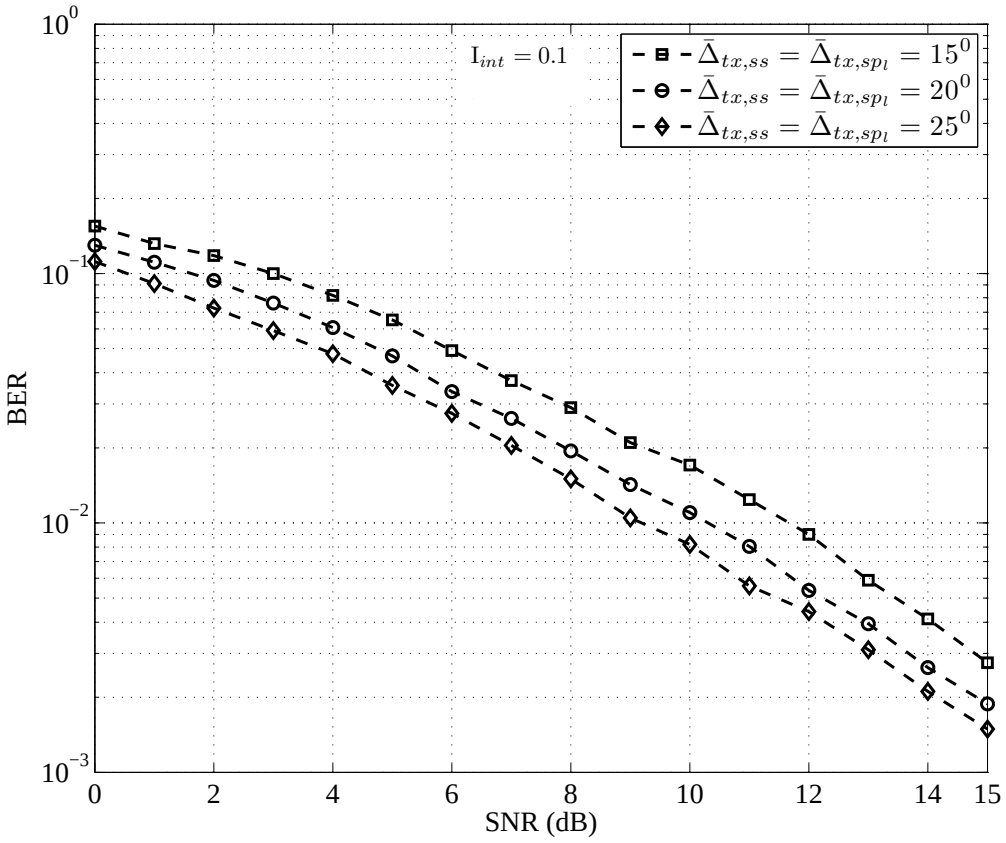

Figure 2.8: The average BER versus SNR of the precoded OSTBC MIMO-OFDM based CR transmission scheme with different $\bar{\Delta}_{tx,ss}$.

power at the PU receiver reach the interference power threshold at a higher SNR value. In Fig. 2.7, the average BER is plotted against SNR for a 2×2 CR system for SU transmit and receive correlations, and for only SU transmit correlation, at a 0.1 interference power threshold. Comparing the plots in Fig. 2.7 clearly shows that the precoding gain decreases due to SU receive antenna correlation. Fig. 2.8 depicts the average BER versus SNR for a 2×2 CR system with different $\bar{\Delta}_{tx,ss}$ for a 0.1 interference power threshold. As expected, BER performance improves significantly with decreased $\bar{\Delta}_{tx,ss}$ at higher SNR regimes.

2.6 Conclusion

This Chapter presents a design of a linear precoder for orthogonal space-time block coded orthogonal frequency division multiplexing-based multiple-input multiple-output (MIMO) antenna cognitive radio (CR). The CR coexists with the primary user (PU) network by opportunistically sharing the originally allocated PU spectrum in correlated Rayleigh fading channels. The optimum linear precoder with respect to error probability performance is obtained by exploiting the partial channel information in the form of transmit and receive correlation matrices at the CR transmitter and by minimizing an upper bound on the average pairwise error probability, while imposing a set of per subcarrier transmit power constraints at the CR transmitter and a set of interference power constraints specified by the PUs. We have shown that the precoder design problem with these constraints is convex and have proposed a Lagrange dual-decomposition-based efficient algorithm to obtain the optimal precoders. Furthermore, the individual effects of the transmit and/or receive correlation on the linear precoder design for CR were investigated. The current study further reveals that for uncorrelated CR transmit antennas, the precoder consists of equally

weighted diagonal elements. Simulation results illustrate that the proposed linear precoder outperforms uniform power loaded systems in a correlated MIMO channel even with the presence of additional interference power constraints.

Bibliography

[1] Federal Communication Commission, *Spectrum Policy Task Force*, ET Docket No. 02-155, Nov. 2002.

[2] J. Mitola III, "Cognitive radio for flexible mobile multimedia communications," *Proc. IEEE Int. Work. MoMuC*, pp. 3-10, Nov. 1999.

[3] S. Haykin, "Cognitive radio: Brain-empowered wireless communications," *IEEE J. Sel. Areas Commun.*, vol. 23, no. 2, pp. 201-220, Feb. 2005.

[4] E. Telatar, *Capacity of Multi-antenna Gaussian Channels*, AT and T Bell Labs Tech. Memo., Mar. 1995.

[5] V. Tarokh, H. Jafarkhani, and A. R. Calderbank, "Space-time block coding for wireless communications: Performance results," *IEEE J. Sel. Areas Commun.*, vol. 17, no. 3, pp. 451-460, Mar. 1999.

[6] V. Tarokh, H. Jafarkhani, and A. R. Calderbank, "Space-time block codes from orthogonal designs," *IEEE Trans. Inf. Theory*, vol. 45, no. 5, pp. 1456-1467, Jul. 1999.

[7] S. M. Alamouti, "A simple transmit diversity technique for wireless communications," *IEEE J. Sel. Areas Commun.*, vol. 16, no. 8, pp. 1451-1458, Oct. 1998.

[8] T. Weiss and F. K. Jondral, "Spectrum pooling: An innovative strategy for the enhancement of spectrum efficiency," *IEEE Commun. Mag.*, vol. 43, no. 3, pp. S8-S14, Mar. 2004.

[9] J. A. C. Bingham, "Multicarrier modulation for data transmission: An idea whose time has come," *IEEE Commun. Mag.*, vol. 28, no. 5, pp. 5-14, May 1990.

[10] R. V. Nee and R. Prasad, *OFDM Wireless Multimedia Communications*, Artech House, 2000.

[11] D. Shiu, J. G. Foschini, M. Gans, and J. M. Kahn, "Fading correlation and its effect on the capacity of multi-element antenna systems," *IEEE Trans. Commun.*, vol. 48, no. 3, pp. 201-220, Mar. 2000.

[12] H. Bolcskei and A. J. Paultry, "Performance of space-time codes in the presence of spatial fading correlation," *Proc. IEEE ASILOMAR*, pp. 687-693, Oct. 2000.

[13] E. Bjornson, B. Ottersten, and E. Jorswieck, "On the impact of spatial correlation and precoder design on the performance of MIMO systems with space-time coding," *Proc. ICASSP*, pp. 2741-2744, Apr. 2009.

[14] H. Sampath and A. Paultry, "Linear precoding for space-time coded systems with known fading correlations," *IEEE Commun. Letters*, vol. 6, no. 6, pp. 239-241, Jun. 2002.

[15] Y. Zeng and A. R. Leyman, "Linear precoding for MIMO STC-OFDM and blind channel estimation," *Proc. IEEE APCCAS*, pp. 127-130, Dec. 2006.

[16] Y. Zhao, R. Adve, and T. J. Lim, "Precoding of orthogonal STBC with channel covariance feedback for minimum error probability," *Proc. IEEE PIMRC*, pp. 503-507, Sep. 2004.

[17] H. R. Bahrami and L. N. Tho, "Precoder design based on correlation matrices for MIMO system," *IEEE Trans. Wireless Commun.*, vol. 5, no. 12, pp. 3579-3587, Dec. 2006.

[18] A. Hjorungnes and D. Gesbert, "Precoding of orthogonal space-time block codes in arbitrarily correlated MIMO channels: Iterative and closed-form solutions," *IEEE Trans. Wireless Commun.*, vol. 6, no. 3, pp. 1072-1082, Mar. 2007.

[19] A. Hjorungnes, D. Gesbert, and J. Akthar, "Precoding of space-time block coded signals for joint transmit-receive correlated MIMO channels," *IEEE Trans. Wireless Commun.*, vol. 5, no. 3, pp. 492-497, Mar. 2006.

[20] Md. H. Islam and Y. C. Liang, "Space-time coding in MIMO cognitive networks with known channel correlations," *Proc. IEEE EuWiT*, pp. 97-102, Oct. 2008.

[21] A. Paultry, R. Nabar, and D. Gore, *Introduction to Space-Time Wireless Communications*, 2nd. ed. Cambridge University Press, 2003.

[22] K. Yu, M. Bengtsson, B. Ottersten, D. McNamara, P. Karlsson, and M. Beach, "Modeling of wide-band MIMO radio channels based on NLoS indoor measurements," *IEEE Trans. Veh. Technol.*, vol. 53, no. 3, pp. 655-665, May 2004.

[23] R. Stridh, K. Yu, B. Ottersten, and P. Karlsson, "MIMO channel capacity and modeling issues on a measured indoor radio channel at 5.8 GHz," *IEEE Trans. Wireless Commun.*, vol. 4, no. 3, pp. 895-903, May 2005.

[24] X. Hong, C. X. Wang, H. H. Chen, and J. Thompson, "Performance analysis of cognitive radio networks with average interference power constraints," *Proc. IEEE ICC*, pp. 3578-3582, May. 2008.

[25] G. Bansal, Md. J. Hossain, and V. K. Bhargava, "Optimal and suboptimal power allocation schemes for OFDM-based cognitive radio systems," *IEEE Trans. Wireless Commun.*, vol. 7, no. 11, pp. 4710-4718, Nov. 2008.

[26] W. Wei, P. Tao, and W. Wenbo, "Optimal Power control under interference temperature constraint in cognitive radio network," *Proc. IEEE WCNC*, pp. 116-120, Mar. 2007.

[27] R. Zhang, Y. C. Liang, and S. Cui, "Dynamic resource allocation in cognitive radio networks: A convex optimization perspective," *To appear in IEEE Sig. Proc. Magazine*.

[28] S. Boyd and L. Vandenberg, *Convex Optimization*, Cambridge University Press, 2004.

[29] D. P. Palomar, *A Unified Framework for Communications through MIMO Channels*, PhD Thesis, May 2003.

[30] W. Yu, "A dual decomposition approach to the sum power Gaussian vector multiple access channel sum capacity problem," *Proc. CISS*, pp. 116-120, Mar. 2003.

[31] M. Codreanu, M. Juntti, and M. Latva-Aho, "On the dual-decomposition-based sum capacity maximization for vector broadcast channels," *IEEE Trans. Veh. Technol.*, vol. 56, no. 6, pp. 3577-3581, Nov. 2007.

[32] D. P. Palomar M. Chiang, "A tutorial on decomposition methods for network utility maximization," *IEEE J. Sel. Areas Commun.*, vol. 24, no. 8, pp. 1439-1451, Aug. 2006.

[33] R. G. Bland, D. Goldfarb, and M. J. Todd, "The ellipsoid method: A survey," *Operations Research*, vol. 29, no. 6, pp. 1039-1091, 1981.

[34] X. Kang, A. Nallanathan, Y. C. Liang, H. K. Garg and R. Zhang, "Optimal power allocation for fading channels in cognitive radio networks: Ergodic capacity and outage capacity," *IEEE Trans. Wireless Commun.*, vol. 8, no. 2, pp. 940-950, Feb. 2009.

[35] R. Zhang and Y. C. Liang, "Exploiting multi-antennas for opportunistic spectrum sharing in cognitive radio networks," *IEEE J. Sel. Topics Signal Proc.*, vol. 2, no. 1, pp. 88-102, Feb. 2008.

[36] X. Kang, Y. C. Liang and A. Nallanathan, "Optimal power allocation for fading channels in cognitive radio networks under transmit and interference power constraints," *Proc. IEEE ICC*, pp. 3568-3572, May 2008.

[37] X. Hong, C-X. Wang, and H-H. Chen and J. Thompson, "Performance analysis of cognitive radio networks with average interference power constraints," *Proc. IEEE ICC*, pp. 3578-3582, May. 2008.

[38] J. G. Proakis, *Digital Communications*, 4th. ed. McGraw-Hill, 2000.

[39] A. Graham, *Kronecker Products and Matrix Calculus With Applications*, Ellis Horwood Ltd., 1981.

[40] R. A. Horn and C. A Johnson, *Matrix Analysis*, 1st. ed. Cambridge University Press, 1985.

Chapter 3

Capacity and Power Allocation for Opportunistic Spectrum Sharing MAC with Imperfect Channel Estimation[3]

3.1 Introduction

Cognitive radio (CR) has emerged as a promising technology to improve the spectrum utilization, while supporting the increasing amount of services and applications in wireless communications [1, 2]. In CR environment, CR (secondary) users (SUs) opportunistically share the licensed (primary) users (PUs) spectrum without causing interference to the PUs. Therefore, CR has the potential to improve spectral utilization efficiently. In practice, CR may coexist with the PUs either on a non-interfering basis or an interference tolerance basis [3]. In CR networks, PUs are given higher priority than the SUs while opportunistically sharing the spectrum. Therefore, the quality of services (QoS) of active PUs in CR network is maintained by introducing an additional interference power constraint into the resource allocation problem [4]. This constraint allows SU transmitters to maintain the interference

[3] A version of this chapter has been submitted for publication. Punchihewa, A. Bhargava V. K. and Despins, C. "Capacity and Power Allocation for Opportunistic Spectrum Sharing MAC with Imperfect Channel Estimation," submitted for publication.

introduced to the active PUs by the SUs below a certain limit defined by regulatory bodies.

Since CR operates in dynamically changing environments with opportunistic spectrum sharing, it is necessary to optimally allocate CR's transmit power to maximize throughput while minimizing the resultant performance degradation of the active PUs in the network. In previous studies [5–11], power allocation policies are presented for single- and multi-antenna CR to obtain the point-to-point CR channel capacity under the interference power constraints. By considering the similar setup, [12] and [13] have studied the ergodic sum capacity of cognitive multiple access channel (MAC) and broadcast channels. However, all these previous studies [5–13], have assumed perfect channel state information (CSI) is available for the channels between the SU transmitters and the SU receivers and channels between the SU transmitters and the PU receivers. Nevertheless, in practice these CSI is often imperfect and the SUs performance and the interference introduced to the PUs highly depend on the accuracy of the CSI.

In recent studies, a power allocation policy is presented in [14] to achieve the ergodic capacity of a single user CR considering only the imperfect CSI for the channel between a SU transmitter and a PU receiver. However, CR network is naturally a multiuser communication environment and therefore, it is necessary to consider design of a power allocation policy between multiple SUs in a CR network incorporating the channel estimation errors. In this Chapter, we propose an optimal power allocation policy for opportunistic spectrum sharing single-input single-output (SISO) MAC to achieve a lover-bound on the ergodic sum capacity considering channel estimation errors for both set of channels between the SU transmitters and the SU receiver and the channels between the SU transmitters and the PU receivers. Furthermore, convex optimization techniques are exploited to derive an efficient algorithm to obtain the power allocation for each SU transmitter under these channel

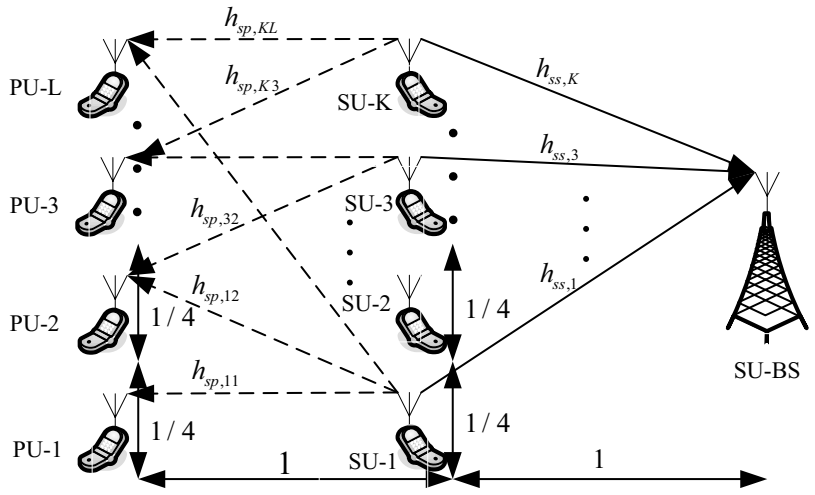

Figure 3.1: An opportunistic spectrum sharing SISO MAC.

estimation errors. Numerical results are also presented to illustrate the effect of channel estimation errors on the performance of SISO MAC.

The rest of the Chapter is organized as follows: The system model and the sum capacity optimization problem formulation is presented in Sections 3.2 and 3.3, respectively. A Lagrange dual-decomposition based efficient algorithm is proposed in Section 3.4, to obtain the power allocation policy for each SU transmitter. Simulation results are discussed in Section 3.5. Finally, conclusions are drawn in Section 3.6. Derivations of theorems are presented in the Appendix B.

3.2 System and Channel Models

An opportunistic spectrum sharing SISO MAC as shown in Fig. 3.1 is considered, where K SU transmitters, SU base station (BS) and L PU receivers share the same spectrum

band. Furthermore, physical locations[4] of the each SU transmitter, BS and the PU receiver is depicted in Fig. 3.1, where the numbers above and the besides the arrows represent the normalized distance between users. At discrete-time instant n, K SUs transmits to the BS, thus the resulting received signal at BS can be written as

$$y(n) = \sum_{k=1}^{K} \alpha_{ss,k}(n) s_{ss,k}(n) + w_{ss}(n), \tag{3.1}$$

where, $s_{ss,k}(n)$ is the transmitted data symbol from the kth SU transmitter, $\alpha_{ss,k}(n)$ is the complex channel coefficient between the kth SU transmitter and the SU receiver and $w_{ss}(n)$ is the additive white Gaussian noise at the SU receiver with zero-mean and variance σ_w^2. The complex channel coefficient between the kth SU transmitter and the lth PU receiver is represented as $\alpha_{sp,kl}(n)$, $l = 1 \ldots, L$. Furthermore, flat-fading channel gains and noise are assumed to be independent. The complex channel coefficients $\alpha_{ss,k}(n)$, $\alpha_{sp,kl}(n)$, $k = 1, \ldots, K$, $l = 1, \ldots, L$ are assumed to be independent and identically distributed (i.i.d.) zero-mean circular symmetric complex Gaussian (CSCG) random variables with variance $1/(1+d)^{\beta}$, where d is the normalized distance between transmitter and receiver and β is the path exponent. From here onwards the discrete time index n is omitted as it is clear from the context.

It is assumed that the BS and each SU transmitter perform the minimum mean square error (MMSE) estimation of the channels $\alpha_{ss,k}(n)$ and $\alpha_{sp,kl}(n)$. Under the MMSE estimation, the channel estimation errors for the channel between the SU transmitter and the BS and the channel between the SU transmitters and the PU receivers can be respectively written as [15]

[4]Note that the theoretical analysis do not depend on the physical location of SUs, BS or PUs. Physical locations will be exploited only for the simulation purposes.

$$\Delta\alpha_{ss,k} = \alpha_{ss,k} - \hat{\alpha}_{ss,k},\ k = 1, \ldots, K, \tag{3.2}$$

$$\Delta\alpha_{sp,kl} = \alpha_{sp,kl} - \hat{\alpha}_{sp,kl},\ k = 1, \ldots, K,\ l = 1, \ldots, L, \tag{3.3}$$

where $\hat{\alpha}_{ss,k}$ and $\hat{\alpha}_{sp,kl}$ are the MMSE estimation of the channels $\alpha_{ss,k}$ and $\alpha_{sp,kl}$, respectively. It is clear from the MMSE estimation that the channel estimation errors ($\Delta\alpha_{ss,k}$, $\Delta\alpha_{sp,kl}$) and channel estimates ($\hat{\alpha}_{ss,k}$, $\hat{\alpha}_{sp,kl}$) are uncorrelated. Furthermore, the estimation errors $\Delta\alpha_{ss,k}$ and $\Delta\alpha_{sp,kl}$ are distributed as zero-mean CSCG with variances $\sigma^2_{ss,k}$ and $\sigma^2_{sp,kl}$, respectively. Hereafter, the fading channel power gains are represented by $h_{ss,k} = |\alpha_{ss,k}|^2$, $\hat{h}_{ss,k} = |\hat{\alpha}_{ss,k}|^2$, $h_{sp,kl} = |\alpha_{sp,kl}|^2$, $\hat{h}_{sp,kl} = |\hat{\alpha}_{sp,kl}|^2$ and the channel power gain estimation errors are represented by $\Delta h_{ss,k} = |\Delta\alpha_{ss,k}|^2$ and $\Delta h_{sp,kl} = |\Delta\alpha_{sp,kl}|^2$.

3.3 Problem Formulation

The main objective is to derive an optimal transmit power allocation policy for each SU transmitter so as to maximize a lower-bound on the ergodic sum capacity of the opportunistic spectrum sharing SISO MAC subject to a set of SUs transmit power constraints and a set of PUs interference power constraints when channel estimation errors are present for the channels between the SU transmitters and the SU receiver and the channels between the SU transmitters and the PU receivers. Towards this objective, the average received power at each PU receiver by the SUs transmission is first examined. The received interference power measure is an important metric in an opportunistic spectrum sharing. In CR network, the QoS of the PUs is maintained by introducing this interference power constraints. The average received signal power at the lth PU can be obtained as

$$q_l^{av} = \mathcal{E}_{\mathcal{H}}\left\{\sum_{k=1}^{K} p_k(\mathcal{H})(\hat{h}_{sp,kl} + \Delta h_{sp,kl})|\tilde{s}_{ss,k}|^2\right\},\ l = 1, \ldots, L, \tag{3.4}$$

where $s_{ss,k} = \sqrt{p_k(\mathcal{H})}\tilde{s}_{ss,k}$ is exploited, $\mathcal{H} = \Big\{\hat{h}_{ss,1}, \ldots, \hat{h}_{ss,K}, \Delta h_{ss,1}, \ldots, \Delta h_{ss,K}, \hat{h}_{sp,11}, \ldots, \hat{h}_{sp,KL}, \Delta h_{sp,11}, \ldots, \Delta h_{sp,KL}\Big\}$ is the set of channel power gains and the channel power gain errors for the nth time slot, $\mathcal{E}_{\mathcal{H}}\{\cdot\}$ is the expectation operation with respect to $\mathcal{H}$ and $p_k(\mathcal{H})$ is the channel estimation dependent transmit power of the kth SU transmitter. Under the assumption of independent channel gains for different users and the properties of MMSE estimation, an average received interference power at the lth PU can be rewritten as

$$q_l^{av} = \sum_{k=1}^{K} \mathcal{E}_{\mathcal{H}}\Big\{p_k(\mathcal{H})\hat{h}_{sp,kl}\Big\} + \sum_{k=1}^{K} p_k^{av}\sigma_{sp,kl}^2,\ l = 1, \ldots, L, \tag{3.5}$$

where p_k^{av} is the average transmit power of the kth SU transmitter. Furthermore, it is assumed that each SU transmitter is subject to its own transmit power constraint. Therefore, under the assumption of Gaussian codebook is used by each SU transmitter, the average transmit power at the kth SU transmission can be written as $p_{ss,k}^{tr} = \mathcal{E}_{\mathcal{H}}\{p_k(\mathcal{H})\},\ k = 1, \ldots, K$.

It should be noted that the exact ergodic capacity of SISO MAC under the channel estimation errors is in general unknown [16]. Therefore, focus will be given on a lower-bound of it [16]. The following theorem will be exploited in obtaining a lower-bound on the ergodic sum capacity of opportunistic spectrum sharing SISO MAC.

Theorem 3.1: A lower-bound on the mutual information of SISO MAC with channel estimation errors can be written as

$$I_{low}(s_{ss,1}, s_{ss,2}, \ldots, s_{ss,K}; y) = \mathcal{E}_{\mathcal{H}}\left\{\log\left(1 + \frac{\sum_{k=1}^{K} p_k(\mathcal{H})\hat{h}_{ss,k}}{\sum_{k=1}^{K} p_k(\mathcal{H})\sigma_{ss,k}^2 + \sigma_w^2}\right)\right\}. \tag{3.6}$$

Proof. See the Appendix B. □

Therefore, one can obtain a lower-bound on the ergodic sum capacity, ($\mathcal{C}_{MAC,lb}$), of K SU opportunistic spectrum sharing SISO MAC solving the optimization problem **P1**:

$$\underset{\mathbf{p}(\mathcal{H})}{\text{maximize}} \quad \mathcal{E}_{\mathcal{H}}\left\{\log\left(1+\frac{\hat{\mathbf{h}}_{ss}^{\dagger}\mathbf{p}(\mathcal{H})}{\sigma_w^2+\mathbf{e}_{ss}^{\dagger}\mathbf{p}(\mathcal{H})}\right)\right\}, \tag{3.7}$$

$$\text{subject to} \quad \mathcal{E}_{\mathcal{H}}\left\{\hat{\mathbf{h}}_{sp,l}^{\dagger}\mathbf{p}(\mathcal{H})\right\}+\mathbf{e}_{sp,l}^{\dagger}\mathbf{p}^{av} \leq \mathcal{Q}_l^{av},\ l=1,\ldots,L, \tag{3.8}$$

$$\mathcal{E}_{\mathcal{H}}\{\mathbf{p}(\mathcal{H})\} \leq \mathbf{p}^{av}, \tag{3.9}$$

$$\mathbf{p}(\mathcal{H}) \geq 0, \tag{3.10}$$

where $\mathbf{p}(\mathcal{H})=[p_1(\mathcal{H}),\ldots,p_K(\mathcal{H})]^{\dagger}$, $\hat{\mathbf{h}}_{ss}=[\hat{h}_{ss,1},\ldots,\hat{h}_{ss,K}]^{\dagger}$, $\hat{\mathbf{h}}_{sp,l}=[\hat{h}_{sp,1l},\ldots,\hat{h}_{sp,Kl}]^{\dagger}$, $\mathbf{p}^{av}=[p_1^{av},\ldots,p_K^{av}]^{\dagger}$, $\mathbf{e}_{ss}=[\sigma_{ss,1}^2,\ldots,\sigma_{ss,K}^2]^{\dagger}$, $\mathbf{e}_{sp,l}=[\sigma_{sp,1l}^2,\ldots,\sigma_{sp,Kl}^2]^{\dagger}$, $\mathcal{Q}_l^{av}$ is the interference power threshold specified by the lth PU and p_k^{av} is the total transmit power available at the kth SU transmitter. Equations (3.8) and (3.9) represent the average interference power constraint for the lth PU receiver and the total transmit power constraint at the kth SU transmitter, respectively. The third constraint implies that the transmit power for each SU transmitter should be greater than or equals to zero. It can be shown that the objective function (3.7) is quasi-concave and constrains are affine functions of $\mathbf{p}(\mathcal{H})$ [17]. An efficient algorithm is proposed in next section to obtain optimal transmit power for each SU transmitter when channel estimation errors are present.

3.4 Power Allocation with Imperfect Channel Estimation

Convex optimization techniques are exploited to derive an optimum power allocation policy for each SU transmitter when the channel estimation errors are present for the channels

between the SU transmitters and the SU receiver and the SU transmitters and the PU receivers. The proposed algorithm is based on the Lagrange dual-decomposition [18–20]. Since the objective function (3.7) is quasi-concave with respect to $\mathbf{p}(\mathcal{H})$, the optimization problem **P1** can be solved by a sequence of optimization problems (**P2**s) as [17]

$$\mathcal{C}_{MAC,lb} = \underset{\tilde{p}:\ 0\leq\tilde{p}\leq\tilde{P}_{max}}{\text{maximize}} \ \{\mathcal{C}_{MAC,lb}(\tilde{p})\}, \tag{3.11}$$

where $\tilde{P}_{max} = \sum_{k=1}^{K} p_k^{av}\sigma_{ss,k}^2$ and for each $\tilde{p}$, $\mathcal{C}_{MAC,lb}(\tilde{p})$ is obtained by solving the optimization problem **P3**:

$$\mathcal{C}_{MAC,lb}(\tilde{p}) = \underset{\{p_k(\mathcal{H})\}}{\text{maximize}} \quad \mathcal{E}_{\mathcal{H}}\left\{\log\left(1+\frac{1}{\sigma_w^2+\tilde{p}}\sum_{k=1}^{K} p_k(\mathcal{H})\hat{h}_{ss,k}\right)\right\}, \tag{3.12}$$

$$\text{subject to} \quad \sum_{k=1}^{K}\mathcal{E}_{\mathcal{H}}\left\{p_k(\mathcal{H})\hat{h}_{sp,kl}\right\} + \sum_{k=1}^{K} p_k^{av}\sigma_{sp,kl}^2 \leq \mathcal{Q}_l^{av}, \quad l=1,\ldots,L, \tag{3.13}$$

$$\mathcal{E}_{\mathcal{H}}\{p_k(\mathcal{H})\} \leq p_k^{av},\ k=1,\ldots,K, \tag{3.14}$$

$$\sum_{k=1}^{K} p_k(\mathcal{H})\sigma_{ss,k}^2 = \tilde{p}, \tag{3.15}$$

$$p_k(\mathcal{H}) \geq 0,\ k=1,\ldots,K. \tag{3.16}$$

It can be noticed that the optimization problem **P3** is convex and the Lagrange dual-decomposition approach can be applied to obtain an optimal power allocation for each SU [17]. First, the optimization problem **P3** is solved.

Theorem 3.2: An optimum power allocation for user k with imperfect channel estimation is given as:

$$p_k^*(\mathcal{H}) = \left(\frac{1}{\nu_k + \sum_{l=1}^{L} \mu_l \hat{h}_{sp,kl} + \delta \sigma_{ss,k}^2} - \frac{(\sigma_w^2 + \tilde{p})}{\hat{h}_{ss,k}} \right)^+ . \tag{3.17}$$

Proof. See the Appendix B. □

Once the problem **P3** is solved, a lower-bound on the ergodic sum capacity of MAC, $\mathcal{C}_{MAC,lb}^*$, is obtained by solving the optimization problem **P2**. The optimization problem **P2** can be solved by a one-dimensional search over $\tilde{p}$. To summarize, the complete algorithm to obtain an optimum power allocation policy and achieve a lover-bound of the ergodic sum capacity of the opportunistic SISO MAC with imperfect channel estimation is given below.

Algorithm 2 Computation of optimum power allocation policy

1: Given $\tilde{p} \in [0, \tilde{p}_{max}]$, initialize $\varrho_0 = 0$ and $\varrho_4 = \tilde{p}_{max}$
2: Set $\varrho_2 = \frac{1}{2}(\varrho_0 + \varrho_4)$, $\varrho_1 = \frac{1}{2}(\varrho_0 + \varrho_2)$, and $\varrho_3 = \frac{1}{2}(\varrho_2 + \varrho_4)$
3: For every $\varrho_i,\ i \in \{1, 2, 3\}$
4: Given $\mathcal{E}_\mu^{(0)}$, $\mathcal{E}_\nu^{(0)}$ initial ellipsoids centered at $\boldsymbol{\mu}^{(0)}$, $\boldsymbol{\nu}^{(0)}$ which contain the optimal dual solution $\boldsymbol{\mu}^*$ and $\boldsymbol{\nu}^*$ and initial value $\delta^{(0)}$.
5: Set $t = 0$.
6: **repeat**
7: Obtain the optimum power allocation ϱ_i for the kth user, from (3.17).
8: Update $\mathcal{E}_\mu^{(t+1)}$, $\mathcal{E}_\nu^{(t+1)}$ using $\mathcal{E}_\mu^{(t)}$, $\mathcal{E}_\nu^{(t)}$ and the sub-gradients of $\nu_l^{(t)}$, $l = 1, \ldots, L$ and $\mu_k^{(t)}$, $k = 1, \ldots, K$ [21]. Update $\delta^{(t+1)}$ using the bisection method [17].
9: Set $\boldsymbol{\mu}^{(t+1)}$ and $\boldsymbol{\nu}^{(t+1)}$ as centers of new ellipsoids $\mathcal{E}_\mu^{(t+1)}$ and $\mathcal{E}_\nu^{(t+1)}$, respectively.
10: Set $t \leftarrow t + 1$.
11: **until** the stopping criteria of the ellipsoid method is satisfied [21].
12: Compute $\mathcal{C}(\varrho_i)$ using (3.12).
13: Find $i^* = \max_{i \in \{0,1,\ldots,4\}} \mathcal{C}(\varrho_i)$.
14: Set $\varrho_0 \leftarrow \varrho_{\max\{i^*-1,0\}}$, $\varrho_4 \leftarrow \varrho_{\min\{i^*+1,4\}}$, $\varrho_2 \leftarrow \frac{1}{2}(\varrho_0 + \varrho_4)$, and compute $\mathcal{C}(\varrho_2)$ through the Steps 3-11.
15: If $|\varrho_4 - \varrho_2| \geq \epsilon$, go to Step 2, where ϵ is a small constant.
16: Else $\tilde{p}^* = \varrho_{i^*}$, and $C_{MAC,lb}^{opt} = C_{MAC}(\tilde{p}^*)$.

Note that in case of a single PU, there is only one Lagrange multiplier ν for the interference temperature constraint. In such a scenario, ν in Step 8 can be updated by the bisection

method [17].

3.5 Numerical Results

In this section, numerical results are presented to illustrate the influence of the channel estimation errors of the SISO channels between the SU transmitter and the SU receiver, and the channels between the SU transmitters and the PU receivers on the mutual information in opportunistic SISO MAC. In all simulations, frequency-flat Rayleigh fading channels are assumed for the aforementioned links. All channel complex coefficients are generated with zero-mean CSCG distributed random variables. A path exponent of 4 is assumed. Furthermore, zero-mean uncorrelated CSCG noise with variance of $\sigma_w^2 = 10^{-6}$ is assumed. The average transmit power available for each SU transmitter is assumed to be 15 μW. Without the loss of geniality, only one PU present is assumed in the network. Unless otherwise mentioned, the average interference power threshold, $\mathcal{Q}_l^{av}$, is set to 10 μW. All simulation results were averaged over $20,000$ independent channel realizations.

Fig. 3.2 presents a lower-bound on the achievable sum capacity versus interference introduced to the PU receiver for $K = 2$ with different channel estimation error variance, $\sigma_{sp}^2 = \sigma_{sp,11}^2 = \sigma_{sp,21}^2$, for the SISO channels between the SU transmitter and PU receiver. We can notice from Fig. 3.2 that a small imperfection in channel estimation errors at low $\mathcal{Q}_l^{av}$ values has a significant impact on the sum capacity. On the other hand, at high $\mathcal{Q}_l^{av}$ values this impact becomes lower.

In Fig. 3.3, a lower-bound on the ergodic sum capacity versus interference introduced to the PU receiver is presented for $K = 2$ with different channel estimation error variances, $\sigma_{ss}^2 = \sigma_{ss,1}^2 = \sigma_{ss,2}^2$, for the channels between the SU transmitters and SU receiver. It is ap-

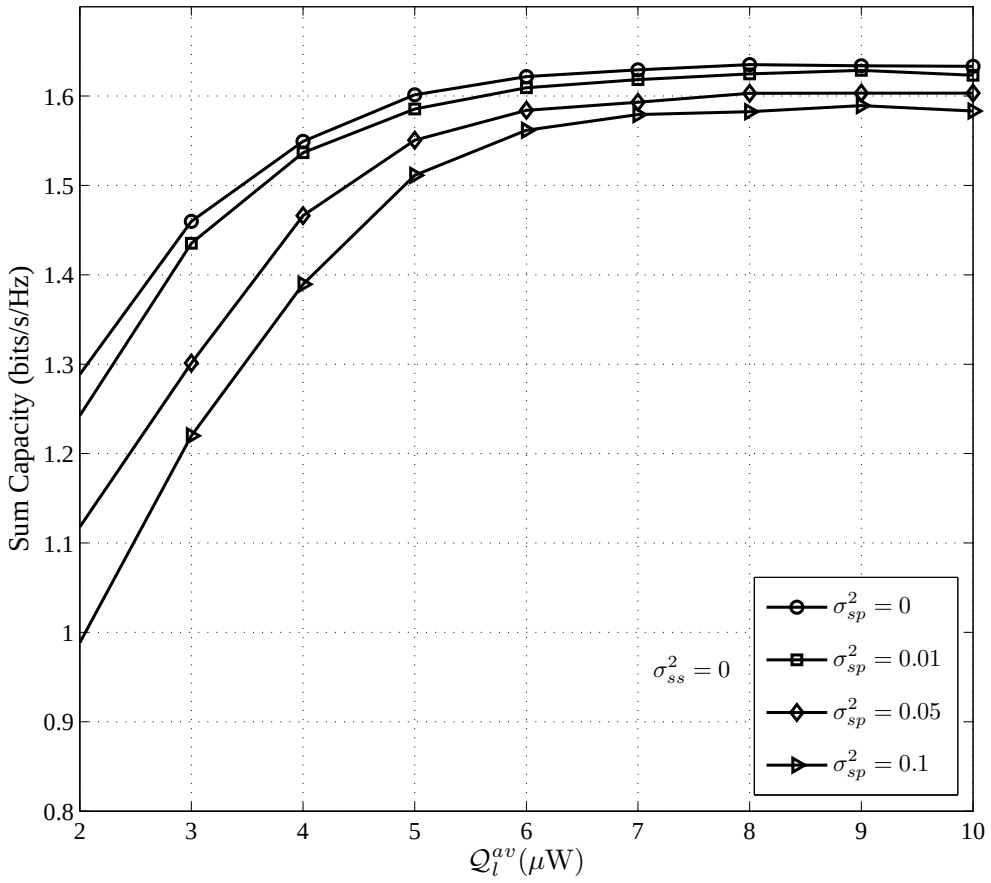

Figure 3.2: Ergodic sum capacity versus $\mathcal{Q}_l^{av}$ for different σ_{sp}^2.

parent from Fig. 3.3, that higher estimation errors have significant detrimental effect on the sum capacity at higher $\mathcal{Q}_l^{av}$ values. In Fig. 3.4, we illustrate a lower-bound on the ergodic sum capacity versus interference introduced to the PU receiver with $K = 2$ for different values of σ_{ss}^2 and σ_{sp}^2 with different power allocation strategies. Solid lines represent the proposed power allocation scheme and dash lines represent the uniform power allocation scheme. It can be noticed that our proposed power allocation scheme outperformed the uniform power allocation scheme. Furthermore, we observe that without channel estimation

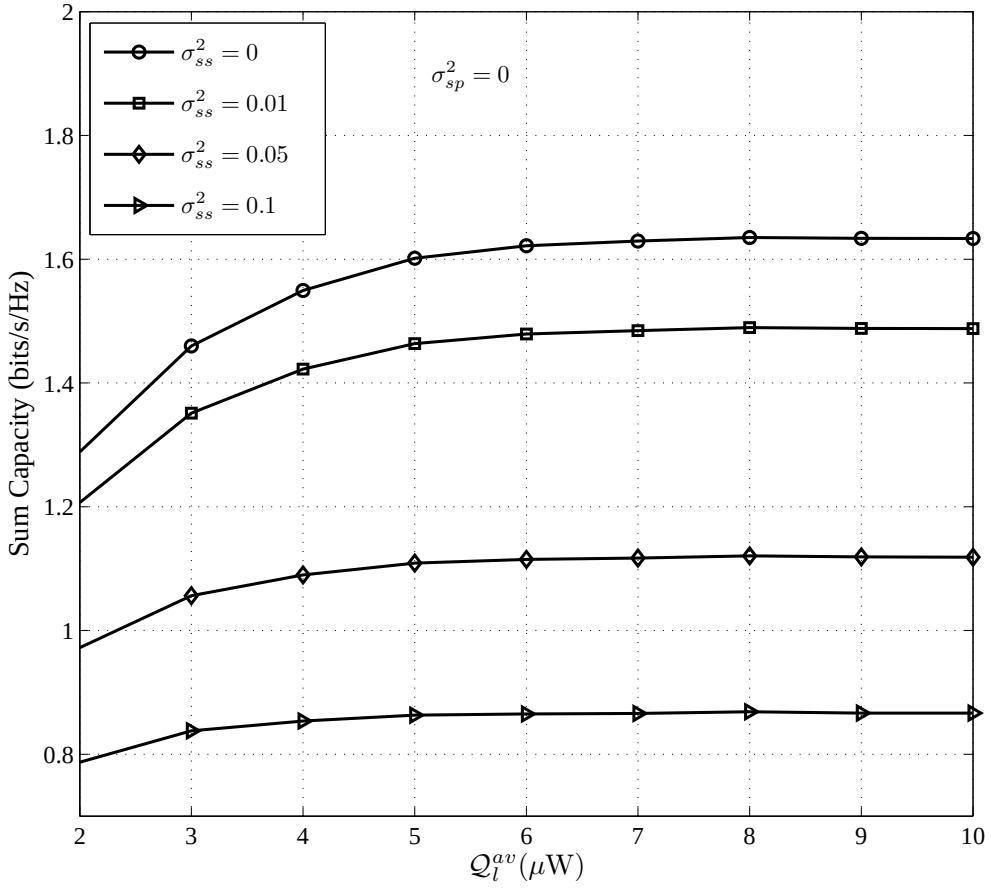

Figure 3.3: Ergodic sum capacity versus $\mathcal{Q}_l^{av}$ for different σ_{ss}^2.

errors, the capacity gain reduces at high $\mathcal{Q}_l^{av}$ values. This trend, however, changes with the channel estimation errors. It can be further noticed from Fig. 3.4 that the growth rate of capacity loss is significant at higher $\mathcal{Q}_l^{av}$ values. Furthermore, as the estimation imperfection increases sum capacity decreases significantly for all $\mathcal{Q}_l^{av}$ values.

Fig. 3.5 shows the average received interference power at the PU receiver versus normalized distance between the PU-1 and the SU-1 for different values of channel estimation error variances σ_{sp}^2. It can be noticed from Fig. 3.5 that the interference introduced to PU

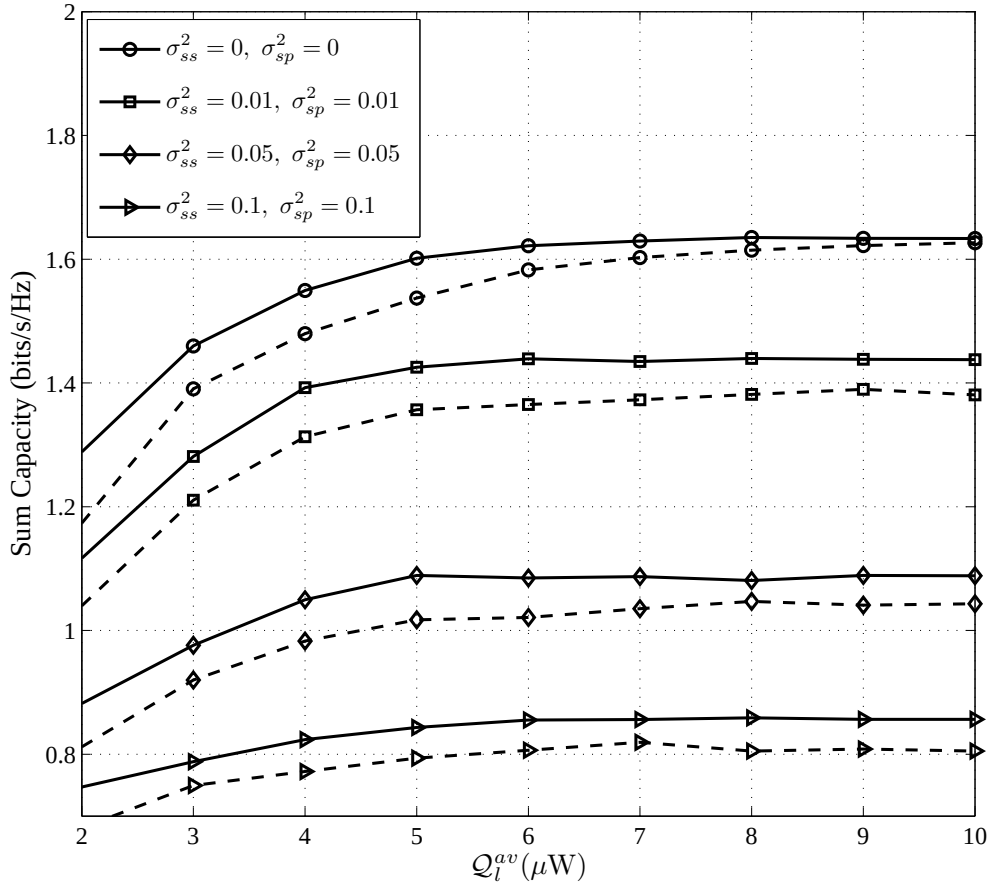

Figure 3.4: Ergodic sum capacity versus $\mathcal{Q}_l^{av}$ for different σ_{ss}^2 and σ_{sp}^2.

increases with the increase of σ_{sp}^2. We further noticed from Fig. 3.5 that higher estimation errors have a larger detrimental effect when PU is located relatively away from the SU. In Fig. 3.6, the average received interference power at the PU receiver versus normalized distance between the PU-1 and the SU-1 is presented for different K. It is apparent from Fig. 3.6 that the interference power increased significantly from $K = 2$ to $K = 3$. Furthermore, when K increases the received interference at the PU also increases for all the distance values. This can be easily explained as the number of SUs increases in the network, the

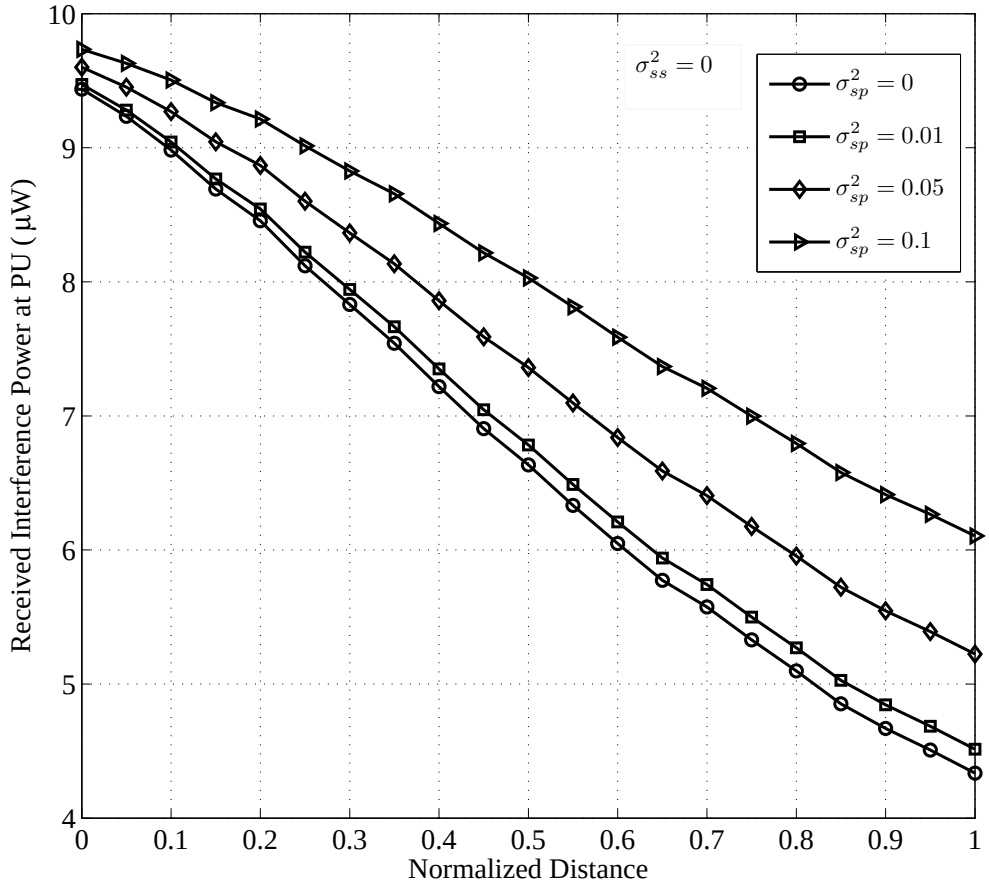

Figure 3.5: Average interference introduced to the PU versus normalized distance between PU and the SU-1 for different σ_{sp}^2.

amount of induced interference at the PU should increase. We can further notice from Fig. 3.6 that for all K values the received interference remain below the threshold specified by the regulatory bodies.

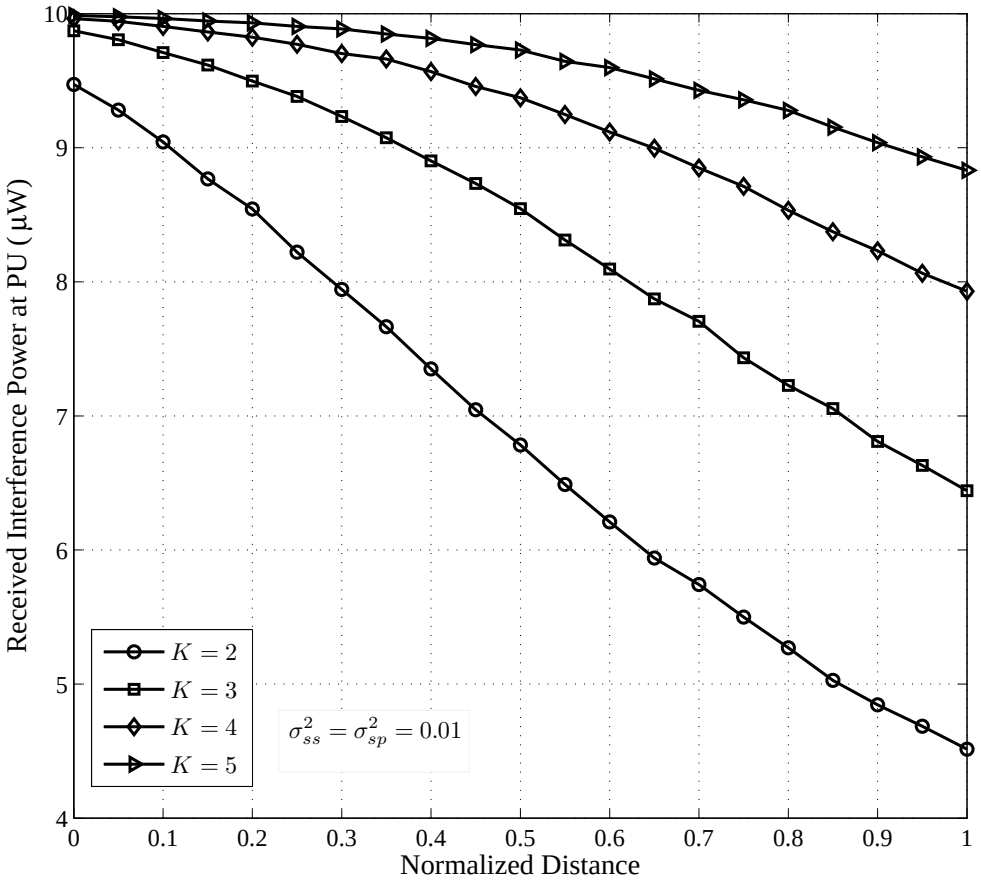

Figure 3.6: Average interference introduced to the PU versus normalized distance between PU and the SU-1 for different K.

3.6 Conclusion

In this Chapter, we have studied a lower-bound on the opportunistic spectrum sharing single-input single-output (SISO) multiple access Rayleigh fading channel by incorporating channel estimation errors. These errors include the channel estimation errors for both the set of SISO channels between the secondary user (SU) transmitters and the primary user (PU) receivers and the channels between the SU transmitters and the SU receiver. An

optimum power allocation policy is designed under the aforementioned channel estimation errors, by maximizing a lower-bound on the sum capacity while imposing a set of transmit power constraint at SU transmitters and a set of interference power constraints specified by PU receivers. The Lagrange dual-decomposition based efficient algorithm is proposed to obtain the optimal power allocation policy for each SU transmitter. The numerical results reveal that channel imperfection on the aforementioned channel links have significant detrimental effect on both sum capacity and the interference introduced to the active PUs in the CR network.

Bibliography

[1] S. Haykin, "Cognitive radio: brain-empowered wireless communications," *IEEE J. Sel. Areas Commun.*, vol. 23, no. 2, pp. 201-220, Feb. 2005.

[2] J. Mitola III, "Cognitive radio for flexible mobile multimedia communications," in *Proc. IEEE Int. Work. MoMuC*, Nov. 1999, pp. 3-10.

[3] H. Hong, C. X. Wang, H. H. Chen, and J. Thompson, "Performance analysis of cognitive radio networks with average interference power constraints," in *Proc. IEEE ICC*, May. 2008, pp. 3578-3582.

[4] W. Wang, T. Peng, and W. Wang, "Optimal power control under interference temperature constraints in cognitive radio network," in *Proc. IEEE WCNC*, Mar. 2007, pp. 116-120.

[5] A. Ghasemi and S. E. Sousa, "Fundamental limits of spectrum-sharing in fading environments," *IEEE Trans. Wireless Commun.*, vol. 6, no. 2, pp. 649-658, Feb. 2007.

[6] L. Musavian and S. Aissa, "Capacity and power allocation for spectrum-sharing communications in fading channels," *IEEE Trans. Wireless Commun.*, vol. 8, no. 1, pp. 148-156, Jan. 2009.

[7] A. Ghasemi and E. S. Sousa, "Capacity of fading channels under spectrum-sharing constraints," in *Proc. IEEE ICC*, Jun. 2006, pp. 4373-4378.

[8] X. Kang, Y. C. Liang, A. Nallanathan, H. K. Garg, and R. Zhang, "Optimal power allocation for fading channels in cognitive radio networks: Ergodic capacity and outage capacity," *IEEE Trans. Wireless Commun.*, vol. 8, no. 2, pp. 940-950, Feb. 2009.

[9] R. Zhang, "Optimal power control over fading cognitive radio channel by exploiting primary user CSI," in *Proc. IEEE GLOBECOM*, Dec. 2008, pp. 1-5.

[10] R. Zhang and Y. C. Liang, "Exploiting multi-antennas for opportunistic spectrum sharing in cognitive radio networks," *IEEE J. Sel. Topics Signal Processing*, vol. 2, no. 1, pp. 88-102, Feb. 2008.

[11] R. Zhang, "On peak versus average interference power constraints for protecting primary users in cognitive radio networks," *IEEE Trans. Wireless Commun.*, vol. 8, no. 4, pp. 2112-2120, Apr. 2009.

[12] R. Zhang, S. Cui, and Y. C. Liang, "On ergodic sum capacity of fading cognitive multiple-access and broadcast channels," *IEEE Trans. Info. Theory*, vol. 55, no. 11, pp. 5161-5178, Nov. 2009.

[13] L. Zhang, Y. C. Liang, and Y. Xin, "Joint beamforming and power allocation for multiple access channels in cognitive radio networks," *IEEE Trans. Selected Areas Commun.*, vol. 26, no. 1, pp. 38-51, Jan. 2008.

[14] L. Musavian and S. Aissa, "Fundamental capacity limits of cognitive radio in fading environments with imperfect channel information," *IEEE Trans. Commun.*, vol. 57, no. 11, pp. 3472-3480, Nov. 2009.

[15] T. Yoo and A. Goldsmith, "Capacity of fading MIMO channels with channel estimation error," in *Proc. IEEE ICC*, Jun. 2004, pp. 808-813.

[16] M. Medard, "The effect upon channel capacity in wireless communications of perfect and imperfect knowledge of the channel," *IEEE Trans. Inf. Theory*, vol. 46, no. 3, pp. 933-946, May 2000.

[17] S. Boyd and L. Vandenberg, *Convex Optimization*. Cambridge University Press, 2004.

[18] W. Yu, "A dual decomposition approach to the sum power Gaussian vector multiple access channel sum capacity problem," in *Proc. CISS*, Mar. 2003.

[19] M. Codreanu, M. Juntti, and M. Latva-Aho, "On the dual-decomposition-based sum capacity maximization for vector broadcast channels," *IEEE Trans. Veh. Technol.*, vol. 56, no. 6, pp. 3577-3581, Nov. 2007.

[20] D. P. Palomar and M. Chiang, "A tutorial on decomposition methods for network utility maximization," *IEEE J. Sel. Areas Commun.*, vol. 24, no. 8, pp. 1439-1451, Aug. 2006.

[21] R. G. Bland, D. Goldfarb, and M. J. Todd, "The ellipsoid method: A survey," *Operations Research*, vol. 29, no. 6, pp. 1039-1091, 1981.

[22] T. Yoo and A. Goldsmith, "Capacity and power allocation for fading MIMO channels with channel estimation error," *IEEE Trans. Inf. Theory*, vol. 52, no. 5, pp. 2203-2214, May 2006.

[23] T. Guess and M. K. Varanasi, "An information-theoretic framework for deriving canonical decision-feedback receivers in Gaussian channels,"*IEEE Trans. Inf. Theory*, vol. 51, no. 1, pp. 173-187, Jan. 2005.

Chapter 4

Blind Estimation of OFDM Parameters in Cognitive Radio Networks[5]

4.1 Introduction

Cognitive radio (CR) has attracted broad attention in both industry and academia due to its capability of improving the spectrum utilization, while providing the increasing amount of applications and services [1, 2]. CR is capable of dynamically recognizing the available spectrum bands, which are initially assigned to licensed users. Then, CR users communicate through these unoccupied spectrum segments without causing harmful interference to licensed users [1, 2]. CR is an intelligent device, which is aware of its propagation environment and adjust to it by making real time changes to its operating parameters, such as modulation strategy, demodulation strategy and operating frequency [2]. In practice, CR utilizes orthogonal frequency division multiplexing (OFDM) to transmit its data due to several advantages of OFDM, such as robustness against frequency selective fading, dynamic allocation of number of subcarriers, simplicity in channel equalization, and multiple access mechanism [3, 4].

[5] A version of this chapter has been accepted for publication. Punchihewa, A. Bhargava V. K. and Despins, C. "Blind Estimation of OFDM Parameters in Cognitive Radio Networks," IEEE Transaction on Wireless Communications.

Since CR has the intelligence of dynamically changing its parameters, it is necessary to develop blind OFDM parameter estimation algorithms to efficiently demodulate the OFDM signals in hostile wireless channels. In this work, a blind parameter extraction algorithm is proposed to estimate the symbol period, useful symbol period, length of the cyclic prefix, number of subcarriers and the carrier frequency offset of the received OFDM signals when affected by additive Gaussian noise, time-dispersive channel, initial phase, timing and frequency offsets. The second-order cyclostationarity of received OFDM signal is exploited for blind estimation of OFDM parameters in time-dispersive channels.

Signal cyclostationarity in communication signals is attached with symbol period, chip rate and carrier frequency [5–14]. The cyclostationarity properties of signal have been exploited in previous studies for blind parameter extraction [5–9], modulation identification [9, 10] and blind channel identification [12]. Although the parameter estimation of OFDM signal has been extensively studied in previous studies [5–9], the analysis considering the time-dispersive channel effect has not been addressed. Parameter extraction algorithms proposed in [7] and [9] assume that the channel effect is composed into the pulse shaping filter. However, this work includes a comprehensive signal model considering the effect of time-dispersive channel, initial phase, timing offset, carrier frequency offset, and additive Gaussian noise. The second-order cyclostatioarity of OFDM signal is derived based on the aforementioned signal model and the proposed algorithm blindly estimates the OFDM parameters. The simulation results indicate that the proposed algorithm performs well even at low signal to noise ratio (SNR) values.

The rest of the Chapter is organized as follows: Fundamental concepts of signal cyclostationarity are introduced in Section 4.2. OFDM signal model and the signal cyclostationarity in time-dispersive channel is presented in Section 4.3. The proposed blind parameter

estimation algorithm is discussed in Section 4.4. Numerical results and conclusions are given in Sections 4.5 and 4.6, respectively. Finally, a cyclostationarity test is presented in the Appendix C.

4.2 Signal Cyclostationarity: Preliminaries

A zero mean complex valued continuous time signal $r(t)$ is called second-order cyclostationarity if its time varying autocorrelation function $\tilde{R}_{rr}(t;\tilde{\tau}) = \mathcal{E}\{r(t)r^*(t+\tilde{\tau})\}$, is a periodic function of time. This time varying autocorrelation function can be expressed as a Fourier series [13, 14]

$$\tilde{R}_{rr}(t;\tilde{\tau}) = \sum_{\{\tilde{\alpha}\}} \tilde{R}_{rr}(\tilde{\alpha};\tilde{\tau}) e^{j2\pi\tilde{\alpha}t}, \tag{4.1}$$

where $\{\tilde{\alpha}\} = \{\tilde{\alpha} | \tilde{R}_{rr}(\tilde{\alpha};\tilde{\tau}) \neq 0\}$ is the set of cycle frequencies (CFs), and $\tilde{R}_{rr}(\tilde{\alpha};\tilde{\tau})$ is the cyclic autocorrelation function (CAF) at CF $\tilde{\alpha}$[6] and at delay $\tilde{\tau}$. Assuming the signal $r(t)$ exhibits second-order cyclostationary with period T_r, the CAF can be expressed as [13, 14]

$$\tilde{R}_{rr}(\tilde{\alpha};\tilde{\tau}) = \frac{1}{T_r} \int_{-T_r/2}^{T_r/2} \tilde{R}_{rr}(t;\tilde{\tau}) e^{-j2\pi\tilde{\alpha}t} dt. \tag{4.2}$$

Under the assumption of no aliasing, the CAF and the corresponding CFs for the discrete time signal $r(n) = r(t)|_{t=nf_s^{-1}}$, are respectively given as [15]

$$R_{rr}(\alpha;\tau) = \tilde{R}_{rr}(\tilde{\alpha}f_s;\tilde{\tau}f_s^{-1}), \tag{4.3}$$

and

[6] It should be noted that the notations $\tilde{\alpha}$ and α are used to denote the CFs for the continuous time and discrete time signals $r(t)$ and $r(n)$, respectively.

$$\{\alpha\} = \{\alpha \in [-1/2, 1/2) |\ \alpha = \tilde{\alpha} f_s^{-1}, R_{rr}(\alpha;\tau) \neq 0\}, \tag{4.4}$$

where f_s is the sampling frequency and $\tau = \tilde{\tau} f_s$. The estimator for the CAF at CF α[6] and for a delay τ, based on $\mathcal{N}$ samples is given by [13, 14]

$$\widehat{R}_{rr}(\alpha;\tau) = \frac{1}{\mathcal{N}} \sum_{n=0}^{\mathcal{N}-1} r(n) r^*(n+\tau) e^{-j2\pi\alpha n}. \tag{4.5}$$

4.3 Signal Model and OFDM Signal Cyclostationarity in Time-Dispersive Channel

4.3.1 Signal Model

The OFDM signal is transmitted over multi-path time-dispersive channel and affected by additive white Gaussian noise, initial phase, timing offset and carrier frequency offset, the received continuous time baseband signal can be written as [11]

$$\begin{aligned} r(t) = \frac{1}{\sqrt{K}} e^{j\Delta\phi} e^{j2\pi\Delta f_e t} \sum_{i=-\infty}^{\infty} \sum_{l=1}^{L_c} \sum_{k=0}^{K-1} d_{k,i} h(\tilde{\tau}_l) e^{j2\pi(k-\frac{K-1}{2})\Delta f(t-\tilde{\tau}_l - iT_s - \epsilon T_s)} \\ \times g(t - \tilde{\tau}_l - iT_s - \epsilon T_s) + w(t), \end{aligned} \tag{4.6}$$

where K is the number of subcarriers, $\Delta\phi$ is the initial phase, Δf_e is the carrier frequency offset, $d_{k,i}$ is the transmitted data symbols in kth subcarrier and in the ith symbol period. The set of data symbols $\{d_{k,i}\}$ are generated from independent and identically distributed zero mean random variables from a M-ary quadrature amplitude modulated (M-QAM) or M-ary phase shift keying (M-PSK) modulated signal constellation. Function $g(t)$ is the

resulting pulse shape with the transmitting root-raised cosine windowing function and the receive low-pass filter. In OFDM transmission schemes, transmit windowing is used to remove the spectrum leakage [3]. The frequency separation between two adjacent subcarriers is given by Δf and the normalized timing offset is represented as ϵ ($0 \leq \epsilon \leq 1$). The OFDM symbol period T_s is given by $T_s = T_{use} + T_{cp}$, where $T_{use} = \Delta f^{-1}$ is the useful symbol period and T_{cp} is the cyclic prefix period. Usually $T_{cp} = \kappa T_{use}$, where κ is a constant which depends on the standard used in the OFDM signal transmission. $h(\tilde{\tau}_l)$ is the path gain at delay $\tilde{\tau}_l$, $l = 1, \ldots, L_c$, and $w(t)$ is the zero mean complex additive Gaussian noise. The discrete time received baseband OFDM signal $r(n)$ is obtained by oversampling the continuous time signal $r(t)$ at a rate $f_s = \varrho K \Delta f$, with ϱ as the oversampling factor.

4.3.2 OFDM Signal Cyclostationarity

By using the signal model in (4.6), the time varying autocorrelation function, $\tilde{R}_{rr}(t;\tilde{\tau})$, of the received continuous time OFDM signal can be obtained as [11]

$$\begin{aligned}\tilde{R}_{rr}(t;\tilde{\tau}) = \frac{\sigma_d^2}{K} e^{-j2\pi\Delta f_e \tilde{\tau}} \sum_{k=0}^{K-1} e^{-j2\pi(k-\frac{K-1}{2})\Delta f \tilde{\tau}} \sum_{i=-\infty}^{\infty} \sum_{l_1=1}^{L_c} h(\tilde{\tau}_{l_1}) g(t - \tilde{\tau}_{l_1} - iT_s - \epsilon T_s) \\ \times \sum_{l_2=1}^{L_c} h^*(\tilde{\tau}_{l_2}) g^*(t - \tilde{\tau}_{l_2} + \tilde{\tau} - iT_s - \epsilon T_s) e^{-j2\pi(k-\frac{K-1}{2})\Delta f(\tilde{\tau}_{l_1} - \tilde{\tau}_{l_2})} + \tilde{R}_{ww}(t;\tilde{\tau}),\end{aligned} \tag{4.7}$$

where σ_d^2 is the variance of the data symbols $d_{k,i}$ and $\tilde{R}_{ww}(t;\tilde{\tau})$ is the autocorrelation function of the additive Gaussian noise. It can be noticed from (4.7) that $\tilde{R}_{rr}(t;\tilde{\tau})$ periodic with period equal to T_s. Therefore, the continuous time received OFDM signal in time-dispersive channel exhibits second-order cyclostationarity with CFs equals to $\{\tilde{\alpha}\} =$

$\{\tilde{\alpha}|\tilde{\alpha} = iT_s^{-1},\ i \text{ integer}\}$. Thus, the CAF of the received OFDM signal can be obtained by taking the Fourier transform of (4.7) with respect to t as

$$\begin{aligned}\tilde{R}_{rr}(\tilde{\alpha};\tilde{\tau}) = &\frac{\sigma_d^2}{KT_s}e^{-j2\pi\tilde{\alpha}\epsilon T_s}e^{-j2\pi\Delta f_e\tilde{\tau}}\\ &\times\int_{-\infty}^{\infty}\sum_{l_1=1}^{L_c}h(\tilde{\tau}_{l_1})g(t-\tilde{\tau}_{l_1})\sum_{l_2=1}^{L_c}h^*(\tilde{\tau}_{l_2})g^*(t-\tilde{\tau}_{l_2}+\tilde{\tau})\\ &\times\sum_{k=0}^{K-1}e^{-j2\pi(k-\frac{K-1}{2})\Delta f(\tilde{\tau}+\tilde{\tau}_{l_1}-\tilde{\tau}_{l_2})}e^{-j2\pi\tilde{\alpha}t}dt+\tilde{R}_{ww}(\tilde{\alpha};\tilde{\tau}),\end{aligned} \tag{4.8}$$

where $\tilde{R}_{ww}(\tilde{\alpha};\tilde{\tau})$ is the CAF of the continuous time additive Gaussian noise process. By using (4.3), (4.4), and (4.8), and under the assumption of no aliasing [15], the CAF of the discrete time OFDM signal, $r(n)$, at CF α and at delay τ, and the corresponding set of CFs can be respectively written as

$$\begin{aligned}R_{rr}(\alpha;\tau) = &\frac{\sigma_d^2}{KN_s}e^{-j2\pi\alpha\epsilon N_s}e^{-j2\pi\Delta f_{ne}\tau}\\ &\times\sum_n\sum_{l_1=1}^{L_c}h(\tau_{l_1})g(n-\tau_{l_1})\sum_{l_2=1}^{L_c}h^*(\tau_{l_2})g^*(n+\tau-\tau_{l_2})e^{-j2\pi\alpha n}\\ &\times\Psi_K(\tau,\tau_{l_1},\tau_{l_2})+R_{ww}(\alpha;\tau),\end{aligned} \tag{4.9}$$

and

$$\{\alpha\} = \{\alpha\in[-1/2,1/2)|\alpha = iN_s^{-1}, i \text{ integer}\}, \tag{4.10}$$

where $N_s = N_{use} + N_{cp}$ is the number of samples over a OFDM symbol with N_{use} and N_{cp} as the number of samples in the useful symbol period and the cyclic prefix period, respectively. $\Delta f_{ne} = \Delta f_e f_s^{-1}$, $\Psi_K(\tau,\tau_{l_1},\tau_{l_2}) = \sum_{k=0}^{K-1}e^{-j2\pi(\varrho K)^{-1}(k-\frac{K-1}{2})(\tau+\tau_{l_1}-\tau_{l_2})} = \frac{sin(\pi(\tau+\tau_{l_1}-\tau_{l_2})/\varrho)}{sin(\pi(\tau+\tau_{l_1}-\tau_{l_2})/\varrho K)}$, and $R_{ww}(\alpha;\tau)$ is the CAF of the discrete time additive Gaussian noise process. From (4.9) we can notice that the magnitude of the CAF does not depends on the

initial phase, timing and carrier frequency offsets. Furthermore, the CAF is non-zero for CFs given in (4.10), otherwise the CAF is identical to zero as a function of delay. It can be further noticed from (4.9) that at zero CF non-zero CAF magnitudes values are obtained at delays around $\tau_{l_1} - \tau_{l_2}$. These non-zero magnitudes are due to the non-zero time varying cumulants resulting from the correlation between the same data symbols within a block of data and the magnitude of the factor $\Psi_K(\tau, \tau_{l_1}, \tau_{l_2})$. Furthermore, additional non-zero CAF magnitudes are obtained at delays around $\pm\varrho K + \tau_{l_1} - \tau_{l_2}$, and at zero CF. These are due to the non-zero time varying cumulants resulting from the correlation between the cyclic prefix data symbols and the corresponding data symbols and the magnitude of the factor $\Psi_K(\tau, \tau_{l_1}, \tau_{l_2})$. In addition to the zero CF, additional non-zero CAF magnitudes can be obtained at delays $\pm\varrho K$ and for different CFs as in (4.10). These non-zero peaks are due to the presence of the cyclic prefix and the magnitude of the factor $\Psi_K(\tau, \tau_{l_1}, \tau_{l_2})$. These attractive features are presented in Figs.[7] 4.1 and 4.2, respectively. The existence of non-zero peaks of the magnitudes of the CAF of OFDM signal will be exploited in the next section to blindly estimate the OFDM parameters in time-dispersive channel.

4.4 Blind Estimation of OFDM Parameters

Blind estimation of OFDM parameters in time-dispersive channel is discussed in this section. As discussed in Section 4.3, the second-order cyclostationarity properties of the received OFDM signal will be exploited to blindly estimate the OFDM signal parameters in time-dispersive channels. These parameters include OFDM symbol period, useful symbol

[7] A static five-tap time-dispersive channel with channel coefficients $\tau_l = [0.2917,\ 0.4941,\ 0.5842,\ 0.4941,\ 0.2917]$, $l = 1, \ldots, 5$ is considered [17]. In addition, other signal parameters are set as in Section 4.5, except for Δf_c, $\Delta\phi$ and ϵ, which are set to zero.

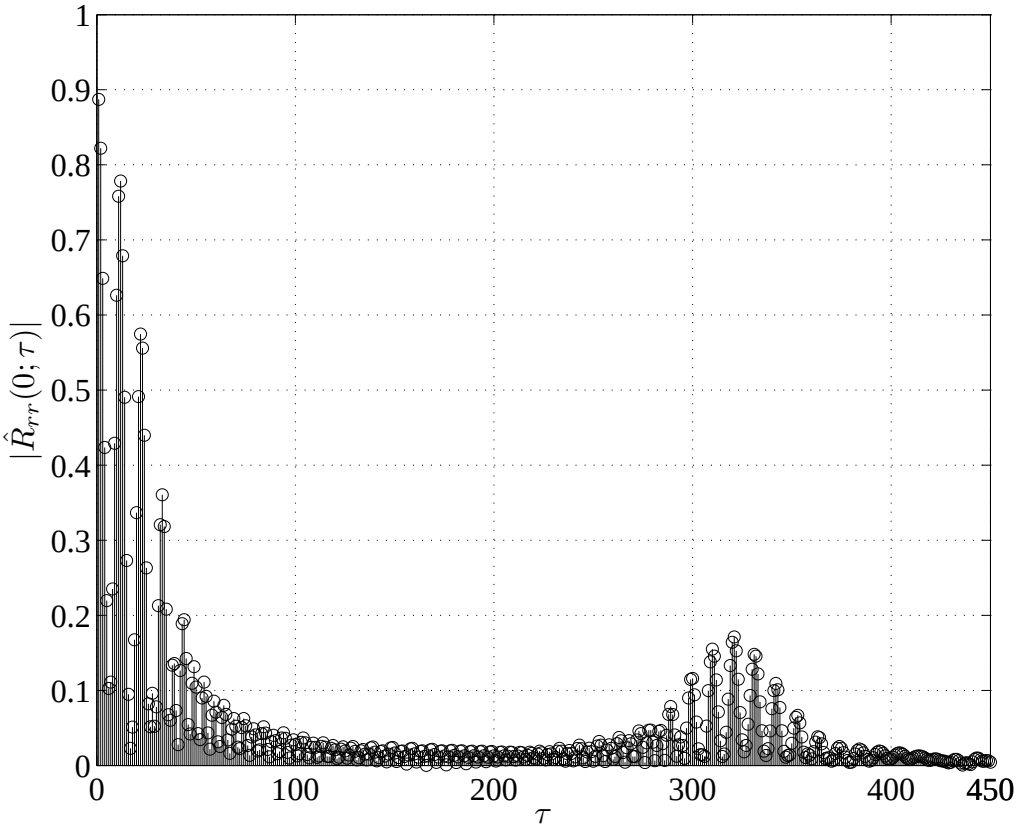

Figure 4.1: The estimated magnitude of the CAF of OFDM signal in time-dispersive channel at zero CF and at different delay values for 20 dB SNR.

period, cyclic prefix factor, number of subcarriers and the carrier frequency offset. Before the estimation of parameters, the received continuous time signal is passed through a low-pass filter to remove the out of band noise. Then, the continuous time signal is oversampled to obtain the discrete time OFDM signal at the receive side. The estimation of OFDM parameters is carried out by following the procedure given in the subsequent subsections.

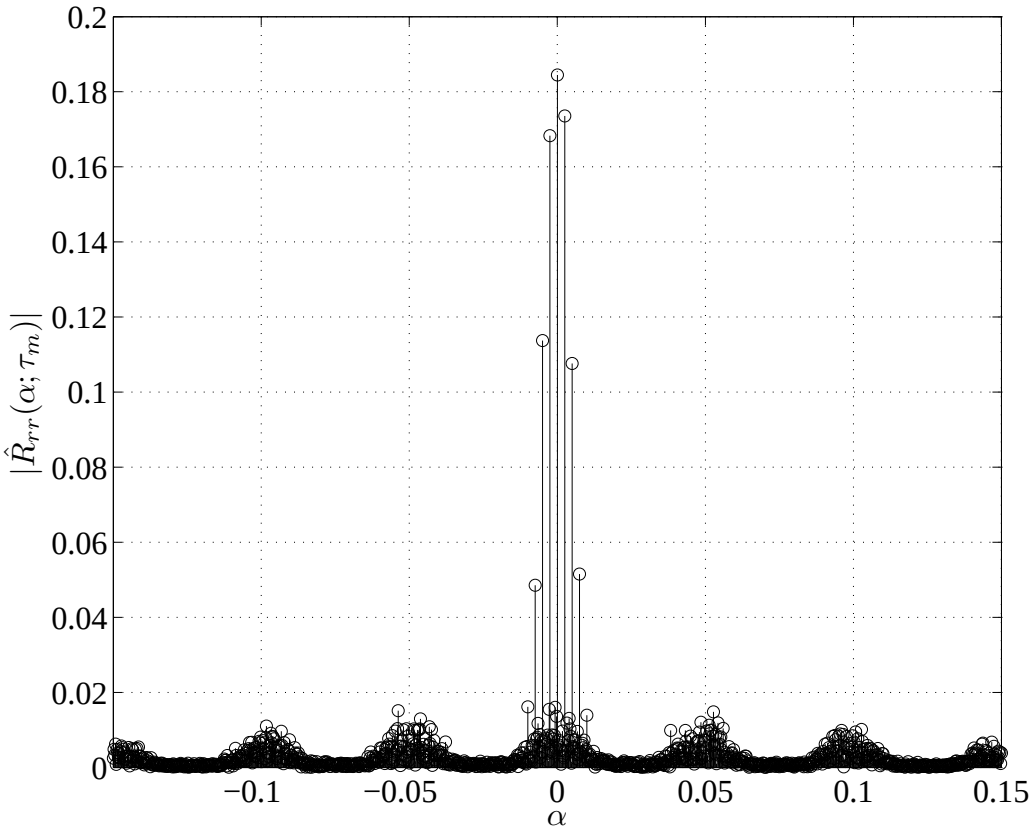

Figure 4.2: The estimated magnitude of the CAF of OFDM signal in time-dispersive channel for different CFs and at delay $\tau = \tau_m$ for 20 dB SNR.

4.4.1 Estimation of Useful Symbol Period

Since the OFDM signal exhibits second-order cyclostationarity at zero CF $(\alpha = 0)$ and at delay $\tau = N_{use}$, a cyclostationarity test [16] is exploited for estimate the useful symbol period. First, the magnitude of the CAF of received discrete time OFDM signal is estimated at $\alpha = 0$ and over a range of positive delay values. The starting value of the delay $\tau_{start} = \varrho K_{min}$, is chosen to cover the possible peaks in the magnitude of the CAF. The K_{min} is the minimum number of subcarriers that we consider and it is assumed to be unknown at the

receive side and a range of possible values are considered based on the OFDM standards. The delay value τ_m, where the CAF magnitude attains a local maximum is chosen. Then, a cyclostationarity test [16] is applied to check whether the $\alpha = 0$ is a CF at delay τ_m. This test consists of calculating a test statistic from the estimated CAF at CF α and at delay τ, and comparing it against a threshold [16][8]. If the calculated test statistic at $\alpha = 0$ and delay τ_m exceeds the threshold, the $\alpha = 0$ is a CF at delay τ_m. Therefore, the useful symbol period can be estimated as $\hat{N}_{use} = \tau_m$.

4.4.2 Estimation of Symbol Period

One can notice that the OFDM signal exhibits second-order cyclostationarity at delay τ_m and at CFs given in (4.10). Therefore, the OFDM symbol period can be estimated by exploiting the non-zero peaks in the magnitude of the CAF at delay $N_{use} = \tau_m$, and over the CF range. First, the magnitude of the CAF is estimated at delay τ_m and over the range of CFs α. Then, a non-zero frequency value α_m where this estimated CAF magnitude achieves a maximum is chosen. This non-zero frequency value corresponds to either N_s^{-1} or $-N_s^{-1}$. This distinguishing feature can be seen from Fig. 4.2. Finally, the cyclostationarity test[8] [16] is applied to check whether the α_m is a CF at τ_m. If the calculated test statistic at frequency α_m and at delay τ_m exceeds the threshold, the α_m is a CF at delay τ_m. Therefore, the OFDM symbol period can be estimated as $\hat{N}_s = |\alpha_m|^{-1}$.

[8]The test description is given in the Appendix C.

4.4.3 Estimation of Number of Subcarriers and the Cyclic Prefix Factor

Once the OFDM symbol period and the useful symbol period are estimated, the number of subcarriers and the cyclic prefix factor can be easily obtained. Since OFDM signal exhibits second-order cyclostationarity at zero CF and at delay $\hat{N}_{use} = \varrho K = \tau_m$, one can easily obtain the number of subcarriers as $\hat{K} = \tau_m \varrho^{-1}$. Furthermore, by exploiting the fact that $\hat{N}_s = |\alpha_m|^{-1}$ and $\hat{N}_{use} = \tau_m$, the cyclic prefix factor can be obtained as $\hat{\kappa} = (1 - (\tau_m |\alpha_m|)^{-1})$.

4.4.4 Estimation of the Carrier Frequency Offset

The frequency offset can also be obtained from the cyclostationary statistics. One can write the CAF of the received OFDM signal at delay τ_m and at CF α as

$$\begin{aligned} R_{rr}(\alpha;\tau_m) = & \frac{\sigma_d^2}{KN_s} e^{-j2\pi\alpha\epsilon N_s} e^{-j2\pi\Delta f_{ne}\tau_m} \\ & \times \sum_n \underbrace{\sum_{l=1}^{L_c} |h(\tau_l)|^2 g(n-\tau_l) g^*(n+\tau_m-\tau_l)}_{g_{g,h}(n;\tau_m)} e^{-j2\pi\alpha n} \Psi_K(\tau_m,\tau_l,\tau_l) \\ & + R_{ww}(\alpha;\tau_m). \end{aligned} \tag{4.11}$$

Note that the contribution of $R_{ww}(\alpha;\tau_m)$ is non-zero only at zero CF. In addition, it can be noticed that for a real valued pulse shape [8], and for any time-dispersive channel, $g_{g,h}(n;\tau_m)$ is a real valued sequence. Therefore, Fourier series of this sequence $G_{g,h}(\alpha;\tau_m) = \sum_n g_{g,h}(n;\tau_m) e^{-j2\pi\alpha n}$, will be Hermitian, i.e. $G_{g,h}(-\alpha;\tau_m) = G^*_{g,h}(\alpha;\tau_m)$ [8]. Therefore, the unwrapped phase of the CAF at CF α and at delay τ_m is given by $\arg\{R_{rr}(\alpha;\tau_m)\} =$

$-j2\pi(\alpha\epsilon N_s + \Delta f_{ne}\tau_m) + \arg\{G_{g,h}(\alpha;\tau_m)\}$. Using the properties of the Hermitian symmetry of $G_{g,h}(\alpha;\tau_m)$, the normalized frequency offset, Δf_{ne} of the received OFDM signal in time-dispersive channel can be estimated as

$$\Delta f_{ne} = \frac{1}{2\pi\tau_m} \arg\{R_{rr}(\alpha;\tau_m)R_{rr}(-\alpha;\tau_m)\}. \tag{4.12}$$

Note that the carrier frequency offset estimation proposed in [5] required prior knowledge of the pulse shape. However, our proposed method obviates the estimation of the pulse shape and the channel while estimating the carrier frequency offset.

4.5 Numerical Results

Simulations are performed to test the performance of the OFDM parameter estimators under different scenarios. The simulations parameters are set as follows. OFDM signal bandwidth of 20 MHz is considered. Number of subcarriers is set to 64, the symbol period and the cyclic prefix period are set to 4 μs and 0.8 μs, respectively. A raised cosine pulse shaping window with 0.025 roll-off factor is used at the transmit side [3]. The transmitted data symbols are generated from 64-QAM constellation with unit variance. The oversampling factor is set to five. The normalized carrier frequency offset is set to 0.1, $\Delta\phi$ and ϵ are generated as a uniformly distributed random variable over the ranges of $[-\pi, \pi)$, and $[0, 1)$, respectively. The ITU-R frequency selective indoor, pedestrian and vehicular A channel models are considered [18]. The SNR considered is the ratio between the received signal power and the noise power at the output of the receive low-pass filter. Simulation results are obtained from 1000 independent trials.

In Fig. 4.3, the probability of correct estimation (P_{ce}) of OFDM symbol period versus

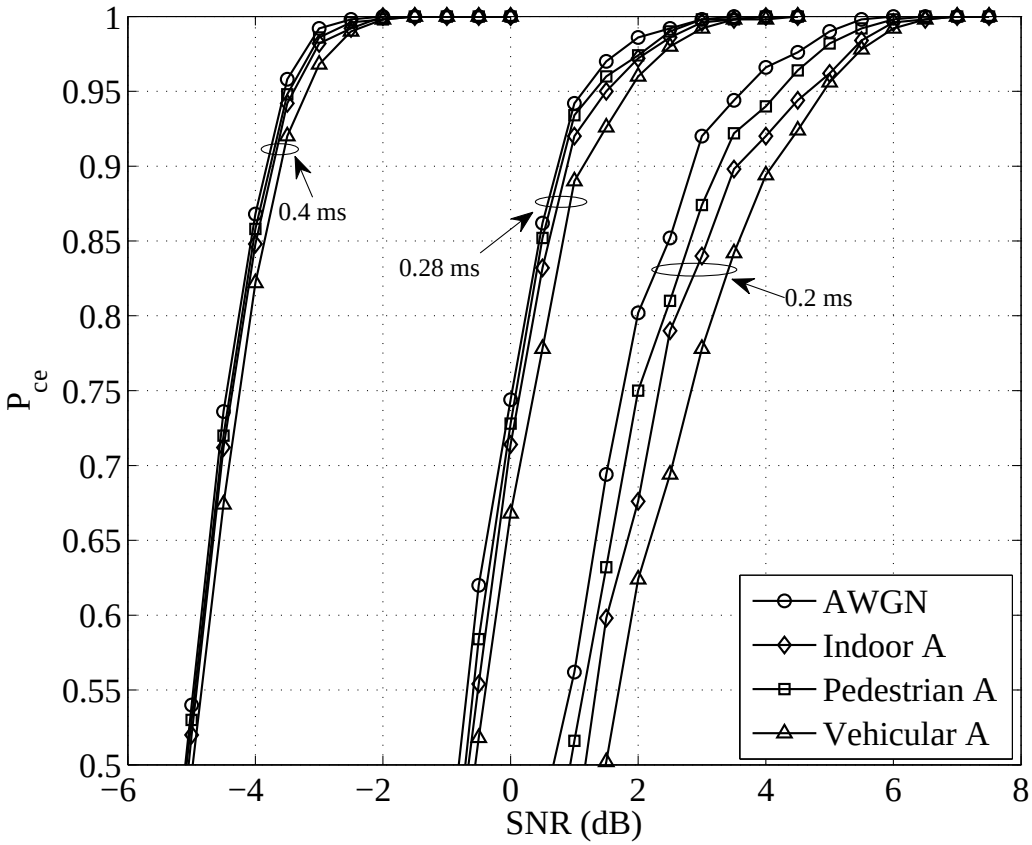

Figure 4.3: The P_{ce} of OFDM symbol period versus SNR for different observation intervals.

SNR is plotted for different observation intervals and for different channel conditions. It can be seen from Fig. 4.3 that for all three observation intervals, the simulation performance is similar for indoor, pedestrian, and AWGN channels, however, falls off in the vehicular channel. Furthermore, as the number of OFDM symbols increased the P_{ce} is also improved. This can be easily explained, as the number of samples increases at the receive side, a better estimate of a test statistic is available for the cyclostationarity test. The result presented in this work out performs the results in [7].

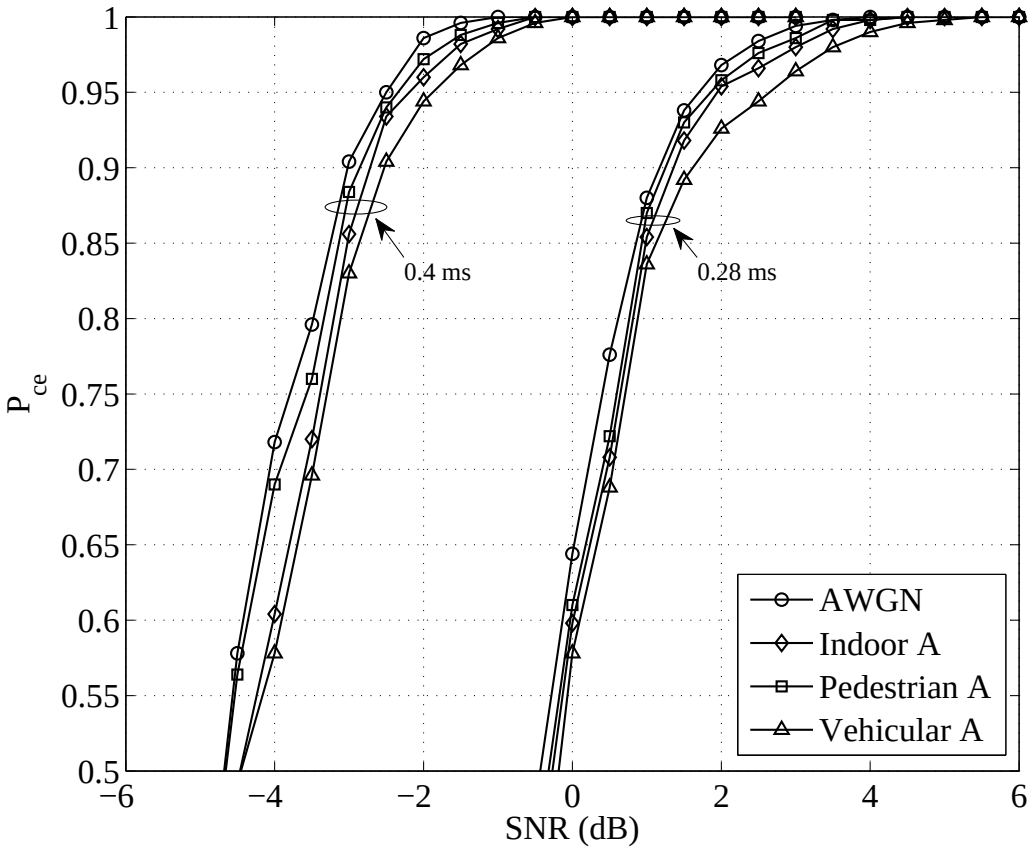

Figure 4.4: The P_{ce} of useful symbol period versus SNR for different observation intervals.

In Fig. 4.4 P_{ce} of useful symbol period versus SNR is presented for different observation intervals and for different channel conditions. It can be noticed from Fig. 4.4 that the P_{ce} performance is similar to the P_{ce} performance of the symbol period. It is apparent from Fig. 4.4 that the P_{ce} of useful symbol period reaches one for all channel conditions at 0 dB and 5 dB for the 0.4 ms and 0.28 ms observation intervals, respectively. In addition, Fig. 4.3 indicates that the P_{ce} of symbol period reaches one for all channel conditions at -2 dB, 3.5 dB and 6.5 dB for the 0.4 ms, 0.28 ms and 0.2 ms observation intervals, respectively. According to these results we can notice that better performance can be achieved even with

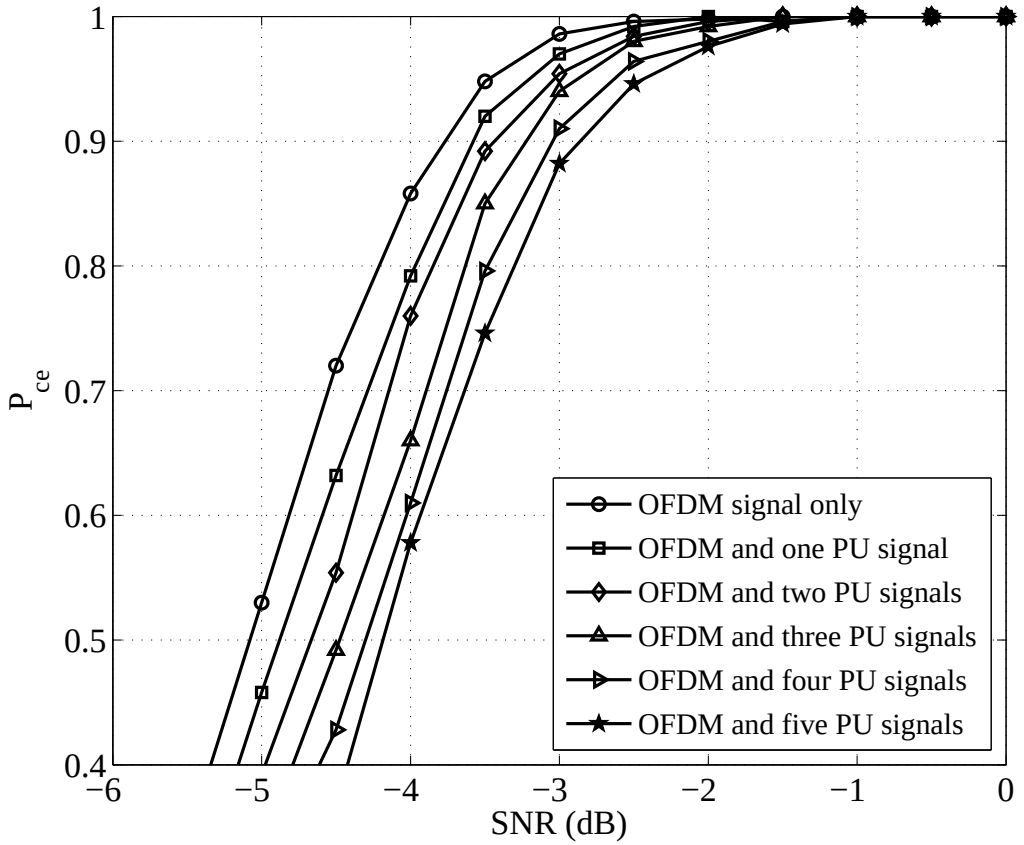

Figure 4.5: The P_{ce} of OFDM symbol period versus SNR for the pedestrian A channel with the presence of NBI.

the short observation intervals.

In Fig. 4.5 the P_{ce} of OFDM symbol period versus SNR is presented for pedestrian A channel when there exist the narrow band interference (NBI) from the other active primary users (PUs) in the network. We consider the BPSK, QPSK, 8-PSK, 8-QAM, 16-QAM, and 64-QAM modulations for the PU signal generation. From Fig. 4.5 we can notice that a small performance degradation due to the presence of NBI. However, the proposed blind estimation scheme is still able to achieve better performance even at low SNR values. In

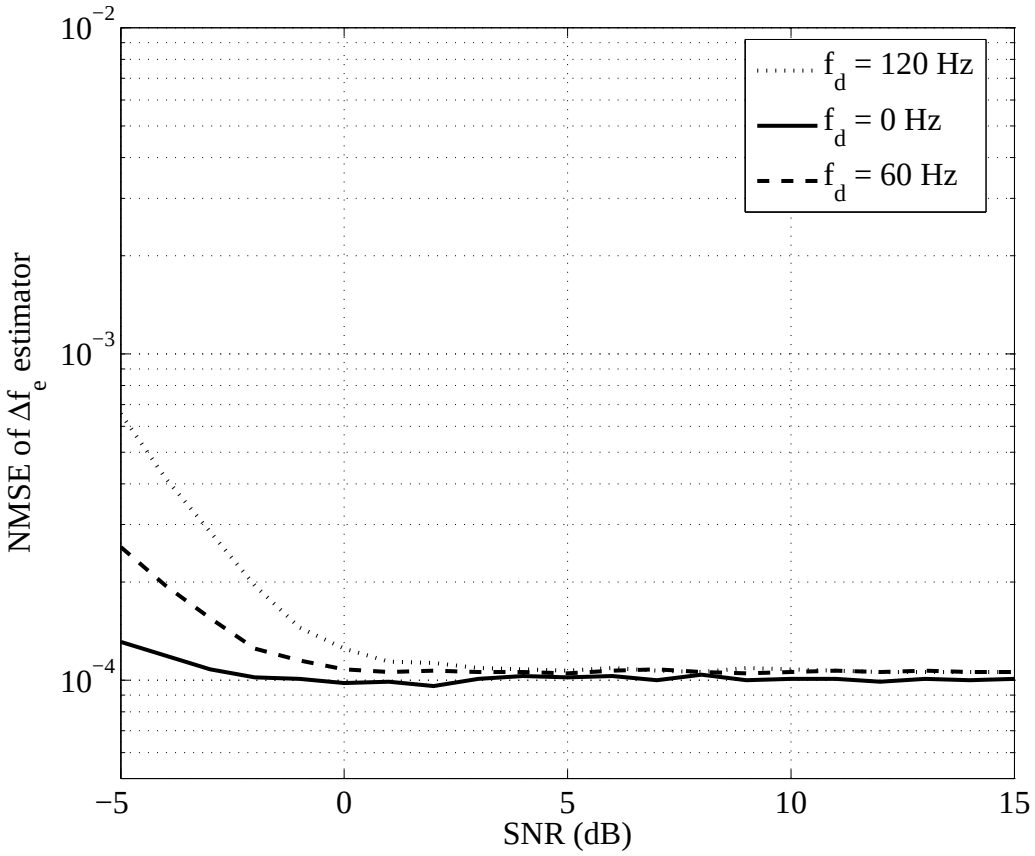

Figure 4.6: NMSE of Δf_e estimator versus SNR for different Doppler frequency (f_d) values.

Fig. 4.6 the normalized mean square error (NMSE) versus SNR for the frequency offset estimator is presented for different Doppler frequency values. It is apparent from the Fig. 4.6 that the frequency offset estimator is quite robust to Doppler frequency even for low SNR values. Fig. 4.7 shows the average bit error rate (BER) performance of 16-QAM OFDM in AWGN and Pedestrian A channels. Solid lines represent the BER results assuming perfect synchronization at the receiver and dashed lines represent the BER results when the receiver employ the proposed parameter estimation algorithm. From Fig. 4.7 we can notice

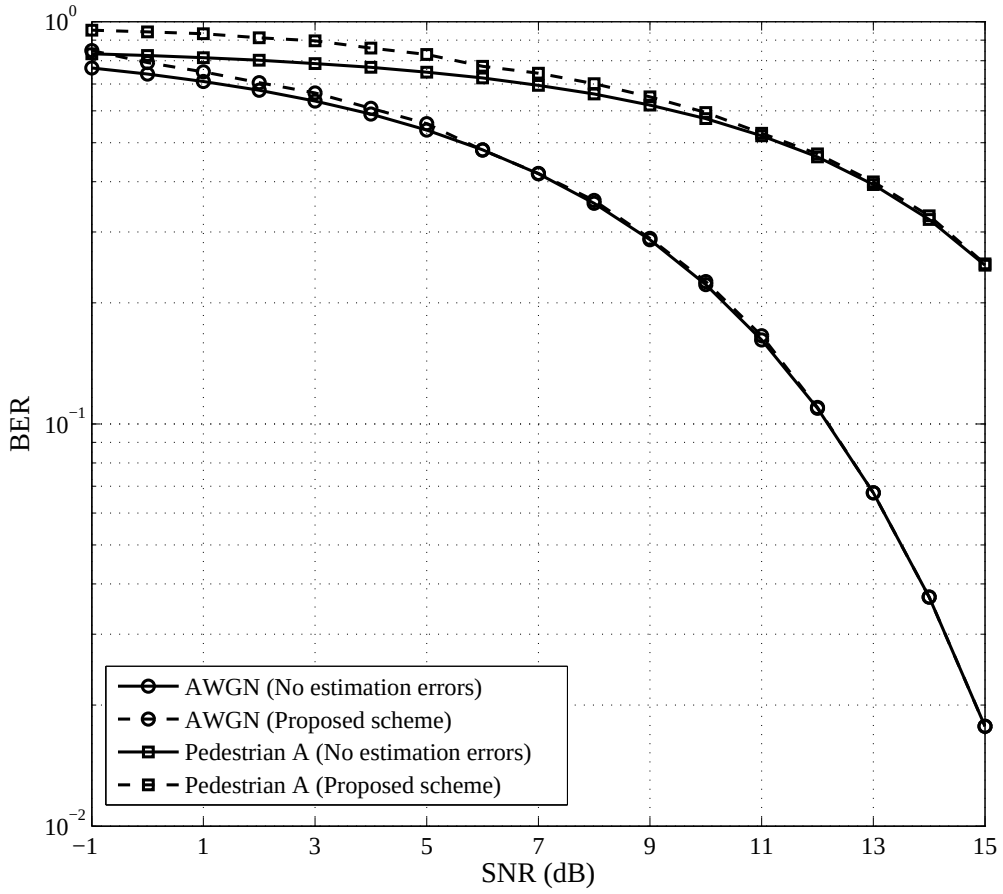

Figure 4.7: BER of 16-QAM OFDM in AWGN and Pedestrian A channels.

that the proposed scheme converges to the no estimation error scheme at high SNR values for both the channel conditions. In addition, AWGN channel performance is better than the Pedestrian A channel as expected. The effect of OFDM parameter estimation errors have detrimental effect on the BER at lover SNR values for both the channel conditions.

4.6 Conclusion

A blind parameter extraction algorithm is proposed for orthogonal frequency division multiplexing (OFDM) signals by considering a comprehensive signal model that takes into account a time-dispersive channel, additive Gaussian noise and other OFDM synchronization parameters. The proposed algorithm extracts some vital OFDM parameters that are necessary for blind demodulation of OFDM signals. A cyclostationarity-based approach is exploited for estimate these OFDM parameters. Simulation results indicate that the proposed algorithm performs well even at relatively low signal to noise ratios in frequency selective fading channels with short observation intervals. This proposed algorithm will play a significant role in cognitive radios, where the radio dynamically changes its fundamental operating parameters in hostile wireless channels.

Bibliography

[1] J. Mitola III, "Cognitive radio for flexible mobile multimedia communications," *Proc. IEEE Int. Work. MoMuC*, pp. 3-10, Nov. 1999.

[2] S. Haykin, "Cognitive radio: Brain-empowered wireless communications," *IEEE J. Sel. Areas Commun.*, vol. 23, no. 2, pp. 201-220, Feb. 2005.

[3] R. V. Nee and R. Prasad, *OFDM Wireless Multimedia Communications*, Artech House, 2000.

[4] T. Weiss and F. K. Jondral, "Spectrum pooling: An innovative strategy for the enhancement of spectrum efficiency," *IEEE Commun. Mag.*, vol. 43, no. 3, pp. S8-S14, Mar. 2004.

[5] H. Bolcskei, "Blind estimation of symbol timing and carrier frequency offset in wireless OFDM systems," *IEEE Trans. Commun.*, vol. 49, no. 6, pp. 988-999, Jun. 2001.

[6] M. Shi, Y. Bar-Ness, and W. Su, "Blind OFDM systems parameters estimation for software defined radio," *Proc. IEEE DySPAN*, pp. 119-122, Apr. 2007.

[7] H. Ishii and G. W. Wornell, "OFDM blind parameter identification in cognitive radio," *Proc. IEEE PIMRC*, pp. 700-705, Sep. 2005.

[8] M. Shi, Y. Bar-Ness, and W. Su, "Revisiting the timing and frequency offset estimation based on cyclostationarity with new improved method," *IEEE Commun. Letters*, vol. 13, no. 7, pp. 537-539, Jul. 2009.

[9] H. Li, Y. Bar-Ness, A. Abdi, O. S. Somekh, and W. Su, "OFDM modulation classification and parameter extraction," *Proc. IEEE CROWCOM*, pp. 1-6, Jun. 2006.

[10] O. A. Dobre, A. Punchihewa, S. Rajan, and R. Inkol, "On the cyclostationarity of OFDM and single carrier linearly digitally modulated signals in time dispersive channels with applications to modulation recognition," *Proc. IEEE WCNC*, pp. 1284 -1289, Apr. 2008.

[11] A. Punchihewa, O. A. Dobre, Q. Zhang, S. Rajan, and R. Inkol, "The nth-order cyclostationarity of OFDM signals in time dispersive channels," *Proc. IEEE ACSSC*, pp. 574-580, Oct. 2008.

[12] R. W. Heath Jr. and G. B. Giannakis, "Exploiting input cyclostationarity for blind channel identification in OFDM systems," *IEEE Trans. Sig. Proc.*, vol. 47, no. 3, pp. 848-856, Mar. 1999.

[13] C. M. Spooner and W. A. Gardner, "The cumulant theory of cyclostationarity time-series. I: Foundation," *IEEE Trans. Sig. Proc.*, vol. 42, no. 12, pp. 3387-3408, Dec. 1994.

[14] C. M. Spooner and W. A. Gardner, "The cumulant theory of cyclostationarity time-series. II: Development and applications," *IEEE Trans. Sig. Proc.*, vol. 42, no. 12, pp. 3409-3429, Dec. 1994.

[15] A. Napolitano, "Cyclic higher-order statistics: input/output relations for discrete- and continuous-time MIMO linear almost- periodically time-variant systems," *IEEE Trans. Sig. Proc.*, vol. 42, no. **xx**, pp. 3409-3429, 1995.

[16] A. V. Dandawate and G. B. Giannakis, "Statistical test for presence of cyclostationarity," *IEEE Trans. Sig. Proc.*, vol. 42, no. 9, pp. 2355-2369, Sep. 1994.

[17] Y. Gu and K. Q. Liao, "An efficient detector for TCM signals transmitted over unknown time-dispersive channels," *Proc. IEEE ICC*, vol. 42, no. 9, pp. 1717-1721, May. 1994.

[18] A. F. Molisch, *Wireless Communications*, 1st. ed. John Wiley, 2005.

Chapter 5

Conclusions and Suggestions for Future Research

In this chapter, we summarize the main contributions and the results obtained in this research study. Furthermore, the directions for future research are also presented.

5.1 Conclusions

In this thesis, we have considered the design of advanced transceiver algorithms for cognitive radio (CR) physical layer with the intention of improving the error rate performance and the throughput. These proposed algorithms will play a significant role in CR, where the radio dynamically changes its fundamental operating parameters in hostile wireless channels. In particular, we have made the following major contributions in this thesis.

First, we have designed a linear precoder for orthogonal space-time block coded orthogonal frequency division multiplexing-based multiple-input multiple-output (MIMO) antenna cognitive radio (CR) when operating in a correlated Rayleigh fading channel. The CR coexists with the primary user (PU) network by opportunistically sharing the originally allocated PU spectrum in correlated Rayleigh fading channels. Theoretical analysis and the proposed linear precoder in this work are based on a comprehensive signal model that takes

into account of multiple antennas at both SUs and PUs, multi-carrier transmission scheme and the correlation effect at SU's both transmit and receive antennas. The optimum linear precoder with respect to error probability performance is obtained by exploiting the partial channel information in the form of transmit and receive correlation matrices at the CR transmitter and by minimizing an upper bound on the average pairwise error probability, while imposing a set of per subcarrier transmit power constraints at the CR transmitter and a set of interference power constraints specified by the PUs. The proposed solution is based on the eigen-beamforming. For this scenario, the linear precoder functions as a multi-mode beamformer based on the knowledge of the transmit and receive correlation matrices of the MIMO channels between the SU transmitter and the SU receiver and between the SU transmitter and the PU receivers. We have shown that the precoder design problem with these constraints is convex and have proposed a Lagrange dual-decomposition-based efficient algorithm to obtain the optimal precoders. Furthermore, the individual effects of the transmit and/or receive correlation on the linear precoder design for CR were investigated. The current study further reveals that for uncorrelated CR transmit antennas, the precoder consists of equally weighted diagonal elements. Simulation results illustrate that the proposed linear precoder outperforms uniform power loaded systems in a correlated MIMO channel even with the presence of additional interference power constraints.

Second, we have proposed a robust power allocation policy for the opportunistic spectrum sharing CR multiple access channel. In this work, we have considered the channel estimation errors at both the set of channels between SU transmitters to the SU receiver and the channels between the SUs transmitters to the PUs receivers. This represents a practical scenario, where there exist channel estimation errors. We have proposed an optimum power allocation policy by maximizing a lower-bound on the sum capacity while

imposing CR transmitter's total transmit power constraint and the set of interference power constraints specified by set of PU receivers under the channel estimation errors. The Lagrange dual-decomposition based efficient algorithm is derived to obtain the optimal allocation policy for each SU transmitter. Simulation results illustrate that the effect of channel estimation errors when compared with no errors.

Third, we have proposed a blind OFDM parameter estimation algorithm for CR when operating in time-dispersive channel. Unlike the previous studies for blind estimation of OFDM parameters, in this work we have considered a comprehensive signal model that takes into account a time-dispersive channel, initial phase, timing offset, carrier frequency offset and additive Gaussian noise. The proposed algorithm extract OFDM parameters such as symbol period, useful symbol period, number of subcarriers, cyclic prefix factor and carrier frequency offsets. Second-order cyclostationarity-based approach is exploited to estimate these OFDM parameters. Simulation results indicates that the proposed algorithm performs well even at relatively low signal to noise ratios (SNR) in frequency selective fading channels with short observation intervals. Since CR changes its parameters dynamically in order to adapt to its surrounding environment, our proposed algorithm can be exploited to blindly estimate and demodulate the received OFDM signal. Thus, the CR transmitter will not have to use a separate frequency band to send its synchronization parameters, which are necessary to demodulate the received signal. Furthermore, the effective SNR at the receive side can be improved by properly estimating these synchronization parameters of the received OFDM signal. This allows CR systems to support higher throughput with the help of higher order modulations.

5.2 Suggested Future Research Directions

Following represents possible extensions to the research studies presented in this thesis.

- In Chapter 2, we proposed a linear precoder for OSTBC MIMO-OFDM based CR to improve the system error performance in frequency-flat correlated Rayleigh fading channels. However, space-time block codes, which were originally designed for frequency-flat fading channels, cannot yield inherent frequency diversity of the channel. Hence, space-frequency codes (SFC), which are capable of achieving maximum diversity have been developed for OFDM systems [1]. Therefore, a possible extension of this work is to design a linear precoder for SFC MIMO-OFDM-based CR systems, when operating in frequency-selective correlated Rayleigh fading channels. The precoder design optimization problem for this scenario can be formulated by minimizing an upper bound on the average pairwise error probability constrained to the similar set of constraints as in Chapter 2. In addition to the interference-limitation, interference cancelation is also a key technology to enable coexisting systems. For conventional MIMO systems, zero-forcing criteria has been exploited in MIMO-broadcast channel (MIMO-BC) when designing downlink precoding [2, 3], which removes any co-channel interference between users. Therefore, another possible extension would be an interference cancelation approach such as transmit zero-forcing (TxZF) to design precoder for MIMO-OFDM-based CR system.

- Spatial multiplexing-based MIMO-OFDM systems, involving smart processing in both the spatial and frequency domains have been proposed in future wireless systems, such as WiFi and WiMAX. These systems operate in unlicensed frequency bands. In addition to these existing systems, CR will also coexist in these unlicensed

bands [4]. Since, CRs and conventional radios are coexist in the same frequency bands in future wireless networks, it is necessary to implement advanced transceiver algorithms for spatial multiplexing based CR systems to improve the performance while minimizing the interference to conventional radios. Therefore, another possible extension of our work is to design of linear precoder and decoder for spatial multiplexing-based MIMO-OFDM CR systems. For a linear minimum mean-square-error (MSE) receiver, design criteria will be the minimization of the symbol MSE under the CR transit power and a set of interference power thresholds on the PUs. Then, this design criteria can be extended for the scenarios when CR employs a linear zero-forcing receiver and a maximum likelihood receiver. This design criteria can be first developed for a uncorrelated Rayleigh fading channels and then can be extended to the correlated Rayleigh fading channels.

- In Chapter 2, we assumed that perfect partial channel state information (CSI) is available at the SU transmitter. However, obtaining an accurate estimate of the channel parameters is difficult in rapidly time-varying channel conditions. In [5], a precoder is designed for conventional single-carrier systems, when the transmitter has the partial but not perfect knowledge about the channel. Thus, another possible extension of our work is to design of a linear precoder for OSTBC MIMO-OFDM based CR system when the imperfect partial CSI is available at the CR transmitter. Channel mean and covariance estimation errors can be incorporate into the precoder design problem.

- In Chapter 3, we considered design of an optimal power allocation scheme for opportunistic spectrum sharing SISO MAC with imperfect channel estimates. In a future

research, design of optimum power allocation schemes for opportunistic spectrum sharing MIMO MAC and MIMO broadcast channel with imperfect channel estimates can be addressed. Furthermore, it can be assumed that no statistical knowledge about the channel estimation errors are available at the base station but error norm is bounded by a spherical or ellipsoid region [6, 7]. In previous studies this spherical or ellipsoid error model has been exploited to characterize the errors originated by estimation and quantization [6, 7].

- The cooperative communication has been an active research area recently [8–10]. Specialized relay stations (RSs) can be installed in the network to facilitate cooperative communication. In addition to improving throughput and coverage, cooperative communication can improve the energy saving performance at the mobile devices, increase reliability in transmission, and decrease the overall interference in the network [11, 12]. With these attractive features, the relay-based communication will form an integral part in future wireless standards. Therefore, combination of cooperative communication and CR will further improve the spectrum efficiency. In practice, the amplify-and-forward (AF) relaying is often preferable than the decode-and-forward relaying due to its simpler processing at the relay station. In future research, design of linear precoders for OFDM-based cooperative CR when the AF relay stations employing multiple antennas can be considered. For this scenario, the precoders have to be designed for the CR transmitter as well as the AF relay station for each OFDM subcarrier. This design can be first carried out considering a single AF relay station and then generalize the precoder design with multiple AF relay stations.

Bibliography

[1] H. Bolcskei and A. J.Paulraj, "Space-frequency coded broadband OFDM systems," in *Proc. IEEE WCNC*, Sep. 2000, pp. 1-6.

[2] Q. H. Spencer, A. L. Swindlehurst, and M. Haardt, "Zero-forcing methods for downlink spatial multiplexing in multiuser MIMO channels," *IEEE Trans. Signal Proc.*, vol. 52, no. 2, pp. 461-471, Feb. 2004.

[3] P. Tejera, W. Utschick, G. Bauch, and J. A. Noessek, "A novel decomposition technique for multiuser MIMO," in *Proc. Int. ITG Workshop on Smart Antennas*, Apr. 2005.

[4] M. Sherman, A. N. Mody, R. Martinez, C. Rodriguez, and R. Reddy, "IEEE standards supporting cognitive radio and networks, dynamic spectrum access, and coexistence," *IEEE Commun. Mag.*, vol. 46, no. 7, pp. 72-79, Jul. 2008.

[5] G. Jongren, M. Skoglund, and B. Ottersten, "Combining beamforming and orthogonal space-time block coding," *IEEE Trans. Info. Theory*, vol. 48, no. 3, pp. 611-627, Mar. 2002.

[6] T. Q. S. Quek, H. Shin, and M. Z. Win, "Robust wireless relay networks: Slow power allocation with guaranteed QoS," *IEEE J. Selected Topics in Signal Processing*, vol. 1, no. 4, pp. 700-713, Dec. 2007.

[7] M. Botros and T. N. Davidson, "Convex conic formulations of robust downlink precoder designs with quality of service constraints," *IEEE J. Selected Topics in Signal Processing*, vol. 1, no. 4, pp. 714-724, Dec. 2007.

[8] A. Sendonaris, E. Erkip, and B. Aazhang, "User cooperation diversity. Part I. System description," *IEEE Trans. Commun.*, vol. 51, no. 11, pp. 1927-1938, Nov. 2003.

[9] A. Sendonaris, E. Erkip, and B. Aazhang, "User cooperation diversity. Part II. Implementation aspects and performance analysis," *IEEE Trans. Commun.*, vol. 51, no. 11, pp. 1939-1948, Nov. 2003.

[10] J. Laneman, D. Tse, and G. Wornell, "Cooperative diversity in wireless networks: Efficient protocols and outage behavior," *IEEE Trans. Inform. Theory*, vol. 50, no. 12, pp. 3062-3080, Dec. 2004.

[11] M. Gastpar and M. Vetterli, "On the capacity of wireless networks: The relay case," in *Proc. INFOCOM*, Nov. 2002, pp. 1577-1586.

[12] R. U. Nabar, H. Bolcskei, and F. W. Kneubuhler, "Fading relay channels: Performance limits and space-time signal design," *IEEE J. Select. Areas Commun.*, vol. 22, no. 6, pp. 1099-1109, Aug. 2004.

Appendix A

Proof of the Theorems 2.1, 2.2 and 2.4[9]

A.1 Proof of the Theorem 2.1

An upper bound of the average PEP of OSTBC MIMO-OFDM, when the SU's transmit and receive antennas are correlated is derived here. Applying the Chernoff bound to (2.8), a tight upper bound on the PEP conditioned on channel matrices $\mathbf{H}_{ss}(k),\ k = 1, \ldots, K$, can be obtained as [38]

$$P(\mathbf{C}_i \rightarrow \mathbf{C}_j | \mathbf{H}_{ss}(1), \ldots, \mathbf{H}_{ss}(K)) \leq \frac{1}{2} \exp^{\frac{-\mathbf{d}^2(\mathbf{C}_i - \mathbf{C}_j)}{2}}, \tag{A.1}$$

where

$$\mathbf{d}^2(\mathbf{C}_i - \mathbf{C}_j) = \sum_{k=1}^{K} \frac{1}{2\sigma_n^2} \left\| \mathbf{H}_{ss}(k)\mathbf{F}(k)(\tilde{\mathbf{C}}_i(k) - \tilde{\mathbf{C}}_j(k)) \right\|^2, \tag{A.2}$$

is the Euclidian distance between two codeword matrices. Due to the orthogonality of the codeword error product matrix, $\mathbf{E}(k) = \tilde{\mathbf{C}}_i(k) - \tilde{\mathbf{C}}_j(k)$, OSTBC has the appealing property that $\mathbf{E}(k)\mathbf{E}(k)^\dagger = \mu_{ij}(k)\mathbf{I}_{M_{st}},\ k = 1, \ldots, K$, where $\mu_{ij}(k)$ is the codeword distance that depends on the two codewords $\tilde{\mathbf{C}}_i(k)$ and $\tilde{\mathbf{C}}_j(k)$. Therefore, exploiting these properties and the standard relations, $Tr\{\mathbf{AB}\} = \text{vec}(\mathbf{A}^\dagger)^\dagger \text{vec}(\mathbf{B})$ and $\text{vec}(\mathbf{ABC}) = (\mathbf{C}^\dagger \otimes \mathbf{A})\text{vec}(\mathbf{B})$ for

[9]Note that the references related to this Appendix are given in the bibliography section of the Chapter 2.

any arbitrary matrices **A**, **B**, and **C** [39], the conditional PEP of OSTBC can be written as

$$\begin{aligned} &P(\mathbf{C}_i \rightarrow \mathbf{C}_j|\mathbf{H}_{ss}(1),\ldots,\mathbf{H}_{ss}(K)) \\ &\qquad \leq \frac{1}{2}\exp^{\sum_{k=1}^{K}\frac{-\mu_{ij}(k)}{4\sigma_n^2}\text{vec}(\mathbf{H}_{ss}(k)^\dagger)^\dagger(\mathbf{I}_{M_{sr}}\otimes\mathbf{F}(k)\mathbf{F}(k)^\dagger)\text{vec}(\mathbf{H}_{ss}(k)^\dagger)}. \end{aligned} \tag{A.3}$$

An upper bound on the average PEP of OSTBC can then be obtained by taking the expectation of (A.3) with respect to $\mathbf{H}_{ss}(k)$, $k = 1,\ldots,K$, as

$$\begin{aligned} P(\mathbf{C}_i \rightarrow \mathbf{C}_j) \leq &\int \exp^{\frac{-\mu_{ij}(1)}{4\sigma_n^2}\tilde{\mathbf{h}}(1)^\dagger\left(\mathbf{I}_{M_{sr}}\otimes\mathbf{F}(1)\mathbf{F}(1)^\dagger\right)\tilde{\mathbf{h}}(1)} p(\tilde{\mathbf{h}}(1))d\tilde{\mathbf{h}}(1)\times\ldots \\ &\times\int \exp^{\frac{-\mu_{ij}(K)}{4\sigma_n^2}\tilde{\mathbf{h}}(K)^\dagger\left(\mathbf{I}_{M_{sr}}\otimes\mathbf{F}(K)\mathbf{F}(K)^\dagger\right)\tilde{\mathbf{h}}(K)} p(\tilde{\mathbf{h}}(K))d\tilde{\mathbf{h}}(K), \end{aligned} \tag{A.4}$$

where $\tilde{\mathbf{h}}(k) = \text{vec}(\mathbf{H}(k)^\dagger)$, $k = 1,\ldots,K$. Note that the probability distribution function (pdf) of the MIMO channel for the kth subcarrier is a complex Gaussian and can be written as $p(\tilde{\mathbf{h}}(k)) = \frac{1}{\pi^{M_{sr}M_{st}}\det[\tilde{\mathbf{R}}_{ss}(k)]}\exp^{-\tilde{\mathbf{h}}^\dagger(k)\tilde{\mathbf{R}}_{ss}^{-1}(k)\tilde{\mathbf{h}}(k)}$, where $\tilde{\mathbf{R}}_{ss}(k) = \mathbf{R}_{rx,ss}(k)\otimes\mathbf{R}_{tx,ss}(k)$, $k = 1,\ldots,K$, is the covariance matrix of $\tilde{\mathbf{h}}(k)$. Therefore, an upper bound on the average PEP can be rewritten as

$$\begin{aligned} &P(\mathbf{C}_i \rightarrow \mathbf{C}_j) \\ &\leq \frac{1}{\pi^{M_{sr}M_{st}}\det[\tilde{\mathbf{R}}(k)]}\int \exp^{-\tilde{\mathbf{h}}(1)^\dagger\left(\left(\mathbf{I}_{M_{sr}}\otimes\frac{\mu_{ij}(1)}{4\sigma_n^2}\mathbf{F}(1)\mathbf{F}(1)^\dagger\right)+\mathbf{R}_{ss}^{-1}(1)\right)\tilde{\mathbf{h}}(1)} d\tilde{\mathbf{h}}(1)\times\ldots \\ &\times\frac{1}{\pi^{M_{sr}M_{st}}\det[\tilde{\mathbf{R}}(k)]}\int \exp^{-\tilde{\mathbf{h}}(K)^\dagger\left(\left(\mathbf{I}_{M_{sr}}\otimes\frac{\mu_{ij}(K)}{4\sigma_n^2}\mathbf{F}(K)\mathbf{F}(K)^\dagger\right)+\mathbf{R}_{ss}^{-1}(K)\right)\tilde{\mathbf{h}}(K)} d\tilde{\mathbf{h}}(K). \end{aligned} \tag{A.5}$$

The integrals in (A.5) can be easily solved by making use of the fact that
$\frac{1}{\pi^{M_{sr}M_{st}}\det[\mathbf{\Phi}^{-1}(k)]}\int\exp^{-\tilde{\mathbf{h}}(k)^\dagger\mathbf{\Phi}(k)\tilde{\mathbf{h}}(k)}d\tilde{\mathbf{h}}(k)$, where
$\mathbf{\Phi}(k) = \frac{\mu_{ij}(k)}{4\sigma_n^2}((\mathbf{I}_{M_{sr}}\otimes\mathbf{F}(k)\mathbf{F}(k)^\dagger)+\tilde{\mathbf{R}}_{ss}^{-1}(k))$, $k = 1,\ldots,K$, is the integral of a complex Gaussian pdf and thus equals one. Therefore, an upper bound on the average PEP of the

OSTBC MIMO-OFDM can be written as

$$P(\mathbf{C}_i \to \mathbf{C}_j) \leq \prod_{k=1}^{K} \left\{ \det \left[\mathbf{I}_{M_{sr}M_{st}} + \frac{\mu_{ij}(k)}{4\sigma_n^2} (\mathbf{I}_{M_{sr}} \otimes \mathbf{F}(k)\mathbf{F}(k)^\dagger)(\mathbf{R}_{rx,ss}(k) \otimes \mathbf{R}_{tx,ss}(k)) \right] \right\}^{-1}. \quad \text{(A.6)}$$

It can be noticed from (A.6) that the dependence on the codeword pair is now only through the codeword distance $\mu_{ij}(k)$s. Furthermore, we can notice that the (A.6) is a decreasing function of $\mu_{ij}(k)$s and PEP is dominated by the codeword pairs corresponding to minimum $\mu_{ij}(k)$. Consequently, only one such pair is considered in the linear precoder optimization procedure, i.e., $\mu_{min} = \min_{\mu_{ij}(k), i \neq j}\{\mu_{ij}(k)\mathbf{I}_{M_{st}} = (\tilde{\mathbf{C}}_i(k) - \tilde{\mathbf{C}}_j(k)(\tilde{\mathbf{C}}_i(k) - \tilde{\mathbf{C}}_j(k))^\dagger\}$, $k = 1, \ldots, K$. The μ_{min} depends on several factors, such as the modulation format of the input signal constellation, the variance of the input signal constellation and the OSTBC generator matrix $\mathbf{G}_{\text{OSTBC}}$ [5]. For example $\mu_{min} = \kappa d_{min}^2$, where the factor κ depends on the OSTBC generator matrix $\mathbf{G}_{\text{OSTBC}}$ [5], and $d_{min}^2 = 4\sigma_s^2 \sin\frac{\pi}{M}$ for M-PSK, $d_{min}^2 = \frac{6\sigma_s^2}{M-1}$ for M-QAM, $d_{min}^2 = \frac{12\sigma_s^2}{M^2-1}$ for M-PAM. Therefore, using this property of OSTBC, the equality $(\mathbf{A} \otimes \mathbf{B})(\mathbf{C} \otimes \mathbf{D}) = (\mathbf{AC}) \otimes (\mathbf{BD})$, and the eigen-decomposition of $\mathbf{R}_{tx,ss}(k) = \mathbf{U}_{tx,ss}(k)\mathbf{\Lambda}_{tx,ss}(k)\mathbf{U}_{tx,ss}(k)^\dagger$, $\mathbf{R}_{rx,ss}(k) = \mathbf{U}_{rx,ss}(k)\mathbf{\Lambda}_{rx,ss}(k)\mathbf{U}_{rx,ss}(k)^\dagger$, $k = 1, \ldots, K$, an upper bound on the average PEP in (A.6) can be rewritten as

$$P(\mathbf{C}_i \to \mathbf{C}_j) \leq \prod_{k=1}^{K} \left\{ \det \left[\mathbf{I}_{M_{st}M_{sr}} + \eta \mathbf{\Lambda}_{rx,ss}(k) \otimes \mathbf{\Lambda}_{tx,ss}^{1/2}(k)^\dagger \tilde{\mathbf{F}}(k) \mathbf{\Lambda}_{tx,ss}^{1/2}(k) \right] \right\}^{-1}, \quad \text{(A.7)}$$

where $\eta = \frac{\mu_{min}}{4\sigma_n^2}$; $\tilde{\mathbf{F}}(k) = \mathbf{F}(k)\mathbf{F}(k)^\dagger$; and $\mathbf{U}_{tx,ss}(k)$, $\mathbf{U}_{rx,ss}(k)$ are the matrices of the eigenvectors; and $\mathbf{\Lambda}_{tx,ss}(k)$, $\mathbf{\Lambda}_{rx,ss}(k)$ are the diagonal eigenvalue matrices of the SU's transmit and receive correlation matrices, respectively. Using the properties of Kroneker

product, one can easily write $\det\left[\boldsymbol{\Upsilon}(k)\right] = \det\left[\mathbf{I}_{M_{st}M_{sr}} + \eta\boldsymbol{\Lambda}_{rx,ss}(k) \otimes \tilde{\mathbf{F}}(k)\boldsymbol{\Lambda}_{tx,ss}(k)\right]$ as

$$\det\left[\boldsymbol{\Upsilon}(k)\right] = \det\begin{bmatrix} \mathbf{I}_{M_{st}} + \eta\lambda_{rx,ss}(k)_1\boldsymbol{\Phi}(k) & \cdots & 0 \\ \vdots & \ddots & \vdots \\ 0 & \cdots & \mathbf{I}_{M_{st}} + \eta\lambda_{rx,ss}(k)_{M_{sr}}\boldsymbol{\Phi}(k) \end{bmatrix}, \quad \text{(A.8)}$$

where $\boldsymbol{\Phi}(k) = \tilde{\mathbf{F}}(k)\boldsymbol{\Lambda}_{tx,ss}(k)$. Furthermore, by using the property that $\det\begin{bmatrix} \mathbf{A} & \mathbf{0} \\ \mathbf{C} & \mathbf{D} \end{bmatrix} = \det\left[\mathbf{A}\right]\det\left[\mathbf{D}\right]$, an upper bound on the PEP can be further written as in (2.9).

A.2 Proof of the Theorem 2.2

The convexity of the linear precoder design problem **P1** given in (2.13)-(2.16), for OS-TBC MIMO-OFDM based CR is proven here. First, we define the function $\mathcal{F}(\boldsymbol{\Psi}(k))$, for subcarrier k as:

$$\mathcal{F}(\boldsymbol{\Psi}(k)) = -\log\det\left[\boldsymbol{\Psi}(k)\right],\ k = 1, \ldots, K, \quad \text{(A.9)}$$

where $\boldsymbol{\Psi}(k) = \mathbf{I}_{M_{st}} + \eta\lambda_{rx,ss}(k)_j\tilde{\mathbf{F}}(k)\boldsymbol{\Lambda}_{tx,ss}(k)$. One can prove the convexity of (2.13) by showing that (A.9) is convex over the set of positive definite matrices. Thus, the convexity of (A.9) is proven using the following theorem [40].

Theorem 2.3 [40]**:** If $\boldsymbol{\Psi}_1 \in \chi$ is Hermitian and $\boldsymbol{\Psi}_2 \in \chi$ is positive definite, then there exists a nonsingular matrix $\mathbf{A} \in \chi$ such that $\mathbf{A}^\dagger\boldsymbol{\Psi}_2\mathbf{A} = \mathbf{I}$, and $\mathbf{A}^\dagger\boldsymbol{\Psi}_1\mathbf{A} = \mathbf{D}$, where $\mathbf{D}$ is a diagonal matrix with all diagonal elements, $d_i > 0$.

The function $\mathcal{F}(\boldsymbol{\Psi}(k))$ is convex, if $\mathcal{F}(\alpha\boldsymbol{\Psi}_1(k) + (1-\alpha)\boldsymbol{\Psi}_2(k)) \leq \alpha\mathcal{F}(\boldsymbol{\Psi}_1(k))$ $+(1-\alpha)\mathcal{F}(\boldsymbol{\Psi}_2(k))$ for any two positive definite Hermitian matrices in χ and for any

$0 \leq \alpha \leq 1$. Equality holds when $\mathbf{\Psi}_1(k) = \mathbf{\Psi}_2(k)$. Using the *Theorem 2.3* and the properties of the logarithm, one can show that $\mathcal{F}(\mathbf{\Psi}(k))$ is convex, if $\mathcal{F}(\alpha\mathbf{I} + (1-\alpha)\mathbf{D}(k)) \leq (1-\alpha)\mathcal{F}(\mathbf{D}(k))$ for all $0 \leq \alpha \leq 1$ and for any diagonal matrix $\mathbf{D}(k)$ with positive diagonal entities. This can be easily proven by using the properties of the determinant and the strict concavity of the logarithmic function itself as

$$\begin{aligned}
\mathcal{F}\left(\alpha\mathbf{I} + (1-\alpha)\mathbf{D}(k)\right) &= -\sum_{i=1}^{n} \log\left(\alpha + (1-\alpha)d(k)_i\right), \\
&\leq -\sum_{i=1}^{n} \left(\alpha \log(1) + (1-\alpha)\log\left(d(k)_i\right)\right), \\
&\leq -(1-\alpha)\log\left(\prod_{i=1}^{n} d(k)_i\right), \\
&\leq -(1-\alpha)\mathcal{F}(\mathbf{D}(k)).
\end{aligned} \tag{A.10}$$

Thus, (A.9) is convex over the set χ. Furthermore, using the property that the sum of convex functions is also a convex function [28], one can easily show that (2.13) is convex. In addition, it can be easily verified that the constraints (2.14)-(2.16) are convex [28]. Therefore the entire optimization problem **P1** is convex.

A.3 Proof of the Theorem 2.4

The proof of the *Theorem 2.4* is presented here. First, the non-negative Lagrange multipliers $\boldsymbol{\nu} = [\nu_1, \ldots, \nu_L]^\dagger$ and $\boldsymbol{\mu} = [\mu_1, \ldots, \mu_K]^\dagger$ associated with the average interference power constraints and per subcarrier power constraints in (2.18) and (2.19) are introduced and the Lagrangian of the primal problem is written as [28, 32]

$$\begin{aligned}\mathcal{L}\left(\{\boldsymbol{\lambda}_{\tilde{\mathbf{F}}}(k)\},\boldsymbol{\nu},\boldsymbol{\mu}\right) &= \sum_{k=1}^{K}\sum_{i=1}^{M_{st}}\sum_{j=1}^{M_{sr}} -\log\left(1+\eta\lambda_{rx,ss}(k)_j\lambda_{tx,ss}(k)_i\boldsymbol{\lambda}_{\tilde{\mathbf{F}}}(k)_i\right)\\ &+\sum_{k=1}^{K}\left(\sum_{l=1}^{L}\nu_l\left(\sum_{i=1}^{M_{st}}\left(\boldsymbol{\lambda}_{\tilde{\mathbf{F}}}(k)_i\mathbf{u}_{tx,ss}(k)_i^{\dagger}\mathbf{R}_{tx,sp_l}(k)\mathbf{u}_{tx,ss}(k)_i\right)-\mathrm{I}_{int,l}\right)\right)\\ &+\sum_{k=1}^{K}\mu_k\left(\sum_{i=1}^{M_{st}}\boldsymbol{\lambda}_{\tilde{\mathbf{F}}}(k)_i-\mathrm{P}_{tot}(k)\right),\end{aligned} \tag{A.11}$$

where $\{\boldsymbol{\lambda}_{\tilde{\mathbf{F}}}(k)\}=\{\boldsymbol{\lambda}_{\tilde{\mathbf{F}}}(k)_i,\ i=1,\ldots,M_{st},\ k=1,\ldots,K\}$ is the set of eigenvalues of the eigenvalue matrices $\Lambda_{\tilde{\mathbf{F}}}(k),\ k=1\ldots,K$. The Lagrange dual function is then defined as [28, 32]

$$\begin{aligned}\mathcal{G}\left(\boldsymbol{\nu},\mu\right) = \quad &\underset{\{\boldsymbol{\lambda}_{\tilde{\mathbf{F}}}(k)\}}{\text{minimize}} \qquad \mathcal{L}\left(\{\boldsymbol{\lambda}_{\tilde{\mathbf{F}}}(k)\},\boldsymbol{\nu},\boldsymbol{\mu}\right),\\ &\text{subject to} \qquad \boldsymbol{\lambda}_{\tilde{\mathbf{F}}}(k)_i\geqslant 0,\ i=1,\ldots,M_{st},\ k=1,\ldots,K.\end{aligned} \tag{A.12}$$

Therefore, the Lagrange dual problem of the primal problem is defined as [28, 32].

$$\begin{aligned}&\underset{\boldsymbol{\nu},\,\boldsymbol{\mu}}{\text{maximize}} \qquad \mathcal{G}\left(\boldsymbol{\nu},\boldsymbol{\mu}\right)\\ &\text{subject to} \qquad \boldsymbol{\nu}\succeq 0,\ \boldsymbol{\mu}\succeq 0.\end{aligned} \tag{A.13}$$

The optimal value $\mathcal{G}^{\star}$ of the dual problem is achieved by the optimal dual variables $\boldsymbol{\nu}^{\star}$ and $\boldsymbol{\mu}^{\star}$. Furthermore, the dual function $\mathcal{G}\left(\boldsymbol{\nu},\boldsymbol{\mu}\right)$ provides a lower bound of the optimal value, $\mathcal{F}^{\star}$, of the primal problem. Since the original problem **P1** is indeed convex and also satisfies Slater's condition, the duality gap ($\mathcal{F}^{\star}-\mathcal{G}^{\star}$) is zero [28, 32]. Therefore, these interesting results suggest that the optimal solution, $\mathcal{F}^{\star}$, for the primal problem can be obtained by first minimizing the Lagrangian $\mathcal{L}(\{\boldsymbol{\lambda}_{\tilde{\mathbf{F}}}(k)\},\boldsymbol{\nu},\boldsymbol{\mu})$ in order to obtain the dual function $\mathcal{G}\left(\boldsymbol{\nu},\boldsymbol{\mu}\right)$

for some given dual variables $\boldsymbol{\nu}$, $\boldsymbol{\mu}$, and then maximizing $\mathcal{G}(\boldsymbol{\nu}, \boldsymbol{\mu})$ over all non-negative values of $\boldsymbol{\nu}$ and $\boldsymbol{\mu}$.

Therefore, consider the minimization of $\mathcal{L}(\{\boldsymbol{\lambda}_{\tilde{\mathbf{F}}}(k)\}, \boldsymbol{\nu}, \boldsymbol{\mu})$ with respect to the variables $\{\boldsymbol{\lambda}_{\tilde{\mathbf{F}}}(k)\}$ and for some given fixed values of $\boldsymbol{\nu}$, $\boldsymbol{\mu}$ to obtain the dual function $\mathcal{G}(\boldsymbol{\nu}, \boldsymbol{\mu})$. One can notice from (A.11) and (A.12) that the dual function $\mathcal{G}(\boldsymbol{\nu}, \boldsymbol{\mu})$ has the following form:

$$\mathcal{G}(\boldsymbol{\nu}, \boldsymbol{\mu}) = \sum_{k=1}^{K} \tilde{\mathcal{G}}_k(\boldsymbol{\nu}, \boldsymbol{\mu}) - \sum_{k=1}^{K} \mu_k \mathrm{P}_{tot}(k) - \sum_{l=1}^{L} \nu_l \mathrm{I}_{int,l}, \tag{A.14}$$

where $\tilde{\mathcal{G}}_k(\boldsymbol{\nu}, \boldsymbol{\mu})$ is given as

$$\begin{aligned} \underset{\boldsymbol{\lambda}_{\tilde{\mathbf{F}}}(k)_i,\ i=1,\ldots,M_{st}}{\text{minimize}} \quad & \sum_{i=1}^{M_{st}} \sum_{j=1}^{M_{sr}} -\log\left(1 + \eta \lambda_{rx,ss}(k)_j \lambda_{tx,ss}(k)_i \boldsymbol{\lambda}_{\tilde{\mathbf{F}}}(k)_i\right) \\ & + \sum_{l=1}^{L} \nu_l \left(\sum_{i=1}^{M_{st}} \left(\boldsymbol{\lambda}_{\tilde{\mathbf{F}}}(k)_i \mathbf{u}_{tx,ss}(k)_i^{\dagger} \mathbf{R}_{tx,sp_l}(k) \mathbf{u}_{tx,ss}(k)_i \right) \right) \\ & + \mu_k \sum_{i=1}^{M_{st}} \boldsymbol{\lambda}_{\tilde{\mathbf{F}}}(k)_i, \\ \text{subject to} \quad & \boldsymbol{\lambda}_{\tilde{\mathbf{F}}}(k)_i \geq 0,\ i = 1, \ldots, M_{st}. \end{aligned} \tag{A.15}$$

Therefore, it is interesting to note that the dual function $\mathcal{G}(\boldsymbol{\nu}, \boldsymbol{\mu})$ can be obtained by solving K independent sub problems (**P3**)s, $\tilde{\mathcal{G}}_k(\boldsymbol{\nu}, \boldsymbol{\mu})$, each for OFDM subcarrier $k = 1, \ldots, K$. This implies that the same computational routine can be repeatedly applied for solving each sub problem **P3**. Thus, the convergence time of the overall algorithm can be dramatically improved. Now it is required to find the optimal solution for a sub problem **P3**. Since the sub problem **P3** is convex, the globally optimal solution can be found by solving the system of Karush-Kuhn-Tucker (KKT) conditions [28]. Therefore, the Lagrangian of the sub problem **P3** can be formulated as

$$\begin{aligned}\tilde{\mathcal{L}}_{tx,rx}\left(\boldsymbol{\lambda}_{\tilde{\mathbf{F}}}(k)_i,\alpha(k)_j\right) &= \sum_{i=1}^{M_{st}}\sum_{j=1}^{M_{sr}} -\log(1+\eta\lambda_{rx,ss}(k)_j\lambda_{tx,ss}(k)_i\boldsymbol{\lambda}_{\tilde{\mathbf{F}}}(k)_i)\\ &+\sum_{l=1}^{L}\nu_l\left(\sum_{i=1}^{M_{st}}\left(\boldsymbol{\lambda}_{\tilde{\mathbf{F}}}(k)_i\mathbf{u}_{tx,ss}(k)_i^{\dagger}\mathbf{R}_{tx,sp_l}(k)\mathbf{u}_{tx,ss}(k)_i\right)\right) \qquad \text{(A.16)}\\ &+\mu_k\sum_{i=1}^{M_{st}}\boldsymbol{\lambda}_{\tilde{\mathbf{F}}}(k)_i-\sum_{i=1}^{M_{st}}\alpha(k)_i\boldsymbol{\lambda}_{\tilde{\mathbf{F}}}(k)_i,\end{aligned}$$

where $\alpha(k)_i$ are the Lagrange multipliers associated with the inequality constraints in (A.15). Then, the KKT conditions for the sub problem **P3** can be written as

$$\begin{aligned}\frac{\partial}{\partial\boldsymbol{\lambda}^{*}_{\tilde{\mathbf{F}}}(k)_i}\tilde{\mathcal{L}}_{tx,rx}\left(\boldsymbol{\lambda}_{\tilde{\mathbf{F}}}(k)_i,\alpha(k)_i\right) &= -\sum_{j=1}^{M_{sr}}\frac{\eta\lambda_{rx,ss}(k)_j\lambda_{tx,ss}(k)_i}{\left(1+\eta\lambda_{rx,ss}(k)_j\lambda_{tx,ss}(k)_i\boldsymbol{\lambda}^{*}_{\tilde{\mathbf{F}}}(k)_i\right)}\\ &+\sum_{l=1}^{L}\nu_l\left(\mathbf{u}_{tx,ss}(k)_i^{\dagger}\mathbf{R}_{tx,sp_l}(k)\mathbf{u}_{tx,ss}(k)_i\right)\\ &+\mu_k-\alpha(k)_i=0,\ i=1,\ldots,M_{st}, \qquad \text{(A.17)}\\ \alpha(k)_i\boldsymbol{\lambda}^{*}_{\tilde{\mathbf{F}}}(k)_i &= 0,\ i=1,\ldots,M_{st}, \qquad \text{(A.18)}\\ \alpha(k)_i &\geq 0,\ i=1,\ldots,M_{st}. \qquad \text{(A.19)}\end{aligned}$$

where $\boldsymbol{\lambda}^{*}_{\tilde{\mathbf{F}}}(k)_i$ is the optimal solution. Therefore, the optimal solution $\boldsymbol{\lambda}^{*}_{\tilde{\mathbf{F}}}(k)_i^{+}$, $i=1,\ldots,M_{st}$, with $x^{+}=\max\{0,x\}$ for the kth subcarrier can be obtained by solving the set of equations as given in (2.21).

Once the dual function $\mathcal{G}\left(\boldsymbol{\nu},\boldsymbol{\mu}\right)$, is obtained for given $\boldsymbol{\nu}$ and $\boldsymbol{\mu}$, the next step of the Lagrange dual-decomposition is to maximize the dual function $\mathcal{G}\left(\boldsymbol{\nu},\boldsymbol{\mu}\right)$, over all possible values of $\boldsymbol{\nu}$ and $\boldsymbol{\mu}$. Searching for the optimal value of $\boldsymbol{\nu}(\boldsymbol{\nu}^{\star})$ and $\boldsymbol{\mu}(\boldsymbol{\mu}^{\star})$ can be done by using, for example, the ellipsoid method [33], which exploits the fact that $\sum_{i=1}^{M_{st}}(\boldsymbol{\lambda}_{\tilde{\mathbf{F}}}(k)_i\mathbf{u}_{tx,ss}(k)_i^{\dagger}\mathbf{R}_{tx,sp_l}(k)\mathbf{u}_{tx,ss}(k)_i)-\mathrm{I}_{int,l}$ and $\sum_{i=1}^{M_{st}}\boldsymbol{\lambda}_{\tilde{\mathbf{F}}}(k)_i-\mathrm{P}_{tot}(k)$ are sub-gradients

of ν_l, $l = 1, \ldots, L$ and $\mu_k, k = 1, \ldots, K$, respectively.

Appendix B

Proof of the Theorems 3.1 and 3.2[10]

B.1 Proof of the Theorem 3.1

A lower-bound on the mutual information, $I_{low}(s_{ss,1}, s_{ss,2}, \ldots, s_{ss,K}; y)$, for the opportunistic spectrum sharing SISO MAC when SU receiver employs MMSE estimation with estimation errors is derived here following the approach presented in [15] and [22]. It is assumed that the signals transmitted from each SU transmitter are independent Gaussian distributed. The received signal in opportunistic spectrum sharing SISO MAC with channel estimation errors can be written as

$$y = \sum_{k=1}^{K} \hat{\alpha}_{ss,k} s_{ss,k} + \sum_{k=1}^{K} \Delta\alpha_{ss,k} s_{ss,k} + w_{ss}. \tag{B.1}$$

A decomposition on the mutual information will be exploited to derive a lower-bound $I_{low}(s_{ss,1}, s_{ss,2}, \ldots, s_{ss,K}; y)$, and it can be written as [23]

$$I(s_{ss,1}, s_{ss,2}, \ldots, s_{ss,K}; y) = \sum_{i=1}^{K} I(s_{ss,i}; y | s_{ss,1}, \ldots, s_{ss,i-1}). \tag{B.2}$$

Therefore, it requires to obtain lower-bounds on the conditional mutual information for $i = 1, \ldots, K$. In the following, lower-bounds on the mutual information for $i = 1$ and K

[10]Note that the references related to this Appendix are given in the bibliography section of the Chapter 3.

are derived and then result for $i = m$ is presented.

When $i = 1$, one can notice that the mutual information $I(s_{ss,K}; y|s_{ss,1}, \ldots, s_{ss,K-1})$ is similar to the mutual information of a single user SISO channel with equivalent noise $w_{ss,eq} = \sum_{k=1}^{K-1} \Delta\alpha_{ss,k} s_{ss,k} + w_{ss}$ and the variance $\sigma^2_{w,eq} = \sum_{k=1}^{K-1} p_k(\mathcal{H})\sigma^2_{ss,k} + \sigma^2_w$. Therefore, these information will be exploited to derive a lover-bound $I_{low}(s_{ss,K}; y|s_{ss,1}, \ldots, s_{ss,K-1})$. It should be noted that $w_{ss,eq}$ is not Gaussian due to the terms $\sum_{k=1}^{K-1} \Delta\alpha_{ss,k} s_{ss,k}$; however, exploiting the similar steps as in [15] and [22], one can derive a lower-bound as

$$I_{low}(s_{ss,K}; y|s_{ss,1}, \ldots, s_{ss,K-1}) = \mathcal{E}_{\mathcal{H}} \left\{ \log \left(1 + \frac{p_K(\mathcal{H})\hat{h}_{ss,K}}{\sum_{k=1}^{K-1} p_k(\mathcal{H})\sigma^2_{ss,k} + \sigma^2_w} \right) \right\}. \tag{B.3}$$

For $i = K$, it can be noticed that the mutual information $I(s_{ss,1}; y)$ is also similar to the mutual information of a single user SISO channel with an equivalent noise $w_{ss,eq} = \sum_{k=2}^{K} \hat{\alpha}_{ss,k} s_{ss,k} + \sum_{k=2}^{K} \Delta\alpha_{ss,k} s_{ss,k} + w_{ss}$ and the variance $\sigma^2_{w,eq} = \sum_{k=2}^{K} p_k(\mathcal{H})\hat{h}_{ss,k} + \sum_{k=2}^{K} p_k(\mathcal{H})\sigma^2_{ss,k} + \sigma^2_w$. Therefore, similarly, a lower-bound on the mutual information, $I_{low}(s_{ss,1}; y)$, can be obtained as [15, 22]

$$I_{low}(s_{ss,1}; y) = \mathcal{E}_{\mathcal{H}} \left\{ \log \left(1 + \frac{p_1(\mathcal{H})\hat{h}_{ss,1}}{\sum_{k=2}^{K} p_k(\mathcal{H})\hat{h}_{ss,k} + \sum_{k=2}^{K} p_k(\mathcal{H})\sigma^2_{ss,k} + \sigma^2_w} \right) \right\}. \tag{B.4}$$

Therefore, following the same procedure, a lower-bond on the mutual information when $i = m$, $I_{low}(s_{ss,m}; y|s_{ss,1}, \ldots, s_{ss,m-1})$, can be obtained as

$$\begin{aligned} &I_{low}(s_{ss,m}; y|s_{ss,1}, \ldots, s_{ss,m-1}) \\ &= \mathcal{E}_{\mathcal{H}} \left\{ \log \left(1 + \frac{p_m(\mathcal{H})\hat{h}_{ss,m}}{\sum_{k=m+1}^{K} p_k(\mathcal{H})\hat{h}_{ss,k} + \sum_{k=m+1}^{K} p_k(\mathcal{H})\sigma^2_{ss,k} + \sigma^2_w} \right) \right\}. \end{aligned} \tag{B.5}$$

Thus, by exploiting (B.2)-(B.5) and the properties of logarithm, a lower-bound on the mutual information of SISO MAC can be obtained as in (3.6).

B.2 Proof of the Theorem 3.2

First, the Lagrangian of the primal problem is formulated by introducing the non-negative Lagrange multipliers $\boldsymbol{\mu} = [\mu_1, \ldots, \mu_L]^\dagger$, $\boldsymbol{\nu} = [\nu_1, \ldots, \nu_K]^\dagger$ and δ associated with constraint in (3.13), (3.14) and (3.15), respectively as

$$\begin{aligned}\mathcal{L}\left(\{p_k(\mathcal{H})\}, \boldsymbol{\mu}, \boldsymbol{\nu}, \delta\right) = \mathcal{E}_{\mathcal{H}}\left\{\log\left(1 + \frac{1}{\sigma_w^2 + \tilde{p}}\sum_{k=1}^{K} p_k(\mathcal{H})\hat{h}_{ss,k}\right)\right\} \\ - \sum_{l=1}^{L}\mu_l\left(\sum_{k=1}^{K}\mathcal{E}_{\mathcal{H}}\left\{p_k(\mathcal{H})\hat{h}_{sp,kl}\right\} + \sum_{k=1}^{K} p_k^{av}\sigma_{sp,kl}^2 - \mathcal{Q}_l^{av}\right) \\ - \sum_{k=1}^{K}\nu_k\left(\mathcal{E}_{\mathcal{H}}\{p_k(\mathcal{H})\} - p_k^{av}\right) - \delta\left(\sum_{k=1}^{K} p_k(\mathcal{H})\sigma_{ss,k}^2 - \tilde{p}\right).\end{aligned} \tag{B.6}$$

Then, the Lagrange dual function, $\mathcal{G}(\boldsymbol{\mu}, \boldsymbol{\nu}, \delta)$ is defined as [17, 20]

$$\begin{aligned}\mathcal{G}\left(\boldsymbol{\mu}, \boldsymbol{\nu}, \delta\right) = \quad & \underset{\{p_k(\mathcal{H})\}}{\text{maximize}} \quad \mathcal{L}\left(\{p_k(\mathcal{H})\}, \boldsymbol{\mu}, \boldsymbol{\nu}, \delta\right) \\ & \text{subject to} \quad p_k(\mathcal{H}) \geq 0,\ k = 1, \ldots, K.\end{aligned} \tag{B.7}$$

The Lagrange dual problem is then defined as [17, 20],

$$\begin{aligned}&\underset{\boldsymbol{\mu},\, \boldsymbol{\nu},\, \delta}{\text{minimize}} \quad \mathcal{G}\left(\boldsymbol{\mu}, \boldsymbol{\nu}, \delta\right) \\ &\text{subject to} \quad \mu_l \geq 0,\ \nu_k \geq 0,\ \delta \geq 0,\ k = 1, \ldots, K,\ l = 1, \ldots, L.\end{aligned} \tag{B.8}$$

Since the original problem **P3** is indeed convex and also satisfies the Slater's condition, the duality gap is zero [17, 20]. Therefore, these interesting results suggested that the optimal solution for the primal problem can be obtained by first maximizing the Lagrangian $\mathcal{L}(\{p_k(\mathcal{H})\}, \boldsymbol{\mu}, \boldsymbol{\nu}, \delta)$ in order to obtain the dual function $\mathcal{G}(\boldsymbol{\mu}, \boldsymbol{\nu}, \delta)$ for some given dual variables $\boldsymbol{\mu}$, $\boldsymbol{\nu}$, δ and then minimizing $\mathcal{G}(\boldsymbol{\mu}, \boldsymbol{\nu}, \delta)$ over all non-negative values of $\boldsymbol{\mu}$, $\boldsymbol{\nu}$ and δ. Therefore, first consider the maximization of $\mathcal{L}(\{p_k(\mathcal{H})\}, \boldsymbol{\mu}, \boldsymbol{\nu}, \delta)$ with respect to variables $\{p_k(\mathcal{H})\}$ and for some given fixed values of $\boldsymbol{\mu}$, $\boldsymbol{\nu}$, δ to obtain the dual function $\mathcal{G}(\boldsymbol{\mu}, \boldsymbol{\nu}, \delta)$. It can be noticed from (B.6) and (B.7), that $\mathcal{G}(\boldsymbol{\mu}, \boldsymbol{\nu}, \delta)$ has the following form:

$$\mathcal{G}\left(\boldsymbol{\mu}, \boldsymbol{\nu}, \delta\right) = \tilde{\mathcal{G}}(\{p_k(\mathcal{H})\}) + \sum_{l=1}^{L} \mu_l \left(\mathcal{Q}_l^{av} - \sum_{k=1}^{K} p_k^{av} \sigma_{ge_k}^2 \right) + \sum_{k=1}^{K} \nu_k p_k^{av} + \delta \tilde{p}, \tag{B.9}$$

where $\tilde{\mathcal{G}}(\{p_k(\mathcal{H})\})$ is given as

$$\begin{aligned} \underset{\{p_k(\mathcal{H})\}}{\text{maximize}} \quad & \mathcal{E}_{\mathcal{H}} \left\{ \log \left(1 + \frac{1}{\sigma_w^2 + \tilde{p}} \sum_{k=1}^{K} p_k(\mathcal{H}) \hat{h}_{ss,k} \right) \right\} \\ & - \sum_{l=1}^{L} \mu_l \left(\sum_{k=1}^{K} \mathcal{E}_{\mathcal{H}} \left\{ p_k(\mathcal{H}) \hat{h}_{sp,kl} \right\} \right) - \sum_{k=1}^{K} \nu_k (\mathcal{E}_{\mathcal{H}} \{ p_k(\mathcal{H}) \}) \\ & - \delta \left(\sum_{k=1}^{K} p_k(\mathcal{H}) \sigma_{ss,k}^2 \right), \\ \text{subject to} \quad & p_k(\mathcal{H}) \geq 0, \ k = 1, \ldots, K, \end{aligned} \tag{B.10}$$

It is interesting to notice that the dual function $\mathcal{G}(\boldsymbol{\mu}, \boldsymbol{\nu}, \delta)$ can be obtained by solving K independent sub problems (**P4**)s, $\tilde{\mathcal{G}}(\{p_k(\mathcal{H})\})$, each for every SU with channel realization $\mathcal{H}$. This implies that the same computational routine can be repeatedly applied for solving each sub problem **P4**. Therefore, the convergence time of the overall algorithm can be dramatically improved. Since the sub problem **P4** is convex, the globally optimal solution

for **P4** can be found by solving the system of Karush-Kuhn-Tucker (KKT) conditions [17]. Therefore, KKT conditions can be written as:

$$\frac{\hat{h}_{ss,k}}{1+\frac{1}{\sigma_w^2+\tilde{p}}\sum_{l=1}^{L} p_l^*(\mathcal{H})\hat{h}_{ss,l}} - \sum_{l=1}^{L}\mu_l\hat{h}_{ss,kl} - \nu_k - \delta\sigma_{ss,k}^2 + \gamma_k^* = 0, \quad k=1,\ldots,K, \tag{B.11}$$

$$p_k^*(\mathcal{H})\gamma_k^* = 0, \quad k=1,\ldots,K, \tag{B.12}$$

where, $p_k^*(\mathcal{H}) \geq 0$, $\gamma_k^* \geq 0$, $k = 1, \ldots, K$ are the optimal solution to the problem **P4**. The following lemma can be obtained by exploiting these KKT conditions:

Lemma 3.1 [12]: The optimal solution of problem **P4** has at most one user $i,\ i \in \{1, \ldots, K\}$, with $p_i^*(\mathcal{H}) > 0$. This suggest that the optimal solution follows the dynamic time-division-multiple-access scheme [12].

Proof. Assume there are two arbitrary users i and j with $p_i^*(\mathcal{H}) > 0$ and $p_j^*(\mathcal{H}) > 0$. Then, from (B.11) and (B.12), one can write that

$$\frac{\hat{h}_{ss,i}}{\sum_{l=1}^{L}\mu_l\hat{h}_{ss,il} + \nu_i + \delta\sigma_{ss,i}^2} = \frac{\hat{h}_{ss,j}}{\sum_{l=1}^{L}\mu_l\hat{h}_{ss,jl} + \nu_j + \delta\sigma_{ss,j}^2}. \tag{B.13}$$

It can be seen that (B.13) is satisfied only with zero probability, because h_i, g_{im}'s are independent of h_j, g_{jm}'s, and λ_i, λ_j, μ_m's are all constant in optimization problem **P2**. Therefore, this shows that there is maximum of one user presence with a positive power value. □

Therefore, by exploiting the *Lemma 3.1*, the optimal power allocation for user k can be obtained as in (3.17). Once the dual function $\mathcal{G}(\boldsymbol{\mu}, \boldsymbol{\nu}, \delta)$, is obtained for given $\boldsymbol{\mu}$, $\boldsymbol{\nu}$, δ, the

next step of the Lagrange dual-decomposition is to minimize $\mathcal{G}(\boldsymbol{\mu}, \boldsymbol{\nu}, \delta)$, over all possible values of $\boldsymbol{\mu}$, $\boldsymbol{\nu}$ and δ. The search of $\boldsymbol{\mu}$ and $\boldsymbol{\nu}$ towards their optimal values $\boldsymbol{\mu}^*$ and $\boldsymbol{\nu}^*$ can be done, e.g. by the ellipsoid method [21].

Appendix C

Cyclostationarity Test[11]

The cyclostationarity test developed in [16] is used to check the presence of cyclostationarity of the received OFDM signal at tested frequency α and at delay τ. The presence of a CF is formulated as a binary hypothesis testing problem. Under the hypothesis $\mathcal{H}_1$ the α is a CF at τ; whereas under hypothesis $\mathcal{H}_0$ the α is not a CF at τ. The following procedure will be employed in the test.

First, the CAF of the received signal is estimated at tested frequency α and at delay τ from the $\mathcal{N}$ samples and the vector $\hat{\mathbf{c}} = [\text{Re}\{\widehat{R}_{rr}(\alpha;\tau)\}\ \text{Im}\{\widehat{R}_{rr}(\alpha;\tau)\}]$ is formed with $\widehat{R}_{rr}(\alpha;\tau)$ as the estimated CAF. Then, a statistic $\Phi = \mathcal{N}\hat{\mathbf{c}}\hat{\Sigma}^{-1}\hat{\mathbf{c}}^{\dagger}$ is computed for the tested frequency α and delay τ, with $\hat{\Sigma}$ being an estimate of the covariance matrix

$$\Sigma = \begin{bmatrix} \text{Re}\{(\mathcal{Q}_{2,0} + \mathcal{Q}_{2,1})/2\} & \text{Im}\{(\mathcal{Q}_{2,0} - \mathcal{Q}_{2,1})/2\} \\ \text{Im}\{(\mathcal{Q}_{2,0} + \mathcal{Q}_{2,1})/2\} & \text{Re}\{(\mathcal{Q}_{2,1} - \mathcal{Q}_{2,0})/2\} \end{bmatrix}, \tag{C.1}$$

where $\mathcal{Q}_{2,0} = \lim_{\mathcal{N}\longrightarrow\infty} \mathcal{N}\text{Cum}[\widehat{R}_{rr}(\alpha;\tau)\}, \widehat{R}_{rr}(\alpha;\tau)\}]$ and
$\mathcal{Q}_{2,1} = \lim_{\mathcal{N}\longrightarrow\infty} \mathcal{N}\text{Cum}[\widehat{R}_{rr}(\alpha;\tau)\}, \widehat{R}^{*}_{rr}(\alpha;\tau)\}]$ are the covariances and Cum$[\cdot]$ as the cumulant operator. These covariances for zero mean processes are given respectively by [16]

[11] Note that the references related to this Appendix are given in the bibliography section of the Chapter 4.

$$\mathcal{Q}_{2,0} = \lim_{\mathcal{N}\longrightarrow\infty} \frac{1}{\mathcal{N}} \sum_{n=0}^{\mathcal{N}-1} \sum_{\xi=n}^{\mathcal{N}-n-1} \text{Cum}[f_r(n;\tau), f_r(n+\xi;\tau)] e^{-j2\pi 2\alpha n} e^{-j2\pi\alpha\xi}, \tag{C.2}$$

and

$$\mathcal{Q}_{2,1} = \lim_{\mathcal{N}\longrightarrow\infty} \frac{1}{\mathcal{N}} \sum_{n=0}^{\mathcal{N}-1} \sum_{\xi=n}^{\mathcal{N}-n-1} \text{Cum}[f_r(n;\tau), f_r^*(n+\xi;\tau)] e^{-j2\pi(-\alpha)n}, \tag{C.3}$$

where $f_r(n;\tau) = r(n+\tau)r^*(n)$ is the second-order lag product. The covariance estimators are respectively given by

$$\hat{\mathcal{Q}}_{2,0} = \frac{1}{\mathcal{N}\mathcal{N}_w} \sum_{n_w=-(\mathcal{N}_w-1)/2}^{(\mathcal{N}_w-1)/2} \omega(n_w)\mathcal{F}(2\pi\alpha - 2\pi n_w\mathcal{N}^{-1})\mathcal{F}(2\pi\alpha + 2\pi n_w\mathcal{N}^{-1}), \tag{C.4}$$

and

$$\hat{\mathcal{Q}}_{2,1} = \frac{1}{\mathcal{N}\mathcal{N}_w} \sum_{n_w=-(\mathcal{N}_w-1)/2}^{(\mathcal{N}_w-1)/2} \omega(n_w)\mathcal{F}^*(2\pi\alpha + 2\pi n_w\mathcal{N}^{-1})\mathcal{F}(2\pi\alpha + 2\pi n_w\mathcal{N}^{-1}), \tag{C.5}$$

where $\mathcal{F}(\alpha) = \sum_{n=0}^{\mathcal{N}-1} r(n+\tau)r^*(n)e^{-j2\pi\alpha n}$ is the discrete-time Fourier transform of the second-order lag product, and $\omega(n_w)$ is a spectral window of length $\mathcal{N}_w$ (odd). It should be noted that $\mathcal{Q}_{2,0}$ and $\mathcal{Q}_{2,1}$, and also their estimators depend on both α and τ. Finally, the calculated test statistic Φ is compared against a threshold Γ. If $\Phi \geq \Gamma$, the tested frequency α is a CF at delay τ and it is not otherwise. The threshold Γ is set for a desired probability of deciding that α is a CF at delay τ given that is not, i.e. $Pr(\Phi \geq \Gamma|\mathcal{H}_0)$. The threshold Γ can be obtained from the tables of chi-squared distribution for the desired probability [16].